

Mechanofluorescent Visualization of Stresses in Polymers and Composites

Citation for published version (APA):

Aerts, A. (2022). *Mechanofluorescent Visualization of Stresses in Polymers and Composites*. [Phd Thesis 1 (Research TU/e / Graduation TU/e), Chemical Engineering and Chemistry]. Eindhoven University of Technology.

Document status and date:

Published: 22/03/2022

Document Version:

Publisher's PDF, also known as Version of Record (includes final page, issue and volume numbers)

Please check the document version of this publication:

- A submitted manuscript is the version of the article upon submission and before peer-review. There can be important differences between the submitted version and the official published version of record. People interested in the research are advised to contact the author for the final version of the publication, or visit the DOI to the publisher's website.
- The final author version and the galley proof are versions of the publication after peer review.
- The final published version features the final layout of the paper including the volume, issue and page numbers.

[Link to publication](#)

General rights

Copyright and moral rights for the publications made accessible in the public portal are retained by the authors and/or other copyright owners and it is a condition of accessing publications that users recognise and abide by the legal requirements associated with these rights.

- Users may download and print one copy of any publication from the public portal for the purpose of private study or research.
- You may not further distribute the material or use it for any profit-making activity or commercial gain
- You may freely distribute the URL identifying the publication in the public portal.

If the publication is distributed under the terms of Article 25fa of the Dutch Copyright Act, indicated by the "Taverne" license above, please follow below link for the End User Agreement:

www.tue.nl/taverne

Take down policy

If you believe that this document breaches copyright please contact us at:

openaccess@tue.nl

providing details and we will investigate your claim.

MECHANOFLUORESCENT VISUALIZATION OF STRESSES IN POLYMERS AND COMPOSITES

PROEFSCHRIFT

ter verkrijging van de graad van doctor aan de Technische Universiteit Eindhoven,
op gezag van de rector magnificus prof.dr.ir. F.P.T. Baaijens, voor een commissie
aangewezen door het College voor Promoties, in het openbaar te verdedigen op
dinsdag 22 maart 2022 om 16:00 uur

door

Annelore Aerts

geboren te Mol, België

Dit proefschrift is goedgekeurd door de promotoren en de samenstelling van de promotiecommissie is als volgt:

Voorzitter: prof. dr. F. Gallucci

1^e promotor: prof. dr. R.P. Sijbesma

2^e promotor: dr. ir. J.P.A. Heuts

Leden: prof. dr. K.U. Loos (Rijksuniversiteit Groningen)

prof. dr. C. Creton (ESPCI Paris)

dr. S.C.J. Meskers

dr. ir. L.C.A. van Breemen

Het onderzoek of ontwerp dat in dit proefschrift wordt beschreven is uitgevoerd in overeenstemming met de TU/e Gedragscode Wetenschapsbeoefening.

Remember to celebrate milestones as you prepare for the road ahead

- Nelson Mandela -

A catalogue record is available from the Eindhoven University of Technology Library
ISBN: 978-90-386-5463-8

Copyright© 2022 by Annelore Aerts

Cover Design: Annelore Aerts

The cover illustrates an iris composed of processed fluorescence microscope images of scratches in mechanophore containing polystyrene.

Printed by Gildeprint, the Netherlands

This research forms part of the research programme of DPI, project #805t15
DPI, P.O. Box 902, 5600 AX Eindhoven, the Netherlands.

Summary

Polymers and composites are extensively used in different types of working fields depending on their mechanical properties. These properties are correlated to their molecular structure and in order to be able to predict the mechanical behavior of a material, it is of paramount interest to create a better understanding of this structure-property relationship. The in-use-performance of polymers has increasingly been studied by incorporating stimuli-responsive molecular units, which generate an output upon exposure to a specific stimulus. An example of these responsive units are mechanochromophores, which undergo a change in optical properties upon exposure to a mechanical force and their application into polymers has already been extensively investigated in the field of polymer mechanochemistry. There is still ample opportunity to improve these damage reporting systems by for example introducing tunability of the activation threshold of the mechanophore. Additionally, most studies are performed on polymer networks or non-crosslinked elastomers, while mechanophore activation in glassy polymers and composites remains a challenge. The aim of this thesis is to tune the ability of the mechanophore to detect relatively small forces in elastomers and to extend the use of mechanochemistry for stress detection in glassy polymers and composites.

The *first* part of the thesis focuses on the development of the mechanophores, polymeric probes and polymer matrices for further activation studies (*Chapter 2*), and the tunability of mechanophores in elastic polyurethanes. Both a supramolecular mechanophore and a covalent mechanophore were synthesized and converted into polymeric probes. The first mechanophore was based on an ion-paired complex of pyranine with pyridinium or bipyridinium as a quencher. No fluorescence was observed when the complex was formed and upon dissociation the fluorescent pyranine was released resulting in an increase in fluorescence intensity. Both the quencher and the fluorescer were converted into an elastic polyurethane probe to study the tunability of the activation threshold in a polyurethane matrix by changing the quencher in the complex (*Chapter 3*). Unexpectedly it was observed that the reference system without quencher forms aggregates in solid state which also function as a mechanophore.

The *second* part of this thesis focuses on visualization of stresses in glassy polymers and composites. The covalent mechanophore based on a Diels-Alder chemistry of π -extended anthracene and maleimide was applied in polystyrene and polycarbonate matrices at

room temperature. When the Diels-Alder adduct was intact, no fluorescence was observed and as soon as a force was applied, the retro-Diels-Alder reaction happened, and fluorescent anthracene was released. Activation was shown in both solution and the solid state. Sliding friction tests with applied normal loads were performed for activation of the mechanophore in the solid state in both polystyrene and polycarbonate. Polystyrene shows more brittle behavior and hence more bond scission compared to polycarbonate with the application of a similar force (*Chapter 4*).

Chapter 5 focuses on mechanophore functionalized silica and MBS nanoparticles which were used in polycarbonate composites. Tensile tests combined with scanning electron microscopy (SEM) and fluorescence microscopy were used to study the failure of the composites. From this was observed that debonding of the particles happens shortly after applying a force.

Lastly, some future perspectives on mechanochemistry in composites and their application in bulk materials are presented in **Chapter 6**.

Samenvatting

Polymeren en composieten worden op grote schaal gebruikt voor verschillende toepassingen, afhankelijk van hun mechanische eigenschappen. Deze eigenschappen worden bepaald door de moleculaire structuur en om het mechanische gedrag van een materiaal te kunnen voorspellen, is het van groot belang om deze structuur-eigenschap relaties beter te begrijpen. De gebruiksprestaties van polymeren zijn in toenemende mate bestudeerd door het inbouwen van op stimuli reagerende moleculaire eenheden, die een respons genereren bij blootstelling aan een specifieke stimulus. Een voorbeeld van deze responsieve eenheden zijn mechanochromoforen, die een verandering in optische eigenschappen ondergaan bij blootstelling aan een mechanische kracht. De toepassing van mechanochromoforen in polymeren is al uitgebreid onderzocht in het veld van polymeermechanochemie. Er zijn nog verschillende mogelijkheden om deze schaderapportagesystemen te verbeteren door bijvoorbeeld de activatierempel van het mechanofoor af te stellen. Bovendien worden de meeste studies uitgevoerd op polymeernetwerken of niet-verknoopte elastomeren, terwijl mechanofooractivering in glasachtige polymeren en composieten een uitdaging blijft. Het doel van dit proefschrift is om het vermogen van de mechanofoor om relatief kleine krachten in elastomeren te detecteren af te stemmen en om het gebruik van mechanochemie voor spanningsdetectie in glasachtige polymeren en composieten uit te breiden.

Het *eerste* deel van het proefschrift richt zich op de ontwikkeling van de mechanoforen, polymere sensoren en polymeermatrices voor verdere activeringsstudies (*Hoofdstuk 2*), en de afstembaarheid van mechanoforen in elastische polyurethanen. Zowel een supramoleculaire mechanofoor als een covalente mechanofoor werden gesynthetiseerd en omgezet in polymere sensoren. Het eerste mechanofoor was gebaseerd op een ion-gepaard complex van pyranine met pyridinium of bipyridinium als quencher. Er werd geen fluorescentie waargenomen toen het complex werd gevormd en bij dissociatie kwam het fluorescerende pyranine vrij, wat resulteerde in een toename van de fluorescentie-intensiteit. Zowel de quencher als de fluorescer werden ingezet als sensor in een elastisch polyurethaan om de afstembaarheid van de activatierempel in een polyurethaan matrix te bestuderen door de quencher in het complex te veranderen (*Hoofdstuk 3*). Onverwacht werd geconstateerd dat het referentiesysteem zonder quencher in vaste toestand aggregaten vormt die tevens als mechanofoor fungeren.

Het tweede deel van dit proefschrift richt zich op visualisatie van spanningen in glasachtige polymeren en composieten. De covalente mechanofoon, gebaseerd op een Diels-Alder-chemie van π -verlengd antraceen en maleïmide, werd toegepast in polystyreen- en polycarbonaatmatrices bij kamertemperatuur. Wanneer het Diels-Alder-adduct intact was, werd geen fluorescentie waargenomen en zodra er kracht op werd uitgeoefend, vond de retro-Diels-Alder-reactie plaats en kwam fluorescerend antraceen vrij. Activering werd zowel in oplossing als in vaste toestand aangetoond. Krastesten werden uitgevoerd met toegepaste normale belastingen voor activering van de mechanofoon in de vaste toestand in zowel polystyreen als polycarbonaat. Polystyreen vertoont een brosser gedrag en dus er treedt meer breuk van de bindingen op in vergelijking met polycarbonaat bij uitoefening van een vergelijkbare kracht (**Hoofdstuk 4**).

Hoofdstuk 5 richt zich op mechanofoon-gefunctionaliseerde silica- en MBS-nanodeeltjes die werden gebruikt in polycarbonaatcomposieten. Trekproeven gecombineerd met scannende elektronenmicroscopie (SEM) en fluorescentiemicroscopie werden gebruikt om het falen van de composieten te bestuderen. Hieruit werd waargenomen dat het uitbelen van de deeltjes plaatsvindt kort na het uitoefenen van een kracht.

Als laatste worden de toekomstperspectieven voor mechanochemie in composieten en hun applicatie in bulk materialen beschreven in **Hoofdstuk 6**.

Table of contents

Chapter 1	Mechanochemical stress visualization in polymers and composites	1-17
1.1	Why stress detection in polymeric materials?	2
1.2	Mechanical failure in polymers and composites	3
1.3	Mechanical stress sensing in polymers	7
1.4	Aim and outline of the thesis	11
1.5	References	13
Chapter 2	Synthesis of a covalent and a supramolecular mechanophore and their incorporation in polymers	19-44
2.1	Introduction	20
2.2	Supramolecular mechanophore	22
2.3	Covalent mechanophore	24
2.4	Polymeric probes	26
2.5	Conclusion	33
	Appendix	34
2.6	Experimental details	35
2.7	References	42
Chapter 3	Tunability of mechanophore strength in thermoplastic polyurethanes	47-61
3.1	Introduction	48
3.2	Aggregation and quenching of HEPTS telechelic polyurethanes	49
3.3	Mechanical activation of HEPTS functionalized polyurethane films	54
3.4	Conclusion	56
3.5	Experimental details	57
3.6	References	60

Chapter 4 Fluorescent visualization of bond breaking in polymer glasses	63-82
4.1 Introduction	64
4.2 Mechanophore synthesis and characterization in solution	65
4.3 Mechanophore activation in solid state	69
4.4 Discussion and conclusion	75
4.5 Experimental details	75
4.6 References	81
Chapter 5 Investigation of interfacial stresses in composites using mechanofluorescent silica fillers	85-104
5.1 Introduction	86
5.2 Synthesis of mechanofluorescent silica fillers	87
5.3 Composite films	91
5.4 Stresses in a polycarbonate composite	92
5.5 Conclusion	97
5.6 Experimental details	97
5.7 References	103
Chapter 6 Epilogue	107-114
6.1 Summary and conclusions	108
6.2 Further developments in composites	110
6.3 Application of mechanochemistry in bulk polymers	112
6.4 Conclusions	113
6.5 References	114
Curriculum vitae	117
List of publications	119
Acknowledgements	121

Chapter 1

**Mechanochemical stress visualization in
polymers and composites**

1.1 WHY STRESS DETECTION IN POLYMERIC MATERIALS?

Polymers and composites are extensively used in different industrial applications such as automotive and aerospace industries because of their excellent properties. In these applications, the materials are often exposed to demanding thermal, mechanical and chemical conditions.¹ Even though the materials are especially designed for these applications and meet the safety requirements, in the long-term the material may gradually deteriorate with diminished performance as a consequence. Hence, examination of the in-use performance of a polymer is required to avoid unexpected catastrophic failure and to predict the long-term mechanical behaviour of materials to ensure their reliability (**Figure 1.1**). Therefore it is important to create a better understanding of the molecular structure and the relation to its macroscopic properties. Stimuli responsive materials and in particular mechanophores, responding to a mechanical force, are the perfect candidates to study the behaviour at the molecular level of a material under mechanical load.²



Figure 1.1. Aloha Airlines Boeing 737-297 a) before catastrophic failure and b) after explosive decompression because of material fatigue. Copyright[©] National Archives photo no. 412-DA-11509 and National Transportation Safety Board, U.S.

1.2 MECHANICAL FAILURE IN POLYMERS AND COMPOSITES

The discovery of Hermann Staudinger in 1920 that polymers are long chains consisting of small building blocks, called monomers or repeating units, linked together by primary and usually covalent bonds, was the head-start of the rapidly developing field of polymer chemistry.³ Later, Carothers was the first to classify polymeric materials based on their polymerization mechanism. Even today all polymers can be classified into step-growth and chain-growth polymerizations.⁴ Step-growth polymerizations require successful reactions between pairs of reactive functional groups provided by the monomers, which are often combined with the release of a small molecule such as water or methanol. Removal of the condensate results in a shift in the equilibrium towards the polymerization product and hence an increase in the molar mass of the polymer.^{4,5} In contrast, chain growth polymerization involves the subsequent addition of monomers to the polymer chain.⁶ Both polymerization mechanisms have been investigated in detail, allowing precise control over the molecular structure, monomer conversion, degree of polymerization and end-group functionality. This knowledge has resulted in an enormous library of synthetic polymers established since Staudinger's introduction of the term 'macromolecule'.^{3,7}

Polymers are often classified as either thermosets or thermoplastics. Thermosets are cross-linked systems which are irreversibly cured at elevated temperatures making them strong and highly thermally and chemically stable. They show a high thermal, chemical and mechanical stability and in addition thermosets are not reshaping which limits their recyclability.^{8,9} Thermoplastics on the other hand, are solid materials that can be reshaped once their melting temperature is reached, and solidify again upon cooling.¹⁰ As the curing process is reversible, the material can be repeatedly reshaped, making thermoplastics easily recyclable.¹¹ This thesis focusses on the latter polymer class.

Within the class of thermoplastic materials, polymers can be distinguished according to their mechanical properties which corresponds to the flow and deformation behaviour under stress.¹² A general sense of the macroscopic mechanical properties of a polymer can be illustrated in a stress-strain curve, which is generated during a tensile or compression test. During these tests, the load is measured as a function of the constantly increasing strain. In a stress-strain diagram, the stress is defined as the load exerted on the sample divided by the initial cross-sectional area of the sample whereas the strain is determined by the instantaneous elongation divided by the initial length of the sample.

Three important parameters can be derived from the stress strain curve: Young's modulus, yield stress and the strain at break (**Figure 1.2a**).^{6,13}

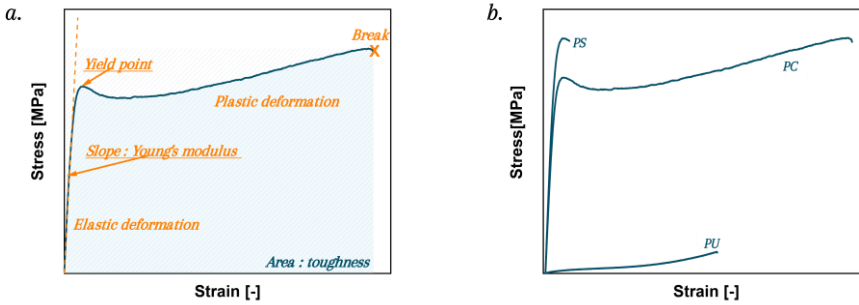


Figure 1.2. a) Illustration of a stress-strain curve for a plastic with the assignment of the modulus, yield stress and strain at break. b) Overview of the difference in mechanical properties of a brittle, ductile and elastic polymer material.

The Young's modulus is equal to the slope of the initial linear part of the tensile curve, and is a measure for the stiffness of the material. This is a measure for the extent to which a material resists deformation. The higher the Young's modulus, the higher the resistance towards deformation and the stiffer the material is.¹² In this region, the material is elastically deformed meaning that dimensional changes are recoverable when the load is removed. After reaching the yield stress, the material starts to plastically deform. After this point the shape of the material is not fully restorable anymore, resulting in permanent deformation. Additionally, upon exceeding the yield stress, the material starts to fail and chains start to slip or bonds start to break. The actual breaking of the material occurs at higher strains (strain at break). One of the polymers that behaves as described above is polycarbonate. However, polymer failure can also occur before the yield point is reached and this is what happens for polystyrene (**Figure 1.3**), this is called brittle failure.

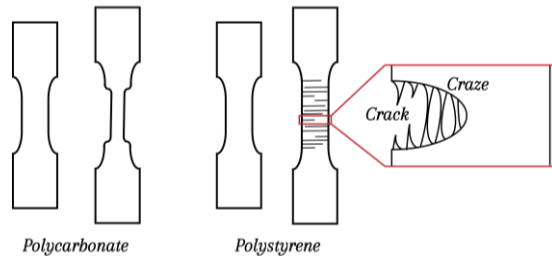


Figure 1.3. Illustration of the deformation in both polycarbonate and polystyrene during a tensile test.

When stretching polystyrene, right before breaking, the material starts to craze which is the formation of microscopically small voids in the material which often can be observed as whitening.^{14,15} Crazes are different from cracks as the two flat fracture surfaces are bridged by fibrils, making crazes able to support stress (**Figure 1.3**). Hence, further stretching of the polymer results in elongation of the fibrils until failure resulting in the formation of a crack.^{13,15} Due to the formation of crazes, polystyrene behaves like a brittle material, which breaks at low strains before the yield point, and hence macroscopically no plastic deformation is observed. Although the elongation of polystyrene before breaking is relatively low, the strain of the fibrils can be extremely high, resulting in local plastic deformation.

A last but not the least important mechanical property that can be derived from a stress-strain curve is toughness, which is the ability to dissipate the applied stresses to result in plastic deformation instead of fracture.¹⁶ Toughness is determined from the area underneath the tensile curve; the larger the area, the tougher the material is and hence the more energy is needed to break the polymer material.¹³

A combination of the above mentioned mechanical properties define the macroscopic properties of a polymer, however, these properties can be tuned by for example adding a secondary phase, often called a reinforcement or a filler (**Figure 1.4a**).

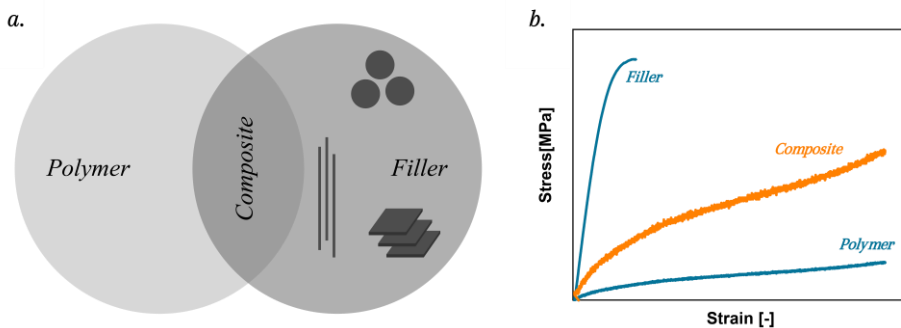


Figure 1.4. a) Composites are formed by adding a filler to a polymer material. b) Illustration of the strength properties of the reinforcement, polymer matrix and a composite.

The addition of a reinforcement material results in the formation of a composite. In general, the composite exhibits combined mechanical properties of the filler and the polymer matrix and sometimes even new properties are obtained (**Figure 1.4b**).¹⁷ For example, when a strong and stiff reinforcement is added to a weaker polymer matrix, the

strength of the composite material will be increased relative to the parent polymer matrix.¹⁸⁻²⁰ In contrast, stiff materials can also be toughened by the addition of fillers, which is often done for glassy polymers such as polycarbonate.^{21,22}

Fillers can be structurally classified as particles, fibers or laminates; this thesis focusses on particulate fillers. The final mechanical properties of a composite depends, next to the geometry of the filler, also on the type of fillers, the filler volume fraction and the interaction between the filler and the polymer matrix.^{18,23,24} In general, particle reinforced composites are less effectively strengthened than fiber reinforced materials and find their applications mostly in increasing wear resistance or toughening. The improvement in mechanical properties is strongly dependent on the strength of the interaction between the particulate filler and the polymer matrix. The higher the surface-to-volume ratio of the filler is, the more important the interfacial region becomes for the final mechanical properties of the material.²⁵⁻²⁸

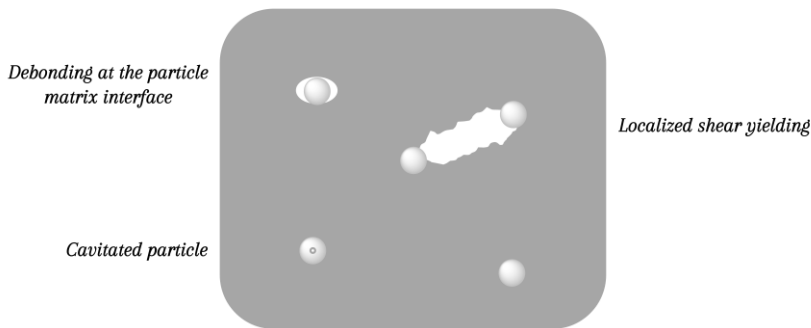


Figure 1.5. Illustration of the different failure modes in polymer composites.

For toughening of a polymer, for example, the proposed mechanism is letting the filler particles act as stress concentrators. When additional load is applied, debonding is thought to occur at the polymer-interface after which the shear yielding mechanism operates as a large energy dissipator, allowing the material to absorb larger energies until fracture.²⁹ In contrast, when the interaction with the polymer matrix is poor, debonding of the particles can lead to failure of the polymer composite. Additionally, matrix failure or particle failure can result in fracture of the polymer material (**Figure 1.5**).³⁰ Hence, investigation of stresses in the polymers, particles and interfacial interactions is of utmost importance for further development of composite materials and the prediction of their long-term mechanical behaviour.

1.3 MECHANOCHEMICAL STRESS SENSING IN POLYMERS

Investigation of crack formation and propagation in polymers has been done by application of dynamic loads to compact tension samples.³¹ However, this technique requires specific loading conditions, which are not fully representative for in-use performance of polymers. In real life, polymers are mainly exposed to tension or compression. Ideally a highly sensitive and self diagnostic technique should be developed to study the microscopic behaviour of a polymer under stress. Mechanochemistry is a branch of chemistry describing chemical or physical transformations upon exposure to mechanical force, making it a perfect candidate for studying stresses in polymeric materials.

Mechanochemistry finds its roots in Ancient Greece: the production of quicksilver upon grinding a cinnabar in a copper morter was the first reported principle of mechanochemistry.³² Over time more and more examples of mechanochemistry were reported and in the beginning of the 20th century, Ostwald introduced the term ‘mechanochemistry’ as a new branch of chemistry.^{33,34} Nowadays, mechanochemistry is a well-established field in chemistry and applied in various materials like polymers, composites, including use in biomedical applications. Polymer mechanochemistry gained attention during the last decades since mechanochemical bond scission was believed to be a cause for premature failure in polymer materials.³⁵

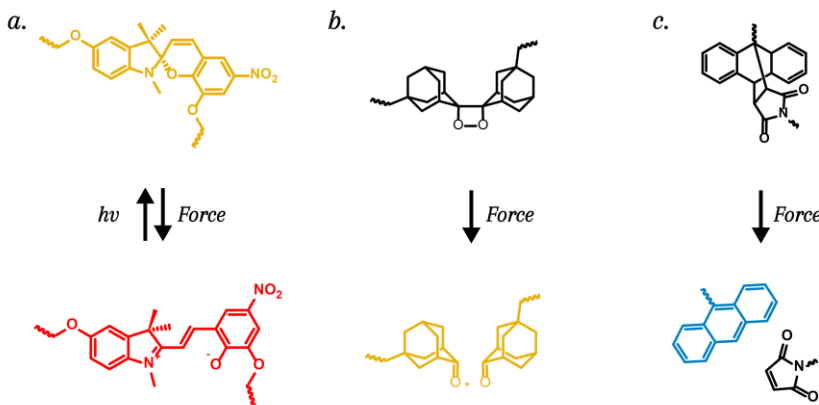
Mechanochemical stress detection

In polymer mechanochemistry the most thoroughly investigated mechanoresponsive moieties are optical mechanophores, which change their optical response under mechanical load.

Different types of organic mechanophores have been investigated regarding to linear polymers and polymer networks.^{36–39} Extensively used mechanophores are spiropyran,³⁸ dioxetanes,³⁹ anthracene or coumarin dimers,^{40,41} and π -extended anthracene-maleimide adducts.^{42,43} These mechanophores require breaking of covalent bonds for activation which limits their use in detection of relatively small stresses. At room temperature, activation of these mechanophores is irreversible, which is convenient for ex-situ measurements but limits the investigation of elastic properties of polymer materials. In order to address these limitations, the array of mechanophores has been expanded with supramolecular mechanophores which require lower energies for dissociation compared to a covalent bonds and can be reformed when the applied load is removed. Only a few

activation thresholds for supramolecular systems have been reported.⁴⁴ Supramolecular mechanophores include systems such as charge transfer interactions, host-guest complexes, rotaxanes, and π-π-stacked mechanophores.⁴⁵⁻⁵¹

Based on the type of optical response, mechanophores can be classified as mechanochromic or mechanoluminescent. Mechanochromic mechanophores change their color when a mechanical force is applied due to a change in conjugation of the mechanochromic moiety. Spiropyran is among the most used and well-investigated mechanophores in polymer mechanochemistry (**Scheme 1.1a**). Moore first reported in 2009 the incorporation of spirobifluorene into poly(methyl acrylate) (PMA) polymer.³⁸ A color change to the red merocyanine form was reported upon application of a mechanical force, demonstrating that the load applied to the polymer is transduced towards the mechanochromic spirobifluorene. Further stretching of the material resulted in an increasing response allowing for quantification of damage in polymer materials. Although mechanochromism is easily quantifiable by UV-VIS absorption, the sensitivity of this method is rather low and relatively high concentrations are required to observe a color change. Additionally, the activation threshold for spirobifluorene is around 0.3 nN,⁵² and the stress dissipates around the formed crack, causing the coloration to spread through the sample.



Scheme 1.1. Overview of the chemical rearrangements upon mechanical loading in a) spirobifluorene, b) dioxetane and c) an anthracene-maleimide Diels-Alder adduct.

Mechanoluminescent moieties, however, offer better sensitivity than absorption because of the emission of light from an excited state that is formed upon activation.⁵³ A subdivision can be made based on the origin of the excited state resulting in a luminescent

response into mechanically induced chemiluminescence (mechanochemiluminescence) and fluorescence (mechanofluorescence). Mechanochemiluminescence is characterized by the formation of an excited state in a chemical reaction such as in the decomposition of 1,2-dioxetanes, firstly reported as strain sensors by our research group (**Scheme 1.1b**).³⁹ Bis(adamantyl)-1,2-dioxetane was incorporated into both a linear PMA polymer and a network and under loading the dioxetane undergoes a cycloelimination reaction followed by the emission of light, allowing localization of bond scission. Furthermore this mechanophore was used in multiple networks showing that the energy dissipation is more efficient in multiple networks than in single networks, in accordance with the observed toughening upon addition of an extra network.⁵⁴ The disadvantage of chemiluminescence is that the chemiluminophore can only undergo reaction once, resulting in transient light emission. Hence, *in situ* monitoring of the bond scission is required. Mechanofluorescence on the other hand addresses this problem because an external light source is used to populate the excited state of the fluorophore. Hence, as long as the mechanochemical reaction is irreversible, the fluorescence emission can be quantified for a longer period of time primarily limited by photobleaching. Cycloreversion reactions dominate the activation mechanisms for mechanofluorophores including anthracene dimers,⁴⁰ and anthracene maleimide Diels-Alder adducts,^{55,56} with the latter as the most extensively researched fluorophore (**Scheme 1.1c**).^{55,57} When the non-fluorescent Diels-Alder adduct is exposed to a mechanical force it undergoes a retro-Diels-Alder, releasing a blue fluorescent anthracene moiety. Later, the sensitivity of these Diels-Alder mechanophores was enhanced by π -extending the anthracene moiety to increase the conjugated system with an increased quantum yield of 0.72.^{37,43} As covalent mechanophore a π -extended anthracene-maleimide Diels-Alder adduct will be discussed in detail in **Chapter 2** and **4** of this thesis.

The library of mechanophores has been expanded by the addition of supramolecular mechanofluorophores with lower thresholds for mechanical activation, often based on mechanoluminescence. Various supramolecular mechanophore systems are based on π - π stacking of molecular dyes. Weder reported a oligo(p-phenylenevinylene) derivative based mechanophore which forms π - π stacks that can be dissociated by the application of a mechanical force resulting in a change in fluorescence emission. The luminescent color can be tuned by the functionalization of the dye.^{50,58} Additionally, Weder developed color-tunable mechanophores based on a fluorophore-quencher complex containing rotaxane, where the off-state is interlocked in the rotaxane. As soon as a force is applied to the material, the quencher is pulled away from the fluorescer, resulting in an increase

in fluorescence intensity. Different emission colors can be obtained by changing the fluorophore built into the rotaxane.^{59,60} Continuing with the π-π- stacked systems, Imato and coworkers developed a system based on non-fluorescent charge transfer complexes between pyrene and naphthalene diimide moieties.⁴⁵ Application of a force dissociates the interactions and fluorescent pyrene is released.

Mechanical activation of bonds

Since mechanophores are intended to undergo a chemical change upon application of mechanical force,⁶¹ researchers have exploited multiple types of experimental methods to investigate mechanochemical changes in polymer materials in both solution and in solid state. An overview of these techniques with their relative strain rates is shown in **Figure 1.6.**⁶²

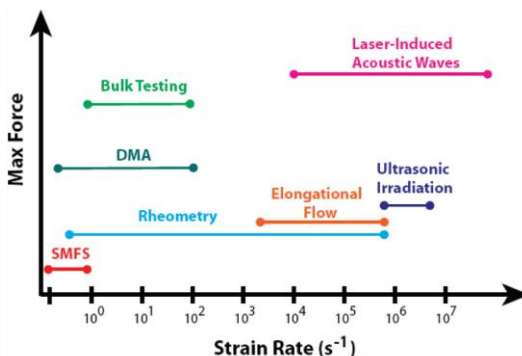


Figure 1.6. Overview of the experimental strategies to characterize mechanochemical activation in solution and solid state.⁶² Copyright © 2009 American Chemical Society

As can be derived from **Figure 1.6**, the maximum strain rates and forces significantly differ between the different techniques. Ultrasound irradiation is a prevalent technique applied for bond scission in dilute polymer solutions, extensively used for fundamental studies on mechanochemistry. High strain rates of 10^6 - 10^7 s^{-1} can be reached, which is much higher than in other solution-based techniques such as contraction flows.⁶³

Upon ultrasonication of a polymer solution, high-frequency pressure waves are formed resulting in the formation and growth of bubbles. When the bubbles reach a critical size, they become unstable and collapse with the introduction of a solvodynamic shear. Polymers close to the shear field will experience a velocity gradient and the polymer chain

will be elongated which ultimately results in chain scission. This process is illustrated in **Figure 1.7**.⁶²

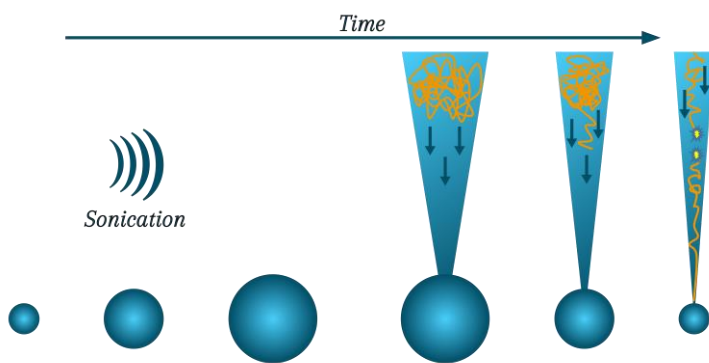


Figure 1.7. Mechanism for the mechanical activation of polymers by ultrasound waves. Bubbles are formed as a consequence of a pressure wave and collapse when a critical size is reached and a solvodynamic shear is generated which uncoils the polymer and finally result in bond scission.

The range of techniques to activate mechanophores in solid state is larger than for mechanophores in solution. In the early years of mechanochemistry, grinding or mastication were used to show the degradation of polymers upon application of mechanical force.^{64–66} With the development of mechanochemistry, the range of techniques to induce a mechanochemical reaction was expanded as well. Examples in literature show mechanochemical activation with less standard techniques such as solvent swelling and crystallization.^{67–69} More generally known techniques used for mechanochemical activation are compression and tension.⁷⁰ In addition, single asperity sliding friction tests can be performed to activate mechanophores.⁷¹ This method will be described in more detail in *Chapter 4*.

1.4 AIM AND OUTLINE OF THE THESIS

The investigation of stresses in polymer materials is important to gain a better understanding of the structure-property relationship in polymeric materials. For this thesis a library of both elastic and glassy polymers was created in which mechanophores are incorporated with the aim to visualize developing stresses and bond scission in polymer materials

Chapter 2 gives a detailed overview of the syntheses of both the mechanophores and the polymers used for this thesis. Two different types of mechanophores are discussed: a supramolecular mechanophore based on pyrene and pyridinium derivatives and a

π -extended anthracene-maleimide Diels-Alder adduct as covalent mechanophore. In order to test their mechanochemical activation in solid polymer films, discussed in **Chapter 3-5**, both elastic polyurethane and glass-like polycarbonate were synthesized as polymer matrix.

The mechanical activation of supramolecular mechanophores in elastic polyurethanes is discussed in **Chapter 3**. Alkylated pyranine (HEPTS) was used as a fluorescer in an ion paired complex, where complex formation with monopyridinium of bipyridinium derivates resulted in quenching of the fluorescence. Additionally, HEPTS aggregates were shown to act as mechanopores as the aggregates change color upon dissociation by mechanical force. Since differences in complex formation were observed, the tunability of the strength of the mechanophore was studied by comparing these three systems for mechanochemical activation under tension.

Chapter 4 describes the mechanical activation of a π -extended anthracene-maleimide Diels-Alder adduct in glassy polymers in single asperity sliding friction tests studied with fluorescence microscopy. In this chapter we show that craze formation in brittle polystyrene goes hand in hand with scission of covalent bonds, whereas plastic deformation in polycarbonate does not require bond scission at lower forces. When higher forces are reached, cracks are formed and hence bond scission occurs in tougher polycarbonate.

As it is hypothesized that in composites the interaction at the interface between the particles and the polymer matrix plays an important role in the enhancement of mechanical properties, it is of utmost importance to create a better understanding of these interfacial stresses or interactions. In **Chapter 5** interfacial interactions were investigated by extending the application of mechanochemistry in glassy polymers to the interfacial region in polycarbonate composites. In this chapter the synthesis and covalent functionalization of silica particles with the Diels-Alder mechanophore is described in detail. Functionalization of the particles was confirmed by heating and sonication experiments. Polycarbonate films with different amounts of silica fillers were solvent cast and tensile tests were performed to study mechanical activation of the mechanophores at the interface. We showed with fluorescence microscopy and SEM that mechanical activation occurs at the interface between the polymer and silica particle.

Future perspectives on the use of mechanochemistry in composites are described in **Chapter 6**.

1.5 REFERENCES

1. Awaja, F.; Zhang, S.; Tripathi, M.; Nikiforov, A.; Pugno, N. Cracks, Microcracks and Fracture in Polymer Structures: Formation, Detection, Autonomic Repair. *Prog. Mater. Sci.* **2016**, *83*, 536–573.
2. Chen, Y.; Mellot, G.; Van Luijk, D.; Creton, C.; Sijbesma, R. P. Mechanochemical Tools for Polymer Materials. *Chem. Soc. Rev.* **2021**, *50*, 4100–4140.
3. Staudinger, H. Über Polymerisation. *Chem. Ber.* **1920**, *1073*–1085.
4. Carothers, W. H. Polymerization. *Chem. Rev.* **1931**, *8*, 353–425.
5. Stille, J. K. Step-Growth Polymerization. *J. Chem. Educ.* **1981**, *58*, 862–866.
6. Young R.J.; Lovell, P. A. *Introduction to Polymers*, 3rd ed.; CRC press, 2011.
7. Kiparissides, C. Polymerization Reactor Modeling : A Review of Recent Developments and Future Directions Classification by the Molecular Structure of Polymers Step-Growth Polymerization. *Chem. Eng. Sci.* **1996**, *51*, 1637–1659.
8. Bîrca, A.; Gherasim, O.; Grumezescu, V.; Grumezescu, A. M. Introduction in Thermoplastic and Thermosetting Polymers. *Mater. Biomed. Eng. Thermoset Thermoplast. Polym.* **2019**, *1*–28.
9. Pickering, S. J. Recycling Technologies for Thermoset Composite Materials-Current Status. *Compos. Part A Appl. Sci. Manuf.* **2006**, *37*, 1206–1215.
10. Van De Velde, K.; Kiekens, P. Thermoplastic Polymers: Overview of Several Properties and Their Consequences in Flax Fibre Reinforced Composites. *Polym. Test.* **2001**, *20*, 885–893.
11. Ibeh., C. C. *Thermoplastic Materials Properties Manufacturing Methods and Applications*; 2011.
12. Odian, G. *Principles of Polymerization*, 4th ed.; John Wiley & Sons, 2015.
13. Vegt, A. K. van der; L. E. G. *Polymeren: Van Keten Tot Kunststof*, 5th ed.; VSSD: Delft, 2003.
14. Van Krevelen, D. W.; te Nijenhuis, K. *Properties of Polymers*, 4th ed.; Elsevier, 2009.
15. Basu, S.; Mahajan, D. K.; Van Der Giessen, E. Micromechanics of the Growth of a Craze Fibril in Glassy Polymers. *Polymer*. **2005**, *46*, 7504–7518.
16. Ritchie, R. O. The Conflicts between Strength and Toughness. *Nat. Mater.* **2011**, *10*, 817–822.
17. Oladele, I. O.; Omotosho, T. F.; Adediran, A. A. Polymer-Based Composites: An Indispensable Material for Present and Future Applications. *Int. J. Polym. Sci.* **2020**, *2020*, 1–11.

18. Fu, S. Y.; Feng, X. Q.; Lauke, B.; Mai, Y. W. Effects of Particle Size, Particle/Matrix Interface Adhesion and Particle Loading on Mechanical Properties of Particulate-Polymer Composites. *Compos. Part B Eng.* **2008**, *39*, 933–961.
19. Dearmitt, C.; Rothon, R.; Consultants, R. Encyclopedia of Polymers and Composites. *Encycl. Polym. Compos.* **2014**, No. 1991, 1–19.
20. Campbell, D. C. *Structural Composite Materials*; ASM International, 2010.
21. Cho, K.; Yang, J.; Yoon, S.; Hwang, M.; Nair, S. V. Toughening of Polycarbonate: Effect of Particle Size and Rubber Phase Contents of the Core–Shell Impact Modifier. *J. Appl. Polym. Sci.* **2005**, *95*, 748–755.
22. Wang, J.; Li, C.; Zhang, X.; Xia, L.; Zhang, X.; Wu, H.; Guo, S. Polycarbonate Toughening with Reduced Graphene Oxide: Toward High Toughness, Strength and Notch Resistance. *Chem. Eng. J.* **2017**, *325*, 474–484.
23. Rothon, R. N. *Particulate-Filled Polymer Composites Second Edition*, 2nd ed.; Rapra, 2003.
24. Lauke, B.; Fu, S. Y. Aspects of Fracture Toughness Modelling of Particle Filled Polymer Composites. *Compos. Part B Eng.* **2013**, *45*, 1569–1574.
25. Pukánszky, B. Interfaces and Interphases in Multicomponent Materials: Past, Present, Future. *Eur. Polym. J.* **2005**, *41*, 645–662.
26. Rothon, R. Fillers for Polymer Applications. *Springer* **2017**, 489.
27. Wang, K.; Wu, J.; Ye, L.; Zeng, H. Mechanical Properties and Toughening Mechanisms of Polypropylene/Barium Sulfate Composites. *Compos. Part A Appl. Sci. Manuf.* **2003**, *34*, 1199–1205.
28. Hatsuo, I.; Ganesh, K. *Molecular Characterization of Composite Interfaces*; Springer, 1985.
29. Zuiderduin, W. C. J.; Westzaan, C.; Huetink, J.; Gaymans, R. J. Toughening of Polypropylene with Calcium Carbonate Particles. *Polymer* **2003**, *44*, 261–275.
30. Onitiri, M.; Ubi, P. A. Failure Modes in Particle Filled Plastic Matrix. *J. Eng. Sci. Technol.* **2021**, *5*, 78–96.
31. Kanders, M. J. W.; Stolk, J.; Govaert, L. E. Direct Comparison of the Compliance Method with Optical Tracking of Fatigue Crack Propagation in Polymers. *Polym. Test.* **2015**, *46*, 98–107.
32. Takacs, L. The First Documented Mechanochemical Reaction? *J. Met.* **2000**, *52*, 12–13.
33. Ostwald, W. *Handbuch Der Allgemeinen Chemie*; Akademische Verlagsgesellschaft: Leipzig, 1919.
34. Takacs, L. The Historical Development of Mechanochemistry. *Chem. Soc. Rev.* **2013**, *42*, 7649–7659.
35. Boulatov, R. *Polymer Mechanochemistry*; Springer: Switzerland, **2015**; Vol. 53.

36. Li, H.; Göstl, R.; Delgove, M.; Sweeck, J.; Zhang, Q.; Sijbesma, R. P.; Heuts, J. P. A. Promoting Mechanochemistry of Covalent Bonds by Noncovalent Micellar Aggregation. *ACS Macro Lett.* **2016**, *5*, 995–998.
37. Morelle, X. P.; Sanoja, G. E.; Castagnet, S.; Creton, C. 3D Fluorescent Mapping of Invisible Molecular Damage after Cavitation in Hydrogen Exposed Elastomers. *Soft Matter* **2021**, *17*, 4266–4274.
38. Davis, D. A.; Hamilton, A.; Yang, J.; Cremar, L. D.; Van Gough, D.; Potisek, S. L.; Ong, M. T.; Braun, P. V.; Martínez, T. J.; White, S. R.; Moore, J. S.; Sottos, N. R. Force-Induced Activation of Covalent Bonds in Mechanoresponsive Polymeric Materials. *Nature* **2009**, *459*, 68–72.
39. Chen, Y.; Spiering, A. J. H.; Karthikeyan, S.; Peters, G. W. M.; Meijer, E. W.; Sijbesma, R. P. Mechanically Induced Chemiluminescence from Polymers Incorporating a 1,2-Dioxetane Unit in the Main Chain. *Nat. Chem.* **2012**, *4*, 559–562.
40. Song, Y. K.; Lee, K. H.; Hong, W. S.; Cho, S. Y.; Yu, H. C.; Chung, C. M. Fluorescence Sensing of Microcracks Based on Cycloreversion of a Dimeric Anthracene Moiety. *J. Mater. Chem.* **2012**, *22*, 1380–1386.
41. Kean, Z. S.; Gossweiler, G. R.; Kouznetsova, T. B.; Hewage, G. B.; Craig, S. L. A Coumarin Dimer Probe of Mechanochemical Scission Efficiency in the Sonochemical Activation of Chain-Centered Mechanophore Polymers. *Chem. Commun.* **2015**, *51*, 9157–9160.
42. Yildiz, D.; Baumann, C.; Mikosch, A.; Kuehne, A. J. C.; Herrmann, A.; Göstl, R. Anti-Stokes Stress Sensing: Mechanochemical Activation of Triplet-Triplet Annihilation Photon Upconversion. *Angew. Chemie - Int. Ed.* **2019**, *58*, 12919–12923.
43. Göstl, R.; Sijbesma, R. P. Π -Extended Anthracenes As Sensitive Probes for Mechanical Stress. *Chem. Sci.* **2016**, *7*, 370–375.
44. van de Laar, T.; Schuurman, H.; van der Scheer, P.; van Doorn, J. M.; van der Gucht, J.; Sprakel, J. Light from Within: Sensing Weak Strains and FemtoNewton Forces in Single Molecules. *Chem* **2018**, *4*, 269–284.
45. Imato, K.; Yamanaka, R.; Nakajima, H.; Takeda, N. Fluorescent Supramolecular Mechanophores Based on Charge-Transfer Interactions. *Chem. Commun. (Camb.)* **2020**, *56*, 7937–7940.
46. Sagara, Y.; Karman, M.; Verde-Sesto, E.; Matsuo, K.; Kim, Y.; Tamaoki, N.; Weder, C. Rotaxanes as Mechanochromic Fluorescent Force Transducers in Polymers. *J. Am. Chem. Soc.* **2018**, *140*, 1584–1587.
47. Crenshaw, B. R.; Weder, C. Deformation-Induced Color Changes in Melt-Processed Photoluminescent Polymer Blends. *Chem. Mater.* **2003**, *15*, 4717–4724.
48. Früh, A. E.; Artoni, F.; Brighenti, R.; Dalcanale, E. Strain Field Self-Diagnostic Poly(Dimethylsiloxane) Elastomers. *Chem. Mater.* **2017**, *29*, 7450–7457.

49. Das, A. D.; Mannoni, G.; Früh, A. E.; Orsi, D.; Pinalli, R.; Dalcanale, E. Damage-Reporting Carbon Fiber Epoxy Composites. *ACS Appl. Polym. Mater.* **2019**, *1*, 2990–2997.
50. Löwe, C.; Weder, C. Oligo(p-Phenylene Vinylene) Excimers as Molecular Probes: Deformation-Induced Color Changes in Photoluminescent Polymer Blends. *Adv. Mater.* **2002**, *14*, 1625–1629.
51. Aerts, A.; Lugger, S. J. D.; Heuts, J. P. A.; Sijbesma, R. P. Pyranine Based Ion-Paired Complex as a Mechanophore in Polyurethanes. *Macromol. Rapid Commun.* **2021**, *42*.
52. Gossweiler, G. R.; Kouznetsova, T. B.; Craig, S. L. Force-Rate Characterization of Two Spiropyran-Based Molecular Force Probes. *J. Am. Chem. Soc.* **2015**, *137*, 6148–6151.
53. Lakowicz, J. R. *Principles of Fluorescence Spectroscopy*, 3rd ed.; Springer: Baltimore, 2006.
54. Ducrot, E.; Chen, Y.; Bulters, M.; Sijbesma, R. P.; Creton, C. Toughening Elastomers with Sacrificial Bonds and Watching Them Break. *Science*. **2014**, *344*, 186–189.
55. Yoshie, N.; Saito, S.; Oya, N. A Thermally-Stable Self-Mending Polymer Networked by Diels-Alder Cycloaddition. *Polymer*. **2011**, *52*, 6074–6079.
56. Konda, S. S. M.; Brantley, J. N.; Varghese, B. T.; Wiggins, K. M.; Bielawski, C. W.; Makarov, D. E. Molecular Catch Bonds and the Anti-Hammond Effect in Polymer Mechanochemistry. *J. Am. Chem. Soc.* **2013**, *135*, 12722–12729.
57. Church, D. C.; Peterson, G. I.; Boydston, A. J. Comparison of Mechanochemical Chain Scission Rates for Linear versus Three-Arm Star Polymers in Strong Acoustic Fields. *ACS Macro Lett.* **2014**, *3*, 648–651.
58. Sagara, Y.; Kubo, K.; Nakamura, T.; Tamaoki, N.; Weder, C. Temperature-Dependent Mechanochromic Behavior of Mechanoresponsive Luminescent Compounds. *Chem. Mater.* **2017**, *29*, 1273–1278.
59. Muramatsu, T.; Sagara, Y.; Traeger, H.; Tamaoki, N.; Weder, C. Mechanoresponsive Behavior of a Polymer-Embedded Red-Light Emitting Rotaxane Mechanophore. *ACS Appl. Mater. Interfaces* **2019**, *II*, 24571–24576.
60. Sagara, Y.; Karman, M.; Seki, A.; Pannipara, M.; Tamaoki, N.; Weder, C. Rotaxane-Based Mechanophores Enable Polymers with Mechanically Switchable White Photoluminescence. *ACS Cent. Sci.* **2019**, *5*, 874–881.
61. Li, J.; Nagamani, C.; Moore, J. S. Polymer Mechanochemistry: From Destructive to Productive. *Acc. Chem. Res.* **2015**, *48*, 2181–2190.
62. Caruso, M. M.; Davis, D. A.; Shen, Q.; Odom, S. A.; Sottos, N. R.; White, S. R.; Moore, J. S. Mechanically-Induced Chemical Changes in Polymeric Materials. *Chem. Rev.* **2009**, *109*, 5755–5798.
63. Nguyen, T. Q.; Kausch, H. H. Chain Extension and Degradation in Convergent Flow. *Polymer*. **1992**, *33*, 2611–2621.

64. Staudinger, H. Über Isopren Und Kautschuk. *Berichte* **1930**, *67*, 1159–1164.
65. Staudinger, H. Über Hochpolymere Verbindungen. *Berichte der Dtsch. Chem. Gesellschaft* **1934**, *67*, 921–934.
66. Takacs, L. M. Carey Lea, the Father of Mechanochemistry. *Bull. Hist. Chem.* **2003**, *28*, 26–34.
67. Clough, J. M.; Van Der Gucht, J.; Sijbesma, R. P. Mechanoluminescent Imaging of Osmotic Stress-Induced Damage in a Glassy Polymer Network. *Macromolecules* **2017**, *50*, 2043–2053.
68. Lee, C. K.; Diesendruck, C. E.; Lu, E.; Pickett, A. N.; May, P. A.; Moore, J. S.; Braun, P. V. Solvent Swelling Activation of a Mechanophore in a Polymer Network. *Macromolecules* **2014**, *47*, 2690–2694.
69. Imato, K.; Irie, A.; Kosuge, T.; Ohishi, T.; Nishihara, M.; Takahara, A.; Otsuka, H. Mechanophores with a Reversible Radical System and Freezing-Induced Mechanochemistry in Polymer Solutions and Gels. *Angew. Chemie - Int. Ed.* **2015**, *54*, 6168–6172.
70. Lenhardt, J. M.; Black, A. L.; Beiermann, B. A.; Steinberg, B. D.; Rahman, F.; Samborski, T.; Elsakr, J.; Moore, J. S.; Sottos, N. R.; Craig, S. L. Characterizing the Mechanochemically Active Domains in Gem-Dihalocyclopropanated Polybutadiene under Compression and Tension. *J. Mater. Chem.* **2011**, *21*, 8454–8459.
71. Davis, C. S.; Rencheck, M. L.; Woodcock, J. W.; Beams, R.; Wang, M.; Stranick, S.; Forster, A. M.; Gilman, J. W. Activation of Mechanophores in a Thermoset Matrix by Instrumented Scratch. *ACS Appl. Mater. Interfaces* **2021**, *13*, 55498–55506.

Chapter 2

Synthesis of a covalent and a supramolecular mechanophore and their incorporation in polymers

| ABSTRACT |

Two new mechanophores and polymer matrices were synthesized and characterized. A supramolecular mechanophore was developed based on complexes of a pyrene derivative which changes emission upon aggregation. Emission of aggregates and unassociated chromophore is quenched by the formation of ion-paired complexes with pyridinium derivatives. A thermoplastic polyurethane was synthesized as a polymer matrix for this supramolecular mechanophore. A covalent mechanophore based on a π -extended anthracene-maleimide Diels-Alder adduct was also synthesized. Here a non fluorescent Diels-Alder diol was synthesized for incorporation in a polycarbonate polymer matrix. A detailed study on the solution transcarbonation reaction to synthesize high molar mass polycarbonate is reported.

Part of the work in this chapter was published in:

Annelore Aerts, Camiel C.E. Kroonen, Jan Henk Kamps, Rint P. Sijbesma, Johan P. A. Heuts; *High Molar Mass Polycarbonate via Dynamic Solution Transcarbonation Using Bis(methyl salicyl) Carbonate, an Activated Carbonate*. *Macromolecular Chemistry and Physics* 2021. 222, 2100186.

2.1 INTRODUCTION

The challenge of understanding the relationship between the macroscopic properties of the material and its chemical structure is one of the main incentives for the development of new mechanophores.^{1,2} Since mechanopores are a specific type of stimuli responsive elements in a polymer that respond to mechanical force, they are the perfect tool to investigate the effect of these forces at the molecular level.^{3,4} Mechanophores can transduce the macroscopically applied force into a physical or chemical change. When activated, mechanochromophores⁵ and mechanoluminophores⁶ both change the optical properties of a material; a color change is induced by the former, whereas the latter results in a change in emission. Mechanochromophores have been extensively investigated in various polymers since a color change is an easily observed signal for detection of stresses or molecular scale damage in polymer materials.^{5,7-9} However, the limited sensitivity of a colorimetric response is a serious drawback of mechanochromophores.¹⁰ Mechanoluminophores provide a more sensitive alternative because they can report stresses in materials at low mechanophore concentrations, even allowing the detection of scission of a single bond.¹¹

There are two classes of luminophores: covalent and supramolecular luminophores. Most mechanophores rely on the rupture of a covalent bond, often a cyclo-elimination reaction of a fluorescent moiety. Anthracene based Diels-Alder adducts are by far the most studied mechanofluorescent systems in polymers. Both the anthracene dimer,¹² and maleimide Diels-Alder adducts^{13,14} have been used as mechanophores in polymer materials. Especially π-extended anthracene derivates offer a more sensitive and more quantitative determination of the bond scission than anthracene itself, and such derivatives will be described in more detail in this thesis. The scission of covalent bonds has a significant activation energy, and hence covalent mechanochemistry is limited for detection of small forces. Supramolecular interactions are weaker and thus dissociation of supramolecular mechanophores requires lower energies which makes them applicable to study the effects of smaller forces. The choice of mechanophores has recently been expanded with supramolecular systems such as host-guest complexes, metal complexes, and rotaxanes.¹⁵⁻¹⁸ Another class of supramolecular mechanophores are charge transfer complexes that are based on π-π interactions.^{19,20} A useful supramolecular mechanophore is a CT complex between pyranine and naphthalenebisimide as part of a polycaprolactone polymer, reported by Imato and coworkers.¹⁹ This complex dissociates when a force is applied to the polymer, but activation is irreversible due to the plastic deformation of the matrix. In this thesis pyranine will be synthesized and characterized

for its mechanophore properties in combination with two quenchers: pyridinium and bipyridinium.

Mechanophores must be incorporated into a polymer chain to enhance force transduction towards the mechanophore. Mechanophore studies have extensively been done in polymer networks and in particular in poly(methyl methacrylate) (PMMA) and poly(methyl acrylate) (PMA) networks.^{6,21-24} In these materials, the mechanophore is built into the chain as a cross-linker. Another approach is to build the mechanophore into a linear polymer chain and this has been mainly done in soft polymers such as polycaprolactone, PMA and polyurethanes.²⁵⁻²⁹ Polyurethanes are commercially important as thermoplastic elastomers and are attractive polymer matrices for mechanochemical study because they are usually transparent and their mechanical properties are highly tunable. Extending mechanophores studies to glassy polymers remains a challenge as brittle failure often occurs before the mechanophore is activated. Despite these intrinsic difficulties with using mechanophores in the glassy state, visualization of stress in polycarbonate, a commercially important glassy polymer, is desirable.

In this chapter a detailed description is given of the synthesis of the mechanophore precursors used for this thesis: a covalent mechanophore based on a π -extended anthracene-maleimide Diels-Alder adduct and a supramolecular mechanophore based on ground-state aggregation. Additionally, the synthesis and characterization of both an elastic polyurethane matrix and a glassy polycarbonate matrix is presented.

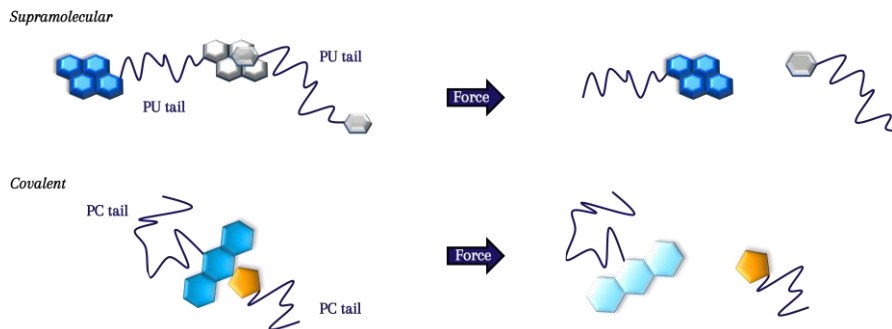
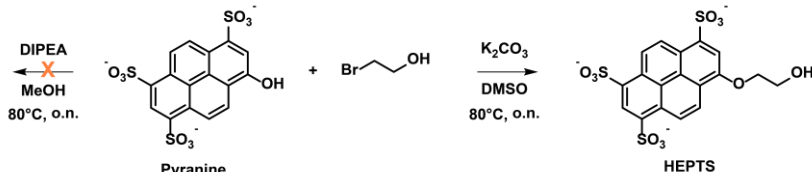


Figure 2.1. Schematic representation of the supramolecular mechanophore in a polyurethane and the π -extended anthracene-maleimide Diels-Alder adduct in a polycarbonate chain.

2.2 SUPRAMOLECULAR MECHANOPHORE

Since phenolic carbamates are not very stable, it is important to first derivatize pyranine with an aliphatic -OH group, which was done with a 2-hydroxylethyl functionality resulting in HEPTS (**Scheme 2.1**).



Scheme 2.1. Synthetic scheme towards the formation of HEPTS.

Since the commercial pyranine starting material contained an impurity, it was purified by precipitation in isopropyl alcohol yielding a bright yellow powder. A first attempt to alkylate the pyranine with a procedure adapted from the literature,³⁰ using N,N-diisopropylethylamine as a base and methanol as a solvent did not give the desired product. When the base was changed to potassium carbonate and the solvent was changed to DMSO, the reaction resulted in 100% conversion of the starting material and formation of the desired product together with some small impurities. Purification of HEPTS required several attempts. Hydrophilic Interaction Liquid Chromatography (HILIC, acetonitrile/water 95/5), reversed-phase chromatography (acetonitrile/water 50/50), ion-exchange chromatography (Amberlite ir-120, tetrabutylammonium) and gel filtration chromatography (Sephadex G-10) did not result in pure HEPTS. Precipitation in isopropanol and drying under vacuum at 150 °C yielded in the desired product as a bright yellow solid.

Pyranine is a fluorescent dye which emits yellow fluorescence in aqueous media when excited at 385 nm or 405 nm. After alkylation, a hypsochromic shift in the emission spectrum and an increase in fluorescence intensity were observed (**Figure 2.2a**). The large Stokes shift in the fluorescence spectrum of pyranine is a consequence of an excited state proton transfer, which is a well-known phenomenon for aromatic photoacids.³¹ The weaker fluorescence emission of pyranine in water is the result of the excited state proton transfer and the formation of hydrogen bonds to the solvent (**Figure 2.2b**).^{32,33} The -OH group of excited state pyranine is a very strong proton donor and has the ability to form strong hydrogen bonds with the solvent, while for the alkylated HEPTS this is not the case

Figure 2.2c). Hence the fluorescence emission appears at lower wavelengths with higher intensity.

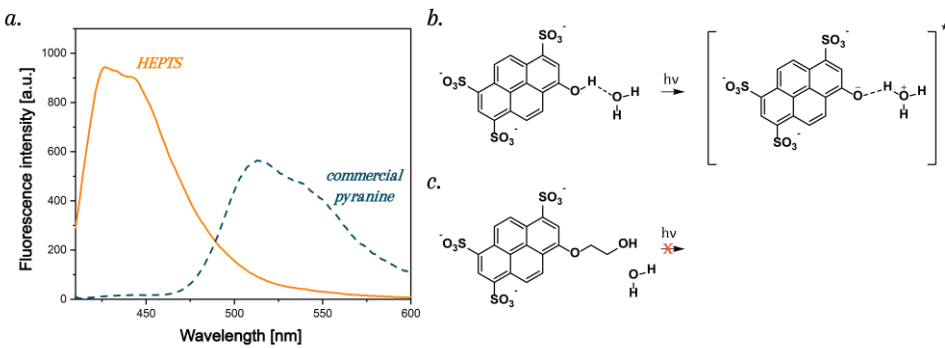


Figure 2.2. a) Normalized fluorescence spectra and pictures of $3 \mu\text{M}$ HEPTS (solid curve) and $3 \mu\text{M}$ pyranine (dashed curve) in water. b) A schematic representation of the quenching mechanism of pyranine by water. The protonated ground state of pyranine forms hydrogen bonds with surrounding water molecules and upon excitation proton transfer will take place. c) functionalization of the phenol inhibits these quenching mechanisms.

Pyranine fluorescence is quenched by pyridinium salts by formation of ground state complexes as shown by Rosenbluth and coworkers.³⁴ In this thesis two different quenchers, Q1 and Q2 (Figure 2.3), were synthesized and they are extensively studied as quenchers in Chapter 4.

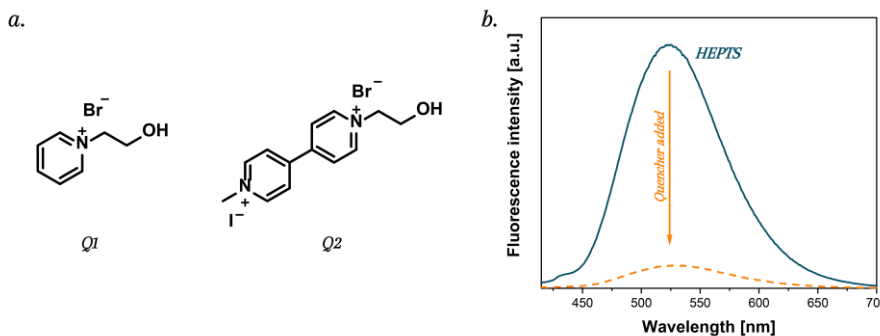
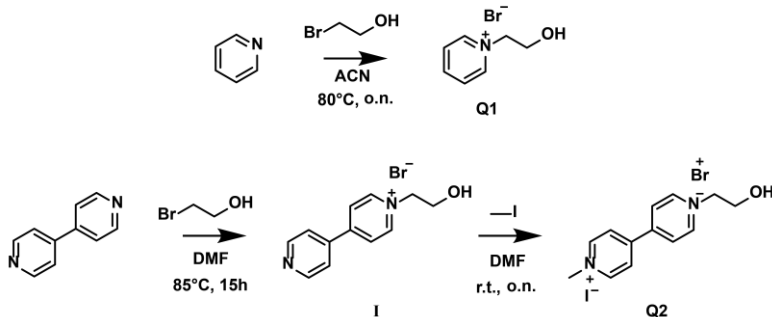


Figure 2.3. a) Schematic overview of the synthesized quenchers Q1 and Q2. b) Illustration of the effect of adding a quencher to HEPTS

Quencher Q1 was synthesized from pyridine and 2-bromoethanol in acetonitrile (Scheme 2.2). The mixture was left stirring overnight at 80°C and white crystals were formed after cooling to room temperature. Recrystallization of the crystals from isopropyl

alcohol resulted in the desired product Q1. Since these pyridinium based compounds are ionic liquids, they tend to form strong hydrogen bonds to for example water, which could interfere with further functionalization. Therefore the products were stored under argon in the freezer to protect them from moisture.



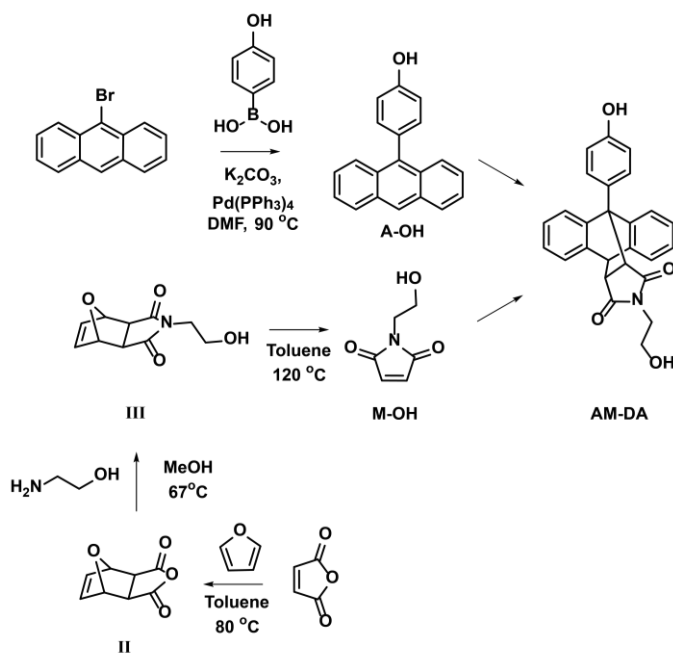
Scheme 2.2. Schematic overview of the synthetic procedure for both quenchers Q1 and Q2.

Quencher Q2 was synthesized according to a procedure reported by Fendler and coworkers (**Scheme 2.2**).³⁵ 4,4'-Bipyridyl was first alkylated on one of the nitrogen atoms with 2-bromoethanol after which the second nitrogen was methylated. The first reaction was performed in DMF at 85 °C overnight and evaporation of the solvent resulted in an off-white solid containing starting material, intermediate **I** (**Scheme 2.3**) and the dialkylated bipyridinium as a side product. The product was washed with DMF followed by a diethylether wash to remove bisalkylated pyridinium and the starting materials, respectively. After filtration, the alkylated bipyridinium (**I**) was collected as an off-white solid which was then methylated at room temperature in DMF using iodomethane. Precipitation in diethyl ether resulted in the desired bright orange quencher Q2 in 28% overall yield.

2.3 COVALENT MECHANOPHORE

A novel mechanophore based on 9- π -extended anthracene was synthesized in the form of its corresponding 9,10-maleimide Diels-Alder adduct. The synthetic pathway towards the mechanophore started with a palladium catalyzed Suzuki coupling of 4-hydroxyphenylboronic acid and 9-bromoanthracene in DMF. Purification by column chromatography yielded the desired 9- π -extended anthracene (A-OH) which was the first precursor of the final anthracene-maleimide Diels-Alder adduct.

In parallel, the synthesis of the N-(2-hydroxyethyl)maleimide precursor was started with the protection of maleic anhydride by a Diels-Alder reaction with furan since the high reactivity of the double bond can provoke unwanted side reactions. With the anhydride protected (**II**), amidation of the succinic anhydride derivate was performed by reaction with amino ethanol. Heating of compound **III** in toluene initiated a retro Diels-Alder reaction resulting in the release of furan to form the unprotected N-(2-hydroxyethyl)maleimide precursor (M-OH) for the final AM-DA. When both precursors M-OH and A-OH were obtained with high purity, the Diels-Alder reaction was performed in a solvent mixture of isopropyl alcohol and toluene. The solution was left to react for two days and the solvent was evaporated. Due to the low solubility of the product, a solid loaded column chromatography was performed to purify the final AM-DA adduct. The use of the off-white product (AM-DA) as chain extender to couple BPA-polycarbonate prepolymers is described in *Chapter 4*.

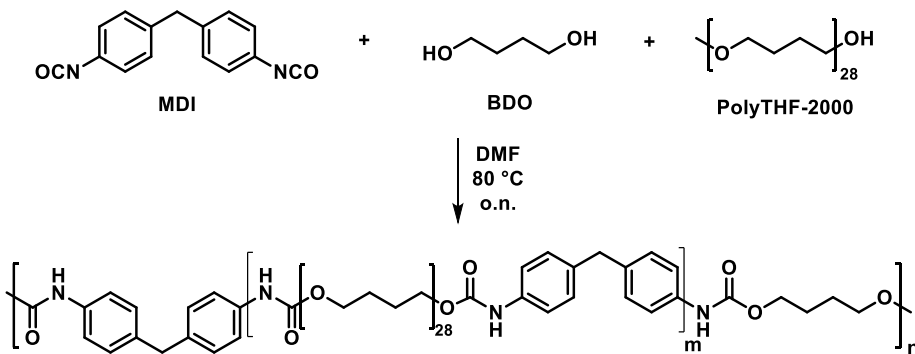


Scheme 2.3. Synthetic pathway towards the π -extended anthracene-maleimide Diels-Alder adduct (AM-DA).

2.4 POLYMERIC PROBES

Thermoplastic polyurethane as an elastic polymer matrix

Thermoplastic polyurethanes based on polyTHF, 4,4'-methylene diphenyl diisocyanate (MDI) and 1,4-butane diol (BDO) were synthesized in a one-pot solution polymerization to facilitate their end-group functionalization with the pyranine or pyridinium mechanophore precursor (**Scheme 2.5**). During several attempts to synthesize well-defined prepolymers of polyTHF and MDI, or MDI-BDO-MDI hard blocks for further extension into a polymer, gelation always occurred. The gelation was a consequence of chemical cross-linking resulting in an insoluble polyurethane network. However, a one-pot reaction with pTHF, BDO and MDI as monomers in a ratio of 0.75 : 1.25 : 2 and dibutyltin dilaurate (DBTDL) as catalyst resulted in the formation of thermoplastic polyurethane with an acceptable molar mass of $85 \cdot 10^3 \text{ g} \cdot \text{mol}^{-1}$.



Scheme 2.5. Synthetic route for the synthesis of MDI based thermoplastic polyurethanes.

Disappearance of the isocyanate groups was monitored with infrared spectroscopy during reaction, and size exclusion chromatography was used to determine the molecular weight. After two hours all isocyanate groups had reacted according to IR (**Figure 2.4a**), but the reaction mixture was left overnight to ensure maximal incorporation of the isocyanates. The polyurethane was quenched with methanol and a molar mass of $M_n = 85 \cdot 10^3 \text{ g} \cdot \text{mol}^{-1}$ was reached after precipitation.

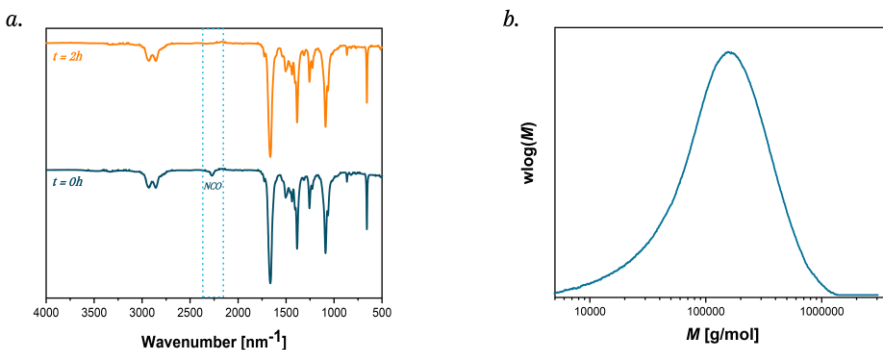
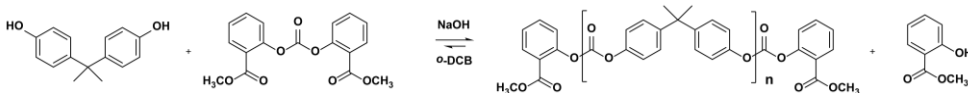


Figure 2.4. a) Infrared spectroscopy showing that the isocyanates react away over time. b) Molecular weight diagram for the final polyurethane synthesized via a one-pot synthesis.

Polycarbonate as a glassy polymer matrix

Due to the thermal stability of the AM-DA, which undergoes a retro Diels-Alder reaction at high temperatures, a low-temperature synthetic approach for aromatic polycarbonates was required. Recently, Kamps *et al.* reported the solution transcarbonation reaction between bisphenol-A (BPA) and activated carbonates.³⁶ Solution transcarbonation with bis(methyl salicyl) carbonate (BMSC) as the carbonate donor was further investigated and high molecular weight aromatic polycarbonates were obtained at temperatures between 60 °C and 120 °C.



Scheme 2.6. Synthesis of BPA-polycarbonate via solution polymerization of BPA and BMSC.

Polymerizations were performed in dried *ortho*-dichlorobenzene (*o*-DCB) and in a closed system; no condensate was removed during the reaction. Further investigation of the kinetics and thermodynamics of this polymerization was performed by determining molar mass distributions with SEC at regular time intervals. The absolute weight-average molar masses, M_w , estimated via the Mark-Houwink parameters are plotted in Figure 2.5a. It is clear from the data in Figure 2.5a that the polymerization rate increases with increasing temperature, but that the maximum achievable M_w decreases. Furthermore, equilibrium constants were determined based on the experimental data (Table 2.1). Details for the determination of the rate constants and equilibrium constants are described in a separate section below (Appendix).

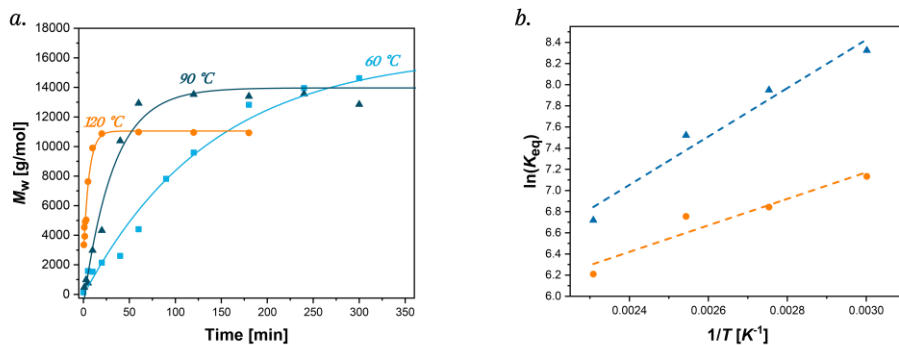


Figure 2.5. a) Weight-average molar masses as a function of time for the solution polymerization of BPA with BMSC in *o*-DCB at 120 °C (●), 90 °C (▲) and 60 °C (■). The curves are a guide to the eye. Experimental conditions as listed in **Table 2.3**, experiments A-C. b) Van 't Hoff plot for the solution transcarbonation of BMSC with BPA in *o*-DCB for $\ln(K_{eq})$ determined using (●) $x_n = M_n/127$ and (▲) $x_n = M_w/254$.

Table 2.1. Summary of temperature-dependent polymerization equilibrium data.

Temperature (°C)	M_w^a (g·mol ⁻¹)	D^b	x_n^c	p^d	K_{eq}^e
60	$16 \cdot 10^3$	3.5	62	0.989	$4.1 \cdot 10^3$
90	$13 \cdot 10^3$	3.4	53	0.986	$2.8 \cdot 10^3$
120	$11 \cdot 10^3$	2.9	43	0.981	$1.8 \cdot 10^3$
160 ^f	$7 \cdot 10^3$	2.6	29	0.972	$0.8 \cdot 10^3$

^a Weight-average molar mass as determined by SEC, ^b $D \equiv M_w/M_n$ as determined by SEC, ^c Number-average degree of polymerization estimated from M_w : $x_n \approx M_w/(2 \cdot 127)$ (see SI for details), ^d Functional group conversion determined via **Equation 2.6**, using r from **Table 2.3**, ^e Equilibrium constant determined via **Equation 2.7**, ^f Data taken from experiment E in **Table 2.3**, all other data from the kinetic experiments shown in **Figure 2.5a** (A-C, **Table 2.3**).

The values of the equilibrium constants were much larger than what is commonly reported for polyesters ($K_{eq} \approx 1$) and polyamides ($K_{eq} \approx 10^2 - 10^3$).³⁷ These high equilibrium constants are explained by the fact that the methyl salicylate condensation product is stabilized by a strong intramolecular hydrogen bond.³⁸ Furthermore, the equilibrium constant decreases with increasing temperature, which is in line with reports in the literature for other systems. The temperature dependence of K_{eq} is most clearly seen in a so-called Van 't Hoff-plot, which is shown in **Figure 2.5b** and allows for the estimation of the standard enthalpy (ΔH^0) and entropy (ΔS^0) of polymerization:

$$\ln K_{\text{eq}} = -\frac{\Delta H^0}{RT} + \frac{\Delta S^0}{R} \quad \text{Eq. 2.1}$$

The linear fits of the two data sets (with K_{eq} based on $x_n = M_w/254$ and $x_n = M_n/127$) lead to slightly different values for ΔH^0 and ΔS^0 . The use of $x_n = M_w/254$ leads to $\Delta H^0 = -19 \text{ kJ}\cdot\text{mol}^{-1}$ and $\Delta S^0 = 13 \text{ J}\cdot\text{mol}^{-1}\cdot\text{K}^{-1}$, whereas the use of $x_n = M_n/127$ results in $\Delta H^0 = -11 \text{ kJ}\cdot\text{mol}^{-1}$ and $\Delta S^0 = 28 \text{ J}\cdot\text{mol}^{-1}\cdot\text{K}^{-1}$. The real values are expected to lie within these ranges. In order to confirm that indeed the polymerization equilibrium was obtained and to establish whether the system is truly reversible, a series of experiments was carried out in which the temperature was varied in a cyclic fashion (experiments D-F in **Table 2.3**). When equilibrium was achieved, a sample was taken and quenched in cold tetrahydrofuran (THF) before determination of the molar mass distribution by SEC.

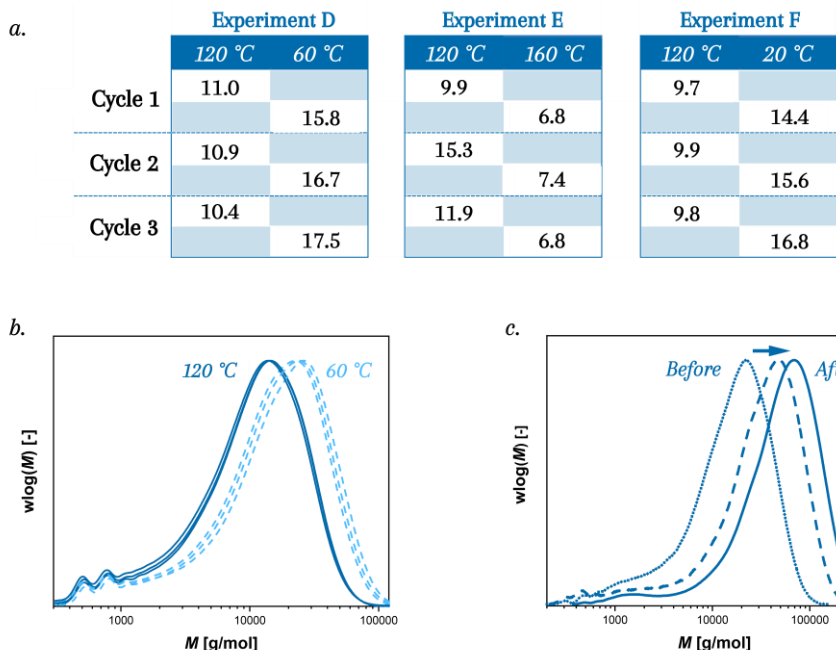


Figure 2.6. a) Overview of the obtained molar masses (in $10^3 \text{ g}\cdot\text{mol}^{-1}$) for the reversibility experiments (experiment D-F, **Table 2.3**). b) Equilibrium molar mass distributions obtained in the temperature cycling experiments between 60 °C and 120 °C with $[BMSC]_0 = 0.30 \text{ M}$ (experiment D, **Table 2.3**). c) Molar mass distributions of polycarbonate synthesized in an equilibrium polymerization at 60 °C before removal of methyl salicylate ($M_w = 16 \cdot 10^3 \text{ g}\cdot\text{mol}^{-1}$, dotted line) and after removal of methyl salicylate and subsequent polymerization at 120 °C: once ($M_w = 46 \cdot 10^3 \text{ g}\cdot\text{mol}^{-1}$, dashed line) and twice ($M_w = 67 \cdot 10^3 \text{ g}\cdot\text{mol}^{-1}$ solid line).

At 120 °C the system was left to react for 2 hours to make sure that the equilibrium weight-average molar mass ($M_{w,eq}$) was reached after which the reaction mixture was slowly cooled to 60 °C and left overnight. This resulted in an increase in $M_{w,eq}$ from $11 \cdot 10^3$ g·mol⁻¹ at 120 °C to $16 \cdot 10^3$ g·mol⁻¹ at 60 °C. This experiment was performed in three cycles in a closed system and without removal of methyl salicylate. Results of the experiments are summarized in **Figure 2.6a**, clearly showing the reversibility of the equilibrium polymerization process. The molar mass distributions for the experiment in which the temperature was cyclically varied between 120 °C and 60 °C are shown in **Figure 2.6b**. The molar mass distributions are the same for every cycle at 120 °C, whereas the distributions of the polymers at 60°C slightly vary. These small differences are attributed to the lower solubility of the high molar mass polycarbonate in *o*-DCB at 60 °C.

The same experiment was also performed between 120 °C and room temperature (**Figure 2.6a**, experiment F) and here a variation at low temperatures was observed because of the low solubility of the polymer. Increasing the temperature to 160 °C results in a decrease in molecular weight. Due to the high solubility at higher temperatures, there is no difference in the molecular mass determined at the same temperature in consecutive cycles.

Because the equilibrium molar masses obtained in these experiments are somewhat lower than molar masses typically found in commercial polycarbonates ($M_w \approx 17 \cdot 10^3$ g·mol⁻¹ for optical quality Lexan™ resin³⁹), attempts were made to increase the molar mass of the polycarbonate by removing methyl salicylate from the reaction mixture. Starting from a polycarbonate synthesized at 60 °C ($M_w \approx 16 \cdot 10^3$ g·mol⁻¹), methyl salicylate was removed by precipitation in hexane (1:15 v/v) and the polymerization was continued at 120 °C due to the lower polymer solubility at 60 °C. In this step M_w increased to $46 \cdot 10^3$ g·mol⁻¹ and after repeating the removal of methyl salicylate and heating at 120 °C for 2 h, a molar mass (M_w) of $67 \cdot 10^3$ g·mol⁻¹ (**Figure 2.6c**) was obtained, very close to the theoretical maximum of $70 \cdot 10^3$ g·mol⁻¹ calculated from the Carothers equation for $p = 1$ and $r = 0.9929$, the stoichiometric balance used in the experiments. This illustrates the favorable equilibrium conditions for this system even at 120 °C.

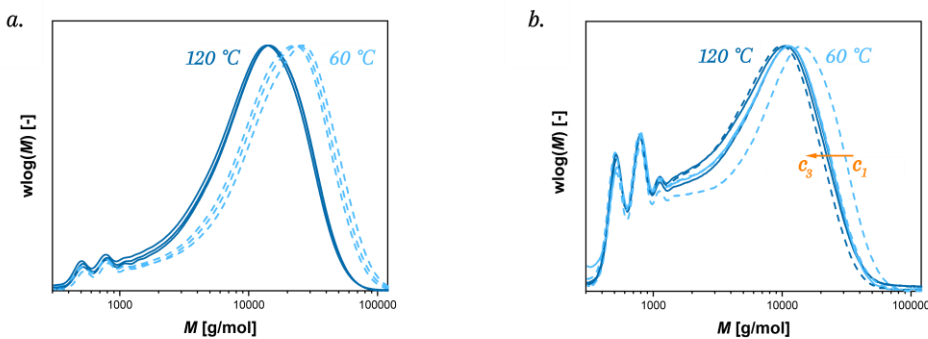


Figure 2.7. Molar mass distribution for the reversibility experiments at $[BMSC]_0 =$ a) 0.30 M (**Table 2.3**, experiment D) and b) 0.07 M (**Table 2.3**, experiment G). More cyclic species were observed for the lowest concentration, resulting in a lower reversibility. In the first cycle (c₁) a higher molar mass was observed at 60°C , while in the last cycle (c₃) the molar mass remained more or less the same at 120°C and 60°C .

Although the polymerizations at lower temperatures reach higher molar masses, further increase in M_w is limited by the solubility of the polymers. In order to increase the solubility, polymerizations were carried out at lower starting concentrations of BMSC (*i.e.*, $[BMSC]_0 = 0.30 \text{ M}$ and 0.07 M) while the ratios of monomers and catalysts were kept the same. Lowering the starting concentration resulted in a significant change in the molar mass distribution at lower molecular weights; the obtained molar mass distributions are shown in **Figure 2.7**. Since at lower concentrations the chance of a reactive end group finding another chain or monomer decreases, the probability for cyclization increases and this seems to be the case here. Experiments at lower concentrations were performed by cyclic heating between 120°C and 60°C . The reactions at lower concentrations are less reversible, as the maximum attainable M_w at 60°C decreases in every cycle. This is also consistent with the presence of cyclized species, which are not able to participate further in chain extensions.

As a final confirmation that the system is an equilibrium polymerization which can be described by an ideal polycondensation mechanism, we studied the effect of the stoichiometric imbalance r at 60°C and 120°C . In addition to the cases in which $r = 0.99$, we studied $r = 0.95$ and $r = 0.98$. The equilibrium molar masses of these three stoichiometric ratios at 60°C and 120°C are shown in **Figure 2.8**. It is clear from these results that the molar mass distributions show the generally expected shift to higher masses for increasing r . Additionally, experimentally obtained M_w (**Table 2.2**) were in good

agreement with the values calculated for the corresponding stoichiometric ratios and using the equilibrium constants from **Table 2.1**.

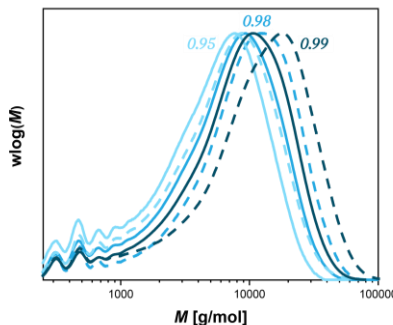


Figure 2.8: Effect of a stoichiometric imbalance of 0.95, 0.98 and 0.99 on the molar mass distribution at 120 °C (solid line) and 60 °C (dashed line) (**Table 2.3**, D, J and K). A higher stoichiometric ratio results in higher molar masses.

Table 2.2. Summary of experimental and predicted molar masses for different stoichiometric ratios and temperatures.

T (°C)	r^a	Experimental		Predicted
		M_w (g·mol ⁻¹)	\bar{D}	M_w (g·mol ⁻¹) ^b
60	0.95	$8.5 \cdot 10^3$	2.9	$8.5 \cdot 10^3$
60	0.98	$12 \cdot 10^3$	3.0	$14 \cdot 10^3$
60 ^c	0.99	$16 \cdot 10^3$	3.5	$16 \cdot 10^3$
120	0.95	$6.7 \cdot 10^3$	3.0	$7.4 \cdot 10^3$
120	0.98	$9.0 \cdot 10^3$	3.0	$10 \cdot 10^3$
120 ^c	0.99	$11 \cdot 10^3$	2.9	$11 \cdot 10^3$

^a Stoichiometric ratio $r = [\text{OH}]_0/[\phi]_0$; ^b Weight-average molar mass as predicted based on K_{eq} obtained from the kinetic experiments (**Table 2.1**); ^c Entries taken from **Table 2.1**, corresponding to the data used to determine K_{eq} .

2.5 CONCLUSIONS

In conclusion, two new mechanophores were synthesized. The synthesis and purification of the pyranine fluorescer was rather challenging, partly because of its low solubility. The synthesis of the pyridinium quenchers was more straightforward and resulted in two pure pyridinium derived quenchers synthesized in moderate yields. Both the fluorescer and the quencher can be used as end-capper of polyurethanes. Synthesis of predefined polyurethanes in solution resulted in gelation and hence an alternative solution-based one-pot synthesis for relatively high molecular weight polyurethanes was developed.

In addition, a covalent mechanophore based on a π -extended anthracene-maleimide Diel-Alder adduct was synthesized. Both precursors, M-OH and A-OH, were obtained via a multi-step synthesis with high purity and in moderate yields. The AM-DA can later be used as a chain coupling agent for incorporation in polycarbonate. A solution transcarbonation polymerization was used to synthesize high molar mass BPA-based polycarbonates. Both the polymerization rate and the degree of polymerization were temperature dependent and high molar masses could be reached at 60 °C without removal of the condensate. The system was completely reversible and produced the theoretical molecular masses predicted in absence of the formation of cyclic products.

Appendix: Determination of the rate constants and equilibrium constants

Assuming a negligible contribution from the reverse reaction on the initial rates and any chain length dependence of the kinetics, the bimolecular rate coefficients, k , for the forward reaction in **Scheme 2.6** and as defined in **Equation 2.2**, were estimated from the data shown in **Figure 2.5a**.

$$-\frac{d[OH]}{dt} = k[OH][\phi] \quad \text{Eq. 2.2}$$

In this equation, $[OH]$ and $[\phi]$ denote the concentrations of hydroxyl and methyl salicylate end groups, respectively. Defining the conversion, p , as

$$p = \frac{[OH]_0 - [OH]}{[OH]_0} \quad \text{Eq. 2.3}$$

and the stoichiometric imbalance, r , as

$$r = \frac{[OH]_0}{[\phi]_0} \quad \text{Eq. 2.4}$$

where the subscript "0" refers to the initial conditions, the following equation can be derived and used to evaluate the rate coefficients:

$$\ln \left\{ \frac{(1 - rp)}{1 - p} \right\} = k([[\phi]_0 - [OH]_0)t \quad \text{Eq. 2.5}$$

The conversions, p , in Equation 2.5, are obtained from the number-average degree of polymerization, x_n , data via Equation 2.6, which is obtained from a rearrangement of the general Carothers equation.

$$p = \frac{(r + 1)(x_n - 1)}{2rx_n} \quad \text{Eq. 2.6}$$

Analysis of the data using Equation 4 yields the following estimates for k : $k \approx 3, 30$ and $80 \text{ L}\cdot\text{mol}^{-1}\cdot\text{s}^{-1}$ at 60°C , 90°C and 120°C , respectively. Hence, the reaction rate at 120°C is about 20 - 30 times faster than at 60°C . A note should be made here that an exact determination for x_n is difficult because of the inherent experimental uncertainties in determining the low M side of the molar mass distribution by SEC. Therefore, we estimated x_n as $M_n/127$ and as $M_w/254$ (assuming a theoretical dispersity, D , of 2 and ignoring the masses of the end-groups); the differences in the obtained values for k using these two approaches were small.

The second important observation in **Figure 2.5a** is that a temperature-dependent maximum M_w is obtained. This observation is not surprising when considering that methyl salicylate, the condensate, was not removed from the reaction and the reaction was expected to stop when equilibrium was reached. The obtained data now enable us to estimate the equilibrium constants, K_{eq} , for this polymerization via **Equation 2.7** which are shown in **Table 2.1**.

$$K_{eq} = \frac{p^2}{(1 - p)(r^{-1} - p)} \quad \text{Eq. 2.7}$$

2.6 EXPERIMENTAL DETAILS

DMSO, DMF and *o*-DCB was dried and stored over molecular sieves for a minimum time of 12 hours prior to use. Deuterated solvents were purchased from Cambridge Isotope Laboratories and stored over 4 Å molecular sieves. Bis(methyl salicyl) carbonate (BMSC, SABIC, 99+ %), bisphenol-A (BPA, SABIC, polymerization grade, > 99%) were kindly provided by SABIC. All other chemicals used were purchased from Sigma Aldrich, TCI, Merck, Cambridge Isotopes Laboratories or Biosolve and used as received unless stated otherwise. Trisodium 8-hydroxypyrene-1,3,6-trisulfonate and potassium carbonate were dried at 80 °C under vacuum overnight. Reactions performed under argon atmosphere were performed in dried glassware and degassed by three purge-and-refill cycles.

Fluorescence emission spectra in solution were acquired using JASCO spectrofluorometer. All experiments were performed at room temperature in a 10x10 mm quartz cuvette (3500 µL chamber volume, Hellma). The fluorescence spectra were recorded with an excitation wavelength of 385 nm between 415–650 nm. Excitation and emission monochromator slits were positioned at 3 nm and measured with 50 nm/min scan speed.

NMR spectra were recorded on a 400 MHz Bruker Avance III spectrometer at room temperature in DMSO-d6 with TMS as internal standard unless stated otherwise. Analysis of the NMR spectra was performed with MestreNova v12.0.4-22023, Mestrelab Research S.I and TopSpin 3.5 pl 5, Copyright© 2016, Bruker BioSpin GmbH.

MALDI-TOF was measured on a Bruker Autoflex Speed MALDI-MS instrument using an α-cyano-4-hydroxycinnamic acid (CHCA) matrix and calibrated with reference list based on cesium triiodide (positive mode). The spectra were obtained from 500 shots and interpreted with Bruker Daltonics flexAnalysis.

Size exclusion chromatography (SEC) was performed in tetrahydrofuran (THF) at 25 °C on a Shimadzu Prominence-I LC-2030C 3D equipped with a RID-20A detector and calibrated by narrow polystyrene standards for the polycarbonate samples and the polyurethanes were measured in DMF with LiBr as a flow marker on a Shimadzu equipped with an RID detector and calibrated with narrow PMMA standards. The following Mark-Houwink-Sakurada parameters were used to convert the polystyrene (PS) masses into polycarbonate (PC) masses: K_{PS} = 1.41 10-4 dL g⁻¹, a_{PS} = 0.70, K_{PC} = 4.12 10 4 dL g⁻¹, a_{PC} = 0.69. The reported molecular weight for the polyurethanes are according to PMMA standards.

Mechanophores synthesis

Purification of commercially purchased pyranine (trisodium 8-hydroxypyrene-1,3,6-trisulfonate): Pyranine (4.50 g, 8.5 mmol) was dissolved in 20 mL water and added dropwise to a beaker with stirring 300 mL cold isopropanol in small aliquots. The resulting yellow suspension was left stirring for 1 hour and then centrifuged (2500 rpm, 3min). The transparent supernatant was discarded, and the yellow pellet was dried under high vacuum yielding a bright yellow solid (96% yield).

¹H-NMR (400 MHz, DMSO-*d*6): δ (ppm) = 10.64 (s, 1H), 9.02 (d, *J* = 9.6 Hz, 1H), 8.98 (t, *J* = 4.9 Hz, 2H), 8.87 (d, *J* = 9.8 Hz, 1H), 8.30 (d, *J* = 9.6 Hz, 1H), 8.16 (s, 1H).

8-(2-hydroxyethoxy)pyrene-1,3,6-trisulfonate: A 250 mL Schlenk-flask was flame dried and charged with pyranine (1.5 g, 2.8 mmol) followed by K₂CO₃ (1.19 g, 8.6 mmol). After degassing the flask, 40 mL DMSO and 2-bromoethanol (1.45 g, 11.4 mmol) were added. The obtained brown reaction mixture was allowed to react at 80 °C under argon atmosphere overnight. Afterwards, the mixture cooled down to room temperature and precipitated in 400 mL stirring cold isopropanol. After continuing stirring the suspension for 1 hour, the mixture was centrifuged (2500 rpm, 3 min) and the yellow pellet was isolated. The residue was dissolved in MeOH, transferred to a round-bottom flask and dried at reduced pressure. Additional drying in the oven at 150 °C under vacuum resulted a yellow powder (85% yield).

¹H-NMR (400 MHz, DMSO-*d*6): δ (ppm) = 9.11 (d, *J* = 9.6 Hz, 1H), 9.03 (m, 2H), 8.94 (d, *J* = 9.8 Hz, 1H), 8.45 (d, *J* = 9.6 Hz, 1H), 8.19 (s, 1H), 5.09 (t, *J* = 5.8 Hz, 1H), 4.36 (t, *J* = 4.9 Hz, 2H), 3.96 (q, *J* = 5.2 Hz, 2H).

¹³C-NMR (101 MHz, DMSO-*d*6): δ (ppm) = 152.12, 143.59, 140.11, 139.89, 128.55, 128.16, 126.83, 126.25, 125.93, 125.60, 124.95, 124.08, 121.10, 120.96, 120.27, 109.53, 71.30, 60.24.

1-(2-Hydroxyethyl)pyridinium Bromide: A 100 mL round-bottom flask was charged with pyridine (5.10 mL, 63.1 mmol) followed by the addition of 28 mL ACN. Then 2-bromoethanol (5.35 mL, 75.5 mmol) was added and the reaction mixture refluxed under argon atmosphere at 80 °C overnight. Afterwards, the reaction mixture cooled down to room temperature and white crystals were formed. The solvent was removed under reduced pressure at the rotary evaporator and the crude was recrystallized in isopropanol resulting in white crystals (56% yield). The product was stored under argon atmosphere at -17 °C to protect it from moisture.

¹H-NMR (400 MHz, DMSO-*d*6): δ(ppm) = 9.03 (d, *J* = 6.0 Hz, 2H), 8.63 (t, *J* = 7.8 Hz, 1H), 8.17 (t, *J* = 7.0 Hz, 2H), 5.25 (t, *J* = 5.3 Hz, 1H), 4.67 (t, *J* = 5.0 Hz, 2H), 3.86 (q, *J* = 5.1 Hz, 2H).
¹³C-NMR (101 MHz, DMSO-*d*6): δ(ppm) = 146.05, 145.66, 128.17, 63.44, 60.48.

Synthesis of 1-(2-hydroxyethyl)-[4,4'-bipyridin]-1-ium bromide (I): 4,4'-bipyridine (2.00 g, 12.81 mmol) was dissolved in 15 mL DMF in a round bottom flask. Then, 2-bromoethanol (0.80 g, 6.40 mmol) was added dropwise to the solution and the reaction mixture heated to 85 °C and left overnight. Afterwards, the reaction mixture was allowed to cool to room temperature and diethyl ether was added to precipitate the product. White crystals were formed and filtered off, washed with cold DMF to remove bisalkylated bipyridinium and finally washed with diethyl ether to remove the starting material. Afterwards the product was dried under vacuum at 60 °C (44% yield).

¹H-NMR (400 MHz, DMSO-*d*6) : δ(ppm) = 9.15 (d, *J* = 7.12 Hz, 2H), 8.88 (d, *J* = 5.7 Hz, 2H), 8.64 (d, *J* = 6.6 Hz, 2H), 8.04 (d, *J* = 5.7 Hz, 2H), 5.28 (t, *J* = 5.2 Hz, 1H), 4.70 (t, *J* = 4.8 Hz, 2H), 3.91 (q, *J* = 4.9 Hz, 2H).

1-(2-hydroxyethyl)-1'-methyl-[4,4'-bipyridine]-1,1'-diium bromide iodide (Q2): **I** (1.50 g, 7.4 mmol) was charged in a round bottom flask and 12 mL of DMF was added. Then, a large excess (8 mL, 120 mmol) of methyl iodide was added dropwise to the solution. The reaction mixture was stirred overnight at room temperature. A precipitate was formed and filtered off after the addition of diethyl ether. The obtained orange solid Q2 was dried under vacuum at 60 °C (80% yield).

¹H-NMR (400 MHz, DMSO-*d*6) : δ(ppm) = 9.30 (t, *J* = 5.8 Hz, 4H), 8.77 (t, *J* = 7.6 Hz, 4H), 5.32 (t, *J* = 5.8 Hz, 1H), 4.77 (t, *J* = 4.7 Hz, 2H), 4.45 (s, 3H), 3.93 (q, *J* = 4.8 Hz, 2H).

4,10-dioxatricyclo[5.2.1.0]dec-8-ene-3,5-dione (II): Maleic anhydride (50 g, 0.51 mol) and furan (55 mL, 1.5 eq.) were dissolved at elevated temperature in toluene. The solution was heated to 80 °C, and left to react overnight. The reaction mixture was left to cool to room temperature and the precipitate was isolated by filtration. The crystals were washed with diethyl ether and dried under vacuum at 40 °C. The final product was obtained as white crystals (76% yield).

¹H-NMR (400 MHz, CDCl₃) : δ(ppm) = 6.57 (s, 2H), 5.46 (s, 2H), 3.17 (s, 2H).

4-(2-Hydroxy-ethyl)-10-oxa-4-aza-tricyclo[5.2.1.0_{2,6}] dec-8-ene-3,5-dione (III): Compound **II** (55 g, 0.33 mol) and aminoethanol (23 mL, 1.2 eq.) were dissolved in methanol (400 mL) and heated to 67 °C. The mixture was reacted overnight, and solvents were evaporated. The crude product was extracted with water and CHCl₃. The organic layer was dried and the product was obtained as a white solid (65% yield).

¹H-NMR (400 MHz, CDCl₃): δ(ppm) = 6.53 (s, 2H) 5.29 (s, 2H) 3.77 (t, 2H) 3.71 (t, J = 4 Hz, 2H) 2.90 (s, 2H).

¹³C-NMR (400 MHz, CDCl₃): δ(ppm) = 176.81, 136.52, 80.96, 60.11, 47.50, 41.71.

N-(2-Hydroxyethyl)maleimide (M-OH): Compound IV (8.0 g, 38.3 mmol) was charged in a 250 mL round bottom flask and dissolved in 80 mL toluene. After stirring the mixture for 28 hours the solvent was evaporated in vacuo. M-OH was obtained as off with crystals (quantitative yield).

¹H-NMR (400 mHz, CDCl₃): δ 6.75 (s, 2H), 3.80 (t, J = 5.2 Hz, 2H), 3.74 (t, J = 5.0 Hz, 2H).

¹³C-NMR (400 mHz, CDCl₃): δ 171.15, 134.26, 60.93, 40.70.

4-(anthracene-9-yl)phenol (A-OH): A 1L 3-neck round bottom flask was dried in the oven and equipped with a tap, septum and cap. 9-bromoanthracene (13.8 g, 53.7 mmol), 4-hydroxyphenylboronic acid (14.9 g, 108 mmol), K₂CO₃ (41.9 g, 303 mmol) and Pd(PPh₃)₄ (3.12 g, 2.7 mmol) were added and the flask was degassed three times. 500 mL of dry DMF was added via a canula after which the reaction mixture was heated to 90°C and reacted for 4 days while stirring under argon atmosphere. After the reaction the precipitate was separated via filtration. The crude product was obtained from the filtrate after evaporating the DMF in vacuo. The crude product was dissolved in CHCl₃ and washed two times with demineralized water and once with brine. Na₂SO₄ was used to remove water from the CHCl₃ fraction and after filtration the filtrate was dried in the rotary evaporator for removal of CHCl₃. The obtained solid was further purified by column chromatography (silica, 4:1 heptane : EtOAc (v/v) resulting in A-OH as a yellow solid (72% yield).

¹H-NMR (400 mHz, CDCl₃): δ 8.48 (s, 1H), 8.04 (d, J = 8.5 Hz, 2H), 7.71 (dd, J = 8.8, 1.0 Hz, 2H), 7.51 – 7.39 (m, 2H), 7.39 – 7.27 (m, 4H), 7.12 – 6.99 (m, 2H), 5.01 (s, 1H).

¹³C-NMR (400 mHz, CDCl₃): δ 155.00, 136.69, 132.52, 131.42, 131.04, 130.54, 128.35, 126.87, 126.43, 125.27, 125.08, 115.31.

Synthesis of Diels-alder diol: A-OH (4.219 g, 15.6 mmol, 1 eq) and M-OH(2.204 g, 15.6 mmol, 1eq) were added to a dried round bottom flask. The reactants were dissolved in a mix of 250 mL toluene and 160 mL isopropanol. The reaction mixture was heated to 100 °C and

reacted for 4 days under reflux while stirring. The solvent was removed by the rotary evaporator and an off-white solid was obtained. This crude product was further purified by washing with CHCl₃. After filtration the residue was isolated and dried in a vacuum oven. AM-OH was obtained as a solid powder (83% yield).

¹H-NMR (400 mHz, DMSO-*d*6): δ 9.58 (s, 1H), 7.83 (s, 1H), 7.51 (d, *J* = 6.9 Hz, 1H), 7.31 (d, *J* = 6.9 Hz, 1H), 7.24 – 6.86 (m, 8H), 6.31 (d, *J* = 7.6 Hz, 1H), 4.84 (d, *J* = 3.0 Hz, 1H), 4.58 (t, *J* = 5.8 Hz, 1H), 4.00 (d, *J* = 8.3 Hz, 1H), 3.28 (dd, *J* = 8.2, 3.0 Hz, 1H), 2.94 (t, *J* = 6.8 Hz, 2H), 2.54 (t, *J* = 8.0 Hz, 2H).

¹³C-NMR (400 mHz, DMSO-*d*6): δ 176.38, 175.56, 156.82, 146.10, 141.57, 141.18, 139.40, 133.37, 131.77, 126.94, 126.90, 126.55, 126.37, 125.99, 125.42, 125.22, 124.93, 123.90, 114.93, 56.83, 55.39, 48.93, 46.91, 45.59.

Polymer Synthesis

PU synthesis

Thermoplastic polyurethanes were synthesized in solution. All glassware was dried at 120 °C for 3 hours prior to use. polyTHF was dried for 3 hours under vacuum at 100 °C and DMF and butane diol were put on molsieves in dried flasks.

A Schlenk fles was equipped with a dried stirrer and charged with 15 g (10.0 mmol) of polyTHF-2000 g·mol⁻¹. 1.57 g (17.4 mmol) BDO was added to the polyTHF and both diols were dissolved into 110 mL dry DMF. The mixture was heated to 50 °C and stirred for 5 minutes to ensure homogeniization. Then 1 μ L of DBTDL was added as a catalyst and 5.03 g (27.6 mmol) MDI was added to the flask. The polymerization was left at 50 °C for 2 hours and then a small sample was taken to check IR after which the temperature was increased to 80 °C and left overnight. The polymer reaction mixture was quenched with methanol, precipitated in ether. A white solid material was obtained (23.7 g).

Polycarbonate synthesis

Details for all polymerizations are shown in **Table 2.3**. In most experiments ~ 2 g (8.9 mmol) BPA, ~ 3 g (9.0 mmol) BMSC and ~ 1 mg (0.02 mmol) NaOH were added to a flame dried three neck round bottom flask, equipped with a septum, reflux cooler, tap and stirring bar. This solid mixture was flushed with argon before the addition of ~10 - 40 mL *o*-DCB to the flask. The resulting reaction mixture was heated to the desired reaction temperature, under constant stirring and argon flow. When the reaction was finished, the reaction mixture was poured into a 15-fold excess of *n*-hexane to precipitate the polymer.

The resulting white polymer was collected by filtration and dried in a vacuum oven at 40 °C overnight.

Table 2.3. Summary of experimental conditions for polymerization reactions.

Exp.	T (°C)	BPA (g)	BMSC (g)	<i>o</i> -DCB (mL)	NaOH (mg)	<i>r</i> ^a	[BMSC] ₀ (mol·L ⁻¹)
A	60	2.054	3.001	24	0.9	0.990	0.30
B	90	2.054	3.002	24	0.9	0.990	0.30
C	120	2.054	3.002	24	0.9	0.990	0.30
D	120 - 60	2.054	3.002	24	0.9	0.990	0.30
E	120 - 160	2.055	3.002	24	0.9	0.991	0.30
F	120 - 20	2.054	3.002	24	0.9	0.990	0.30
G	120 - 60	0.686	1.000	40	0.9	0.993	0.07
H	60	0.683	1.000	4	0.5	0.988	0.76
I	120	0.648	1.000	4	0.4	0.989	0.76
J	120 - 60	2.054	3.032	24	1.0	0.980	0.31
K	120 - 60	2.054	3.120	24	1.0	0.953	0.30

^a stoichiometric ratio $r = [\text{BPA}]_0/[\text{BMSC}]_0$

Kinetic experiments

First a reaction mixture of BPA and BMSC in *o*-DCB was prepared. The resulting mixture was heated to the desired temperature and stirred under argon flow. NaOH was added via an aluminum weighing boat when the temperature was stabilized and both monomers were dissolved. Samples were quenched in cold THF.

Temperature-cycle experiment

The reaction mixture was first heated to 120 °C and allowed to react for two hours. A temperature switch was performed by heating or cooling down the oil bath to the desired temperature. After cooling, the reaction was left overnight in order to let the equilibrium settle. For the experiments carried out at 120 °C and 160 °C the reaction times were kept at 2 h.

Continuation of the polymerization after removal of methyl salicylate

250 mg of a previously synthesized polymer ($M_w = 16 \cdot 10^3 \text{ g} \cdot \text{mol}^{-1}$, synthesized at 60 °C) was added to a flame dried, argon flushed Schlenk flask equipped with a stirring bar. 4 mL of *o*-DCB was added and the resulting reaction mixture was allowed to react overnight at 120 °C under inert conditions; no additional NaOH was required. *n*-Hexane was used to precipitate the polymer, which was subsequently collected by filtration and dried in a vacuum oven at 40 °C overnight.

Sample preparation for analysis

Samples were taken from the reaction mixture with an argon flushed needle and syringe. The preparation of SEC samples was performed by quenching ~ 0.1 mL of the reaction mixture in 0.5 mL cold THF. After evaporation of the solvent using a rotary evaporator, the obtained polymer was dissolved in 1.5 mL THF and filtered through a 0.2 µm PTFE syringe filter.

2.7 REFERENCES

1. Meijer, H. E. H.; Govaert, L. E. Mechanical Performance of Polymer Systems: The Relation between Structure and Properties. *Prog. Polym. Sci.* **2005**, *30*, 915–938.
2. Black, A. L.; Lenhardt, J. M.; Craig, S. L. From Molecular Mechanochemistry to Stress-Responsive Materials. *J. Mater. Chem.* **2011**, *21*, 1655–1663.
3. Clough, J. M.; Van Der Gucht, J.; Sijbesma, R. P. Mechanoluminescent Imaging of Osmotic Stress-Induced Damage in a Glassy Polymer Network. *Macromolecules* **2017**, *50*, 2043–2053.
4. Yuan, Y.; Chen, Y. Ian. Visualized Bond Scission in Mechanically Activated Polymers. *Chinese J. Polym. Sci.* **2017**, *35*, 1315–1327.
5. Davis, D. A.; Hamilton, A.; Yang, J.; Cremar, L. D.; Van Gough, D.; Potisek, S. L.; Ong, M. T.; Braun, P. V.; Martínez, T. J.; White, S. R.; Moore, J. S.; Sottos, N. R. Force-Induced Activation of Covalent Bonds in Mechanoresponsive Polymeric Materials. *Nature* **2009**, *459*, 68–72.
6. Chen, Y.; Spiering, A. J. H.; Karthikeyan, S.; Peters, G. W. M.; Meijer, E. W.; Sijbesma, R. P. Mechanically Induced Chemiluminescence from Polymers Incorporating a 1,2-Dioxetane Unit in the Main Chain. *Nat. Chem.* **2012**, *4*, 559–562.
7. Zhang, H.; Gao, F.; Cao, X.; Li, Y.; Xu, Y.; Weng, W.; Boulatov, R. Mechanochromism and Mechanical-Force-Triggered Cross-Linking from a Single Reactive Moiety Incorporated into Polymer Chains. *Angew. Chemie.* **2016**, *55*, 3040–3044.
8. McFadden, M. E.; Robb, M. J. Force-Dependent Multicolor Mechanochromism from a Single Mechanophore. *J. Am. Chem. Soc.* **2019**, *141*, 11388–11392.
9. Robb, M. J.; Kim, T. A.; Halmes, A. J.; White, S. R.; Sottos, N. R.; Moore, J. S. Regioisomer-Specific Mechanochromism of Naphthopyran in Polymeric Materials. *J. Am. Chem. Soc.* **2016**, *138*, 12328–12331.
10. Shanker, N.; Bane, S. L. Basic Aspects of Absorption and Fluorescence Spectroscopy and Resonance Energy Transfer Methods. *Methods Cell Biol.* **2008**, *84*, 213–242.
11. van de Laar, T.; Schuurman, H.; van der Scheer, P.; van Doorn, J. M.; van der Gucht, J.; Sprakel, J. Light from Within: Sensing Weak Strains and FemtoNewton Forces in Single Molecules. *Chem* **2018**, *4*, 269–284.
12. Song, Y. K.; Lee, K. H.; Hong, W. S.; Cho, S. Y.; Yu, H. C.; Chung, C. M. Fluorescence Sensing of Microcracks Based on Cycloreversion of a Dimeric Anthracene Moiety. *J. Mater. Chem.* **2012**, *22*, 1380–1386.
13. Li, H.; Göstl, R.; Delgove, M.; Sweeck, J.; Zhang, Q.; Sijbesma, R. P.; Heuts, J. P. A. Promoting Mechanochemistry of Covalent Bonds by Noncovalent Micellar Aggregation. *ACS Macro Lett.* **2016**, *5*, 995–998.

14. Göstl, R.; Sijbesma, R. P. Π -Extended Anthracenes As Sensitive Probes for Mechanical Stress. *Chem. Sci.* **2016**, *7*, 370–375.
15. Sagara, Y.; Karman, M.; Verde-Sesto, E.; Matsuo, K.; Kim, Y.; Tamaoki, N.; Weder, C. Rotaxanes as Mechanochromic Fluorescent Force Transducers in Polymers. *J. Am. Chem. Soc.* **2018**, *140*, 1584–1587.
16. Balkenende, D. W. R.; Coulibaly, S.; Balog, S.; Simon, Y. C.; Fiore, G. L.; Weder, C. Mechanochemistry with Metallosupramolecular Polymers. *J. Am. Chem. Soc.* **2014**, *136*, 10493–10498.
17. Filonenko, G. A.; Khusnutdinova, J. R. Dynamic Phosphorescent Probe for Facile and Reversible Stress Sensing. *Adv. Mater.* **2017**, *29*, 1–6.
18. Crenshaw, B. R.; Weder, C. Deformation-Induced Color Changes in Melt-Processed Photoluminescent Polymer Blends. *Chem. Mater.* **2003**, *15*, 4717–4724.
19. Imato, K.; Yamanaka, R.; Nakajima, H.; Takeda, N. Fluorescent Supramolecular Mechanophores Based on Charge-Transfer Interactions. *Chem. Commun. (Camb).* **2020**, *56*, 7937–7940.
20. Löwe, C.; Weder, C. Oligo(p-Phenylen Vinylene) Excimers as Molecular Probes: Deformation-Induced Color Changes in Photoluminescent Polymer Blends. *Adv. Mater.* **2002**, *14*, 1625–1629.
21. Celestine, A. D. N.; Sottos, N. R.; White, S. R. Strain and Stress Mapping by Mechanochemical Activation of Spiropyran in Poly(Methyl Methacrylate). *Strain* **2019**, *55*, 1–17.
22. Celestine, A. D. N.; Beiermann, B. A.; May, P. A.; Moore, J. S.; Sottos, N. R.; White, S. R. Fracture-Induced Activation in Mechanophore-Linked, Rubber Toughened PMMA. *Polymer* **2014**, *55*, 4164–4171.
23. Degen, C. M.; May, P. A.; Moore, J. S.; White, S. R.; Sottos, N. R. Time-Dependent Mechanochemical Response of SP-Cross-Linked PMMA. *Macromolecules* **2013**, *46*, 8917–8921.
24. Hemmer, J. R.; Smith, P. D.; Van Horn, M.; Alnemrat, S.; Mason, B. P.; De Alaniz, J. R.; Osswald, S.; Hooper, J. P. High Strain-Rate Response of Spiropyran Mechanophores in PMMA. *J. Polym. Sci. Part B Polym. Phys.* **2014**, *52*, 1347–1356.
25. Peterson, G. I.; Larsen, M. B.; Ganter, M. A.; Storti, D. W.; Boydston, A. J. 3D-Printed Mechanochromic Materials. *ACS Appl. Mater. Interfaces* **2015**, *7*, 577–583.
26. Peterson, G. I.; Yurtoglu, M.; Larsen, M. B.; Craig, S. L.; Ganter, M. A.; Storti, D. W.; Boydston, A. J. Additive Manufacturing of Mechanochromic Polycaprolactone on Entry-Level Systems. *Rapid Prototyp. J.* **2015**, *21*, 520–527.
27. Potisek, S. L.; Davis, D. A.; Sottos, N. R.; White, S. R.; Moore, J. S. Mechanophore-Linked Addition Polymers. *J. Am. Chem. Soc.* **2007**, *129*, 13808–13809.

- 2
- 28. Lee, C. K.; Beiermann, B. A.; Silberstein, M. N.; Wang, J.; Moore, J. S.; Sottos, N. R.; Braun, P. V. Exploiting Force Sensitive Spiropyrans as Molecular Level Probes. *Macromolecules* **2013**, *46*, 3746–3752.
 - 29. Filonenko, G. A.; Sun, D.; Weber, M.; Müller, C.; Pidko, E. A. Multicolor Organometallic Mechanophores for Polymer Imaging Driven by Exciplex Level Interactions. *J. Am. Chem. Soc.* **2019**, *141*, 9687–9692.
 - 30. Legenzov, E. A.; Dirda, N. D. A.; Hagen, B. M.; Kao, J. P. Y. Synthesis and Characterization of 8-Ocarboxymethylpyranine (CM-Pyranine) as a Bright, Violet-Emitting, Fluid-Phase Fluorescent Marker in Cell Biology. *PLoS One* **2015**, *10*, 1–18.
 - 31. Spry, D. B.; Goun, A.; Fayer, M. D. Deprotonation Dynamics and Stokes Shift of Pyranine (HPTS). *J. Phys. Chem. A* **2007**, *111*, 230–237.
 - 32. Dobretsov, G. E.; Syrejschikova, T. I.; Smolina, N. V. On Mechanisms of Fluorescence Quenching by Water. *Biophys. Russian Fed.* **2014**, *59*, 183–188.
 - 33. Wang, Q.; Berglund, K. A. Pyranine Fluorescence Quenching for the Characterization of Solutions. *Am. J. Anal. Chem.* **2016**, *07*, 43–56.
 - 34. Rosenbluth, H.; Weiss-Lopez, B.; Olea, A. F. Thermodynamic and Kinetic Study of the Interaction between Alkylpyridinium Ions and Pyrene Derivatives in Aqueous Solution. *Photochem. Photobiol.* **1997**, *66*, 802–809.
 - 35. Tundo, P.; Kippenberger, D. J.; Politi, M. J.; Klahn, P.; Fendler, J. H. Active Functionally Polymerized Surfactant. **1982**, No. 19, 5352–5358.
 - 36. Kamps, J. H.; Groote, R.; Baus, M.; Vermeulen, H.; Hoeks, T.; van der Heijden, R.; Sijbesma, R. P.; Heuts, J. P. A. Activated Carbonates: Enabling the Synthesis of Differentiated Polymers via Solution Carbonation. *Eur. Polym. J.* **2020**, *135*.
 - 37. Odian, G. *Principles of Polymerization*, 4th ed.; John Wiley & Sons, **2015**.
 - 38. Kamps, J. H.; Hoeks, T.; Kung, E.; Lens, J. P.; McCloskey, P. J.; Noordover, B. A. J.; Heuts, J. P. A. Activated Carbonates: Enabling the Synthesis of Differentiated Polycarbonate Resins via Melt Transcarbonation. *Polym. Chem.* **2016**, *7*, 5294–5303.
 - 39. Brunelle, D. J. Encyclopedia of Polymer Science and Technolog. In *Encyclopedia of Polymer Science and Technology* **2005**. Vol. 7.

Chapter 3

Tunability of mechanophore strength in thermoplastic polyurethanes

| ABSTRACT |

A new strength tunable strain sensor for polyurethane thermoplastic elastomers based on ion-paired complexes is developed. 8-(2-Hydroxyethoxy)pyrene-1,3,6-trisulfonate (HEPTS), incorporated into polyurethanes as an end-capper was found to aggregate in apolar media. Aggregation of the ionic HEPTS end groups in solution depends on concentration and solvent polarity. Fluorescence of the HEPTS groups was quenched efficiently by pyridinium derivates in THF and in the solid state. However, complete quenching was only observed when a large excess of quencher was used. Dissociation of HEPTS aggregates by mechanical force results in a shift in fluorescence from yellow to blue, and for the quenched mechanophores an increase in the blue intensity is monitored. The same shift in fluorescence emission was induced by stretching the solid polymer. HEPTS aggregates show mechanical activation upon plastic deformation, while the stronger HEPTS-quencher complexes only show an increase in fluorescence emission when strain hardening occurs.

Part of the work in this chapter was published in:

Aerts, A.; Lugger, S. J. D.; Heuts, J. P. A.; Sijbesma, R. P.; Pyranine Based Ion-Paired complex as mechanophore in polyurethanes; Macromolecular rapid communications, 2021, 2000476

3.1 INTRODUCTION

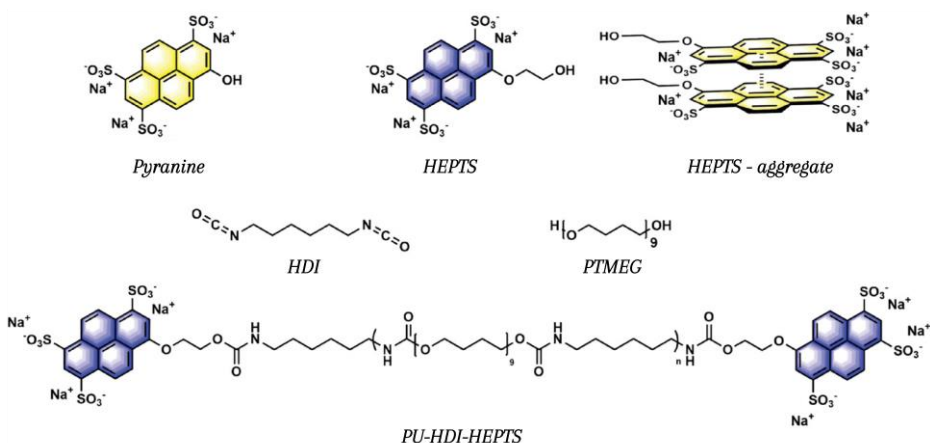
The field of mechanochemistry has emerged as a powerful tool to study polymer materials on the molecular level. Lately, the array of mechanophores has been expanded with supramolecular mechanophores which fluorescence can be turned on by extremely low stresses of 300 fN.¹ Multiple examples of supramolecular mechanophores including host-guest complexes, metal complexes, charge transfer complexes, and rotaxanes have been reported in literature.²⁻⁶ Among supramolecular mechanophores, those based on π-π-interactions, offer a wide range of activation energies. Weder has reported systems in which π-π-interactions were disrupted by a mechanical force resulting in a change of photoluminescence.^{5,7} Some of these mechanophores are based on the aggregation of a fluorescent moiety, in which the polymer changes color upon stretching as a result of dissociation of aggregates.⁷ Another way to create a supramolecular mechanophore is to incorporate a fluorescer-quencher pair into a polymer, like it was done with interlocked rotaxanes by Sagara and Weder.^{2,8} Additionally, Imato and coworkers recently reported a mechanophore based on pyrene derivatives which form a charge-transfer complex via π-π-interactions.⁹ These interactions were disrupted by a mechanical force and immediately reformed in the absence of this stimulus.^{2,10} The sulfonated derivative of pyrene, trisodium 8-hydroxypyrene-1,3,6-trisulfonate or pyranine, exhibits excellent fluorescence properties with a quantum yield near 1.^{11,12} Hann and coworkers showed the effective quenching of anthracene derivatives using methyl pyridinium, while Rosenbluth reported the effective fluorescence quenching of pyranine by the formation of ground-state complexes with various alkyl pyridinium salts.¹³ In this chapter, we focus on the mechanical activation of trisodium 8-(2-Hydroxyethoxy)pyrene-1,3,6-trisulfonate aggregates and ground-state complexes with pyridinium derivatives in MDI based polyurethanes.

3.2 AGGREGATION AND QUENCHING OF HEPTS TELECHELIC POLYURETHANES

Before films were solvent cast and mechanochemical tests could be performed, it was important to first get a better understanding of the mechanophore behavior in solution. Due to the low solubility of HEPTS and both quenchers in organic solvents, their solubility was increased by functionalization with HDI-based polyurethanes via a one-pot polyurethane synthesis with poly(tetramethylene ether)glycol (PTMEG) and hexamethylene diisocyanate (HDI) without using a chain extender (Scheme 3.1).

HEPTS aggregates

The optical properties of pyranine end-capped polyurethane with a molecular mass of $M_n = 54 \cdot 10^3 \text{ g} \cdot \text{mol}^{-1}$ (PU-HDI-HEPTS, Scheme 3.1) were compared in dimethylformamide (DMF) and tetrahydrofuran (THF). In a solution of PU-HDI-HEPTS in DMF with $5 \cdot 10^{-5} \text{ M}$ end groups, monomer emission at 426 nm was observed due to the high solubility of the HEPTS end-groups in this solvent. In contrast, in THF, which is a poor solvent for HEPTS, the strongest emission was observed at $\lambda_{\max} = 510 \text{ nm}$ due to the formation of aggregates, with a relatively small shoulder present at $\lambda_{\max} = 426 \text{ nm}$.



Scheme 3.1. a) Schematic overview of pyranine, HEPTS, HEPTS aggregate, HDI, PTMEG, and the HEPTS functionalized polyurethane (PU-HDI-HEPTS) and the non-functionalized polyurethane (PU).

In order to confirm the solvent dependent aggregation, emission spectra were measured at different solvent compositions at a constant concentration of $5 \cdot 10^{-5} \text{ M}$ PU-HDI-HEPTS. A higher monomer emission ($\lambda_{\max} = 426 \text{ nm}$) was observed at higher DMF content. A solution with equal monomer and aggregate emission intensities was obtained in 3 v/v%

of DMF in THF at a total concentration of $5 \cdot 10^{-5}$ M PU-HDI-HEPTS (solution I). In order to obtain a ratio of emission intensities equal to 1 in 100% THF, dilution to $2 \cdot 10^{-5}$ M was required (**Figure 3.1b**). The effect of dilution of both solutions with THF was investigated. Diluting solution I with THF (**Figure 3.1c** and **d**) results in a 20-fold increase of the monomer-to-aggregate intensity ratio upon dilution by a factor of 5.5, while for the PU-HEPTS in pure THF solution (**Figure 3.1a** and **b**) there is only a 4-fold increase in intensity ratio upon 10-fold dilution. Hence, dissociation of aggregates by dilution is more effective in the presence of DMF.

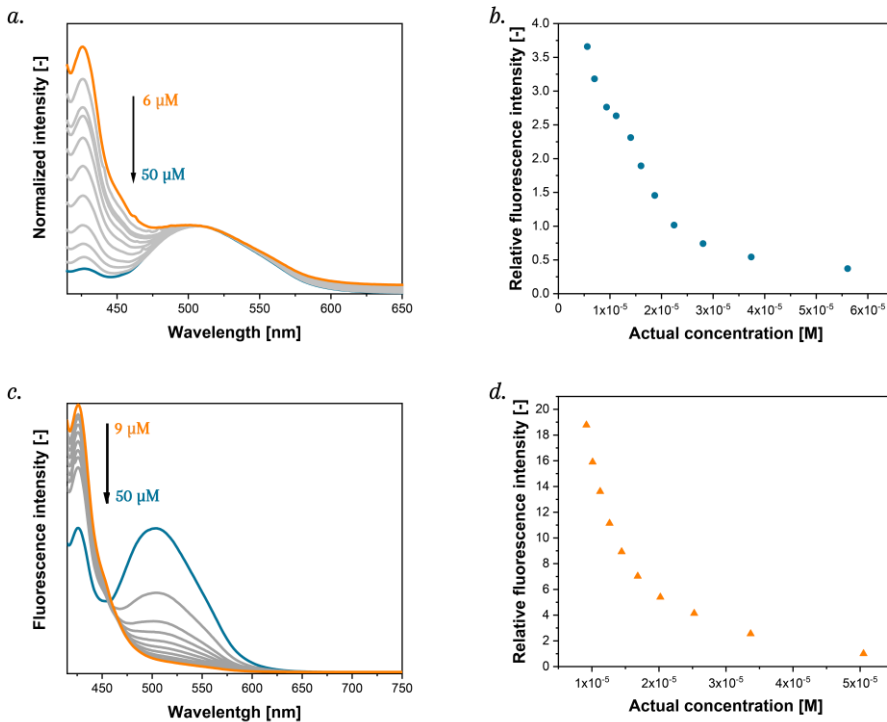


Figure 3.1. a) Fluorescence emission spectra of a dilution series of a $5 \cdot 10^{-5}$ M PU-HDI-HEPTS solution in THF. The dilution series was obtained by diluting the stock solution with THF. b) Relative fluorescence intensity (426 nm/510 nm) decreases with an increasing concentration of PU-HDI-HEPTS in graph a. c) Fluorescence emission spectra of a dilution series of a one-to-one monomer-to-aggregate mixture of PU-HEPTS with THF. The mixture with equal monomer and aggregate emissions (blue, solid line) was obtained by the addition of 38 μL of a $5 \cdot 10^{-5}$ M solution of PU-HDI-HEPTS in DMF to a $5 \cdot 10^{-5}$ M solution of PU-HDI-HEPTS in THF. d) The relative fluorescence intensity (426 nm/510 nm) decreases with increasing concentration of the dilution series in c.

Quenched ion-paired complexes

In addition to the aggregate formation of HEPTS in organic solvents, examples of fluorescence quenching of pyranine are reported in literature. Rosenbluth *et al.* reported the effective quenching of HEPTS by pyridinium salts.¹³ The quenching behavior was investigated for two types of pyridinium salts: a monopyridinium derivative Q1 (**Figure 3.2a**) and a bipyridinium derivate Q2. However, the bromide counter ions in Q1 and Q2 are also known to be fluorescence quenchers. Therefore, the effect of the presence of bromide on HEPTS fluorescence was tested by adding NaBr to a solution of HEPTS. Upon addition of 7500 μM of NaBr to a 3 μM aqueous HEPTS solution, no quenching of HEPTS was observed (**Figure 3.2b-left**). When 7500 μM of Q1 was added, full quenching of HEPTS was achieved, suggesting that Q1 is a much better quencher than to bromide, as was also established by Rosenbluth and coworkers.¹³ Quenching experiments for PU-HDI-HEPTS were performed with similar polyurethane functionalized Q1 (PU-HDI-Q1) with a molecular mass of $M_n = 19 \cdot 10^3 \text{ g} \cdot \text{mol}^{-1}$ in both DMF and THF where the monomeric form and the aggregates were the dominating appearance of HEPTS, respectively. Upon addition of 1 equivalent PU-HDI-Q1 to a PU-HDI-HEPTS solution, no quenching and hence a similar effect as for aqueous media was observed. Due to the high solubility of both HEPTS and Q1 in DMF, the end groups have a low tendency to form quenched complexes.¹⁴ Replacing the solvent by THF resulted in the formation of aggregates, and upon addition of 1 equivalent of PU-HDI-Q1 partial quenching was observed (**Figure 3.2b-right**). Further investigation of the quenching behavior in solution was performed in THF.

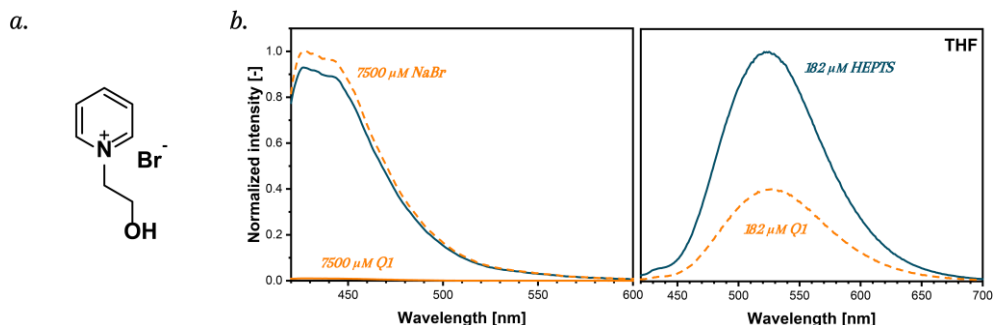


Figure 3.2. a) Chemical structure of quencher Q1. b-left) Quenching of a 3 μM aqueous HEPTS solution (blue solid line) upon the addition of 7500 μM of Q1, while the addition of a similar amount of NaBr did not result in effective quenching of HEPTS (orange dashed line). b-right) Quenching of a 182 μM HEPTS solution in THF (blue solid line) upon the addition of 182 μM of Q1 (orange dotted line)

Lastly, the quenching of HEPTS with Q1 and Q2 was compared **Figure 3.3**; stock solutions of both methylene diphenyl diisocyanate (MDI) based polymeric fluorescer and quenchers (**Figure 3.4**, **Table 3.1**) were prepared in THF and fluorescence was measured of the mixed solutions. Fluorescence quenching was observed for both systems upon addition of 1 equivalent of quencher. We assume that the low solubility of the ionic HEPTS and the quenching end groups increases the tendency to form contact complexes. Quencher 1 required at least a twofold excess to reach maximal quenching in solution, while for Q2 only 0.1 equivalents were required to obtain maximal quenching. 100% quenching was impossible without the addition of a large excess of quenchers.

3

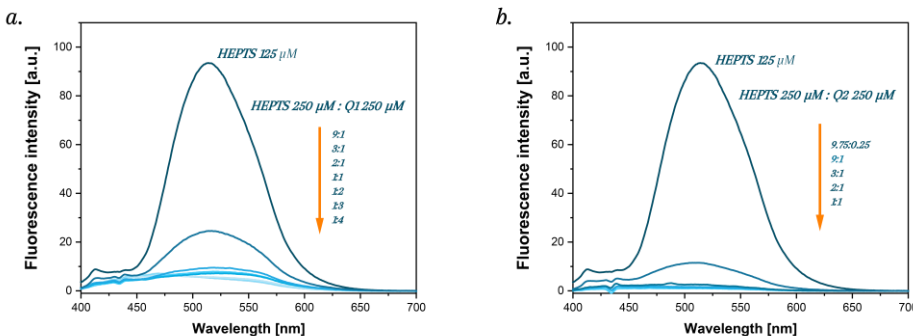


Figure 3.3. Quenching of a 250 μM solution of HEPTS by a) Q1 and b) Q2. Only 2 equivalents of Q2 were required to obtain maximal quenching. Fluorescence spectra were measured upon excitation at 385 nm.

Solid state

Materials for characterization in the solid state were prepared from telechelic MDI based polyurethanes due to the better mechanical properties of MDI-based polyurethanes compared to HDI-based polyurethanes.¹⁵ As described in **Chapter 2**, these polymers were synthesized via a one-pot synthesis in DMF using butanediol (BDO) as a chain extender and randomly built into the chain. Similarly, as for the HDI polyurethanes, the mechanophore functionalities were incorporated as end-groups. Relatively high molar masses were obtained for all polymers after precipitation, for which the distributions are given in **Figure 3.4** and molar masses given in **Table 3.1**. Polyurethane films were cast from a 5 mL THF solution of polyurethane containing 153 mg PU-MDI-HEPTS and quencher in a molar ratio of 1:2 for PU-MDI-Q1 and 39:1 for PU-MDI-Q2, topped up to a total of 900 mg of polymeric solutes with unfunctionalized polyurethane matrix PU-MDI-M. The films were dried overnight at room temperature under THF saturated atmosphere, after which they were heated to 50 °C and dried under vacuum overnight. Upon full

removal of the solvent, the PU-MDI-HEPTS films were bright yellow with a monomer-to-aggregate emission intensity ratio smaller than 1 indicating extensive aggregation of HEPTS end-groups in the bulk. Films containing quenched complexes were significantly quenched in yellow intensity.

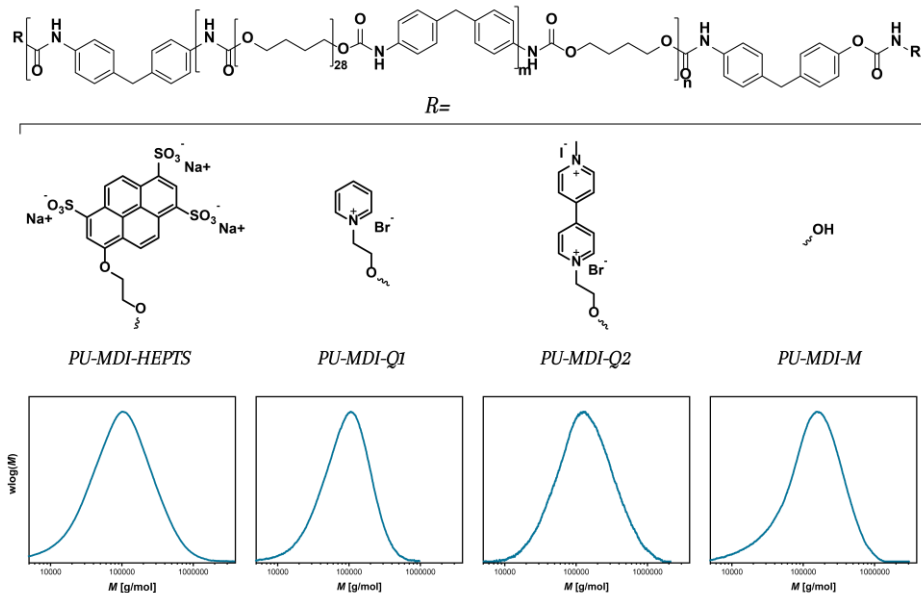


Figure 3.4. Chemical structures of the MDI-based polyurethanes with the defined end groups and the corresponding molar mass distributions as determined by SEC in DMF relative to PMMA standards.

Table 3.1. Summary of experimental molar masses for different end group containing polyurethanes.

	M_n^a ($\cdot 10^3$ g·mol $^{-1}$)	D^b
PU-MDI-HEPTS	56528	2.6
PU-MDI-Q1	65314	1.74
PU-MDI-Q2	89793	2.03
PU-MDI-M	84573	2.2

^a Number-average molar mass as determined by SEC, ^b $D \equiv M_w/M_n$ as determined by SEC.

3.3 MECHANICAL ACTIVATION OF HEPTS FUNCTIONALIZED POLYURETHANE FILMS

Since HEPTS aggregates and HEPTS-quencher complexes were found to dissociate upon dilution, the possibility to revert aggregation and ion-pairing in the bulk by use of mechanical force was studied next. Based on the strength of different non-covalent interactions like π - π - stacking versus ion-pairing, we hypothesized that activation force of the mechanophore could be tuned by changing the charge of the counterion, for example from +1 in pyridinium (Q1) to +2 in bipyridinium (Q2).

Tensile tests were performed on two different types of test specimens: a rectangular strip and a dogbone shaped specimen as shown in **Figure 3.5a**; a clear change in fluorescence intensity was observed upon straining (**Figure 3.5b**). Fluorescence spectra were recorded in situ while straining the sample and the real-time fluorescence spectra as a function of engineering strain (eng. strain) are shown in **Figure 3.5c**. The tensile curves of all polymer samples were compared with rectangular specimens and were very similar, so the mechanical properties were unaffected by incorporation of the mechanophore.

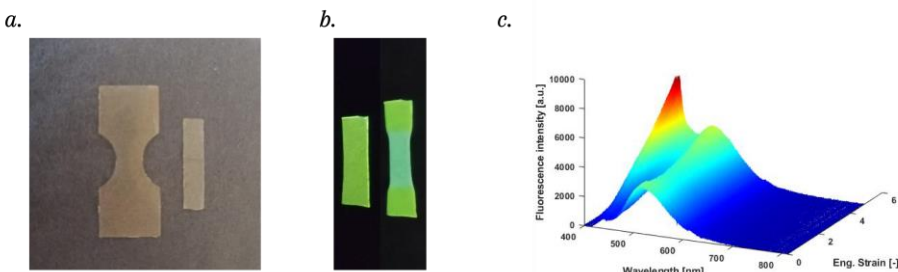


Figure 3.5. a) Illustration of the two different shapes in test specimens used for tensile tests. b) Mechanical activation of the mechanophore in a PU-MDI-HEPTS strip. c) Real-time fluorescence spectra as a function of engineering strain in a rectangular sample.

In the rectangular strip deformation can be assumed to be relatively homogeneous due to the elastic nature of the material and the strip experiences minimal stress localization. In contrast, when a dogbone-shaped specimen is stretched, high stress localization is introduced in the narrowest part. When stress-strain curves of the two geometries were compared for similar strains, higher stresses were observed in the dogbone shaped sample, resulting in a shift of the inflection points of the tensile curves towards smaller strains. Additionally, strain hardening occurs at earlier stages of straining the sample

except for Q2 quenched samples. This is possibly caused by the stronger interaction between Q2 and HEPTS, resulting in a better stress dissipation in the polymer and hence a more homogeneous deformation compared to weaker complexes.

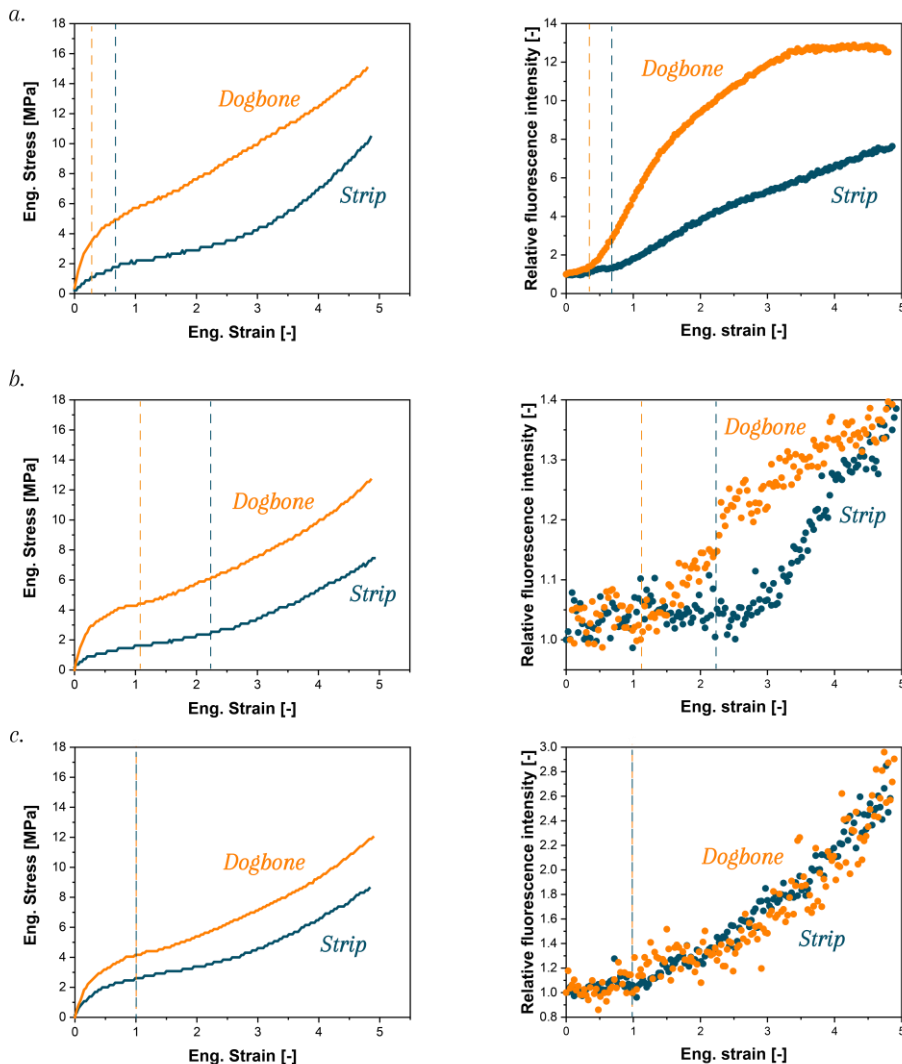


Figure 3.6. Engineering stress-strain curves (left) and the corresponding mechanophore activation as a function of engineering strain (right) for a) PU-MDI-HEPTS b) 1:2 PU-MDI-HEPTS : PU-MDI-Q1 and c) 4:1 PU-MDI-HEPTS : PU-MDI-Q2. The mechanophore activation was determined by the relative fluorescence intensity of the monomer-to-aggregate emission. The fluorescence intensities were averaged over 10 datapoints around 422 nm (monomer) and 514 nm (aggregate). The dashed lines indicate the onset of the mechanophore activation and its corresponding engineering strain in the stress strain curves.

Real-time fluorescence data were obtained by in situ measurements and in order to correct for changing thicknesses of the sample, relative fluorescence intensities of the monomer-to-aggregate emission were plotted versus strain and used to compare the dogbone with the strip. For HEPTS aggregate containing polyurethanes a clear change in fluorescence intensity was observed at low strains (**Figure 3.6a**). In a strip, mechanical dissociation of the HEPTS aggregates was observed around 60% strain, which correlates to the first inflection point of the tensile curve. This is the point where the samples start to deform plastically. When the strip was exchanged for a dogbone, stress localization was introduced, and plastic deformation occurred around 40 % strain, resulting in earlier activation of the mechanophore. Additionally, a relatively stronger increase in fluorescence intensity was observed until a plateau was reached, which might be the result of maximal activation of the mechanophore at the probed spot on the sample. In contrast, the threshold for the mechanical activation of the quenched complexes is higher, and dissociation of the quenched complexes was observed right at the onset of strain hardening of the polymer, which is the point where hard segments in the material start to fail. A similar trend was observed for both quenched systems. Shifting the onset of strain hardening to lower strains by using a dogbone shaped specimen instead of a strip resulted in earlier activation of the mechanophore as shown in **Figure 3.6b**. There is a clear relation between the mechanical behavior and the mechanophore activation. In the PU-MDI-HEPTS:PU-MDI-Q2 system the onset of strain hardening was found at the same strain for the rectangular and the dogbone-shaped sample and a strongly correlated fluorescent response is shown in **Figure 3.6c**, in which the mechanophore activation of both the dogbone and the strip almost completely overlap.

3.4 CONCLUSIONS

Telechelic polyurethanes with ionic end groups were successfully synthesized. Aggregate formation of HEPTS telechelic urethanes was investigated in both DMF and THF and was shown to be concentration dependent and less efficient in DMF compared to THF due to solubility. Quenching of HEPTS aggregates in THF was investigated for both pyridinium and bipyridinium salts: more effective quenching of the HEPTS aggregates was obtained by bipyridinium where only 0.1 equivalents of Q2 was required to reach maximal quenching of the HEPTS end groups. Both HEPTS aggregates and quenched complexes of HEPTS were shown to be reversible upon straining resulting in either a shift in fluorescence from yellow to blue for HEPTS aggregates or an increase in blue emission upon dissociating the quenched complexes. HEPTS aggregates dissociate as soon as the polymer plastically deforms, which is in line with the findings of Filonenko and coworkers where they showed that mechanical activation of the mechanophores in prestrained

samples was slightly delayed in hard phase labelled polyurethanes compared to soft phase labelled polyurethanes.⁶ In contrast, the mechanical activation of the quenched complexes only show an increase in fluorescence intensity at higher strains when strain hardening occurs in the material. Hence the activation threshold of the mechanophore is tunable to higher strengths for ion-paired complexes compared to π-π-stacked aggregates.

3.5 EXPERIMENTAL DETAILS

PU-HDI-HEPTS

A 100 mL schlenk flask was charged with polytetrahydrofuran (PTMEG) (3.52 g, 6.29 mmol) and allowed to stir at 65 °C under vacuum for 1 hour. HEPTS (50.48 mg, 0.09 mmol) was dissolved in dry DMF (10 mL) and added to the flask while stirring. Dry DMF (20 mL), DBTDL catalyst (15 µL) and HDI (0.88 g, 5.23 mmol) were added. The obtained mixture was degassed with 3 argon purge-and-refill cycles and allowed to react at 65 °C under inert atmosphere overnight. Afterwards, the viscous reaction mixture was cooled to room temperature and precipitated in MeOH (500 mL). The obtained precipitate was filtered and dried under high vacuum at room temperature. The dry polymer was redissolved in chloroform (20 mL), precipitated in pentane (500 mL) (3.93 g).

SEC (DMF, 0.1M LiBr): $M_n = 54$ kDa and $\bar{D} = 1.4$

PU-HDI-Q1

A schlenk tube was charged with PTMEG (1.955 g, 2.94 mmol) and allowed to stir at 65 °C under vacuum for 1 hour. Afterwards, ACN (18 mL), Q1 (10.08 mg, 0.05 mmol), DBTDL catalyst (20 µL) and HDI (0.513 g, 3.05 mmol) were added, and the mixture was degassed thoroughly with 3 argon purge-and-refill cycles. The obtained reaction mixture was allowed to stir at room temperature under argon atmosphere overnight. After 1 hour the mixture was not able to stir anymore due to the formation of sticky precipitate. Afterwards, the ACN phase was dried at the rotary evaporator but according to ¹H-NMR did not contain any polyurethane and was therefore discarded. The precipitate was dissolved in CHCl₃ (10 mL), quenched with MeOH (1 mL) in order to terminate all present isocyanate groups and precipitated in pentane (300 mL). The obtained precipitate was stirred in fresh pentane for 1 hour. The solvent was decanted, and the precipitate was dried at 50 °C under vacuum which yielded 5 as white solid (1.93 g).

SEC (DMF, 0.1M LiBr): $M_n = 19.3$ kDa $\bar{D} = 1.7$.

MDI based polyurethanes

Thermoplastic polyurethanes were synthesized in solution. All glassware was dried at 120 °C for 3 hours prior to use. polyTHF was dried for 3 hours under vacuum at 100 °C and DMF and butane diol were put on molsieves in dried flasks.

General procedure: A Schlenk flas was equipped with a dried stirrer and charged with 5 g (2.5 mmol) of polyTHF-2000 g·mol⁻¹. 0.383 g (4.2 mmol) BDO was added to the polyTHF and both diols were dissolved into 50 mL dry DMF. The mixture was heated to 80 °C and stirred for 5 minutes to ensure homogeniization. Then 1µL of DBTDL was added as a catalyst and 1.73 g (6.9 mmol) MDI was added to the flask. 0.1 mmol of fluorescer or quencher was added. The polymerization was left at 80 °C for overnight. Th polymer reaction mixture was quenched with methanol, precipitated in ether. A white solid material was obtained.

Table 3.2. summary of the masses for the end groups used in the synthesis for telechelic polyurethanes.

	End groups			
	mmol	mass (g)	M_n^a (·10 ³ g·mol ⁻¹)	D^b
PU-MDI-HEPTS	0.1	0.058	57	2.6
PU-MDI-Q1	0.1	0.021	65	1.74
PU-MDI-Q2	0.1	0.043	90	2.03
PU-MDI-M	0.1	0.003	85	2.2

^a Number-average molar mass as determined by SEC, ^b $D \equiv M_w/M_n$ as determined by SEC.

Solvent casting of the PU-films

Films were cast from a 900 mg polyurethane solution in 5 mL THF in a round Teflon mold of 10 cm in diameter. Films were dried overnight at room temperature and afterwards kept at 50 °C under vacuum for overnight.

Table 3.3. Summary of the composition of the films for tensile testing.

	mass HEPTS (mg)	mass Q (mg)	mass Matrix (mg)
PU-MDI-HEPTS	153	-	747
1:2 PU-MDI-HEPTS : PU-MDI-Q1	153	354	394
4:1 PU-MDI-HEPTS : PU-MDI-Q2	153	61	686

^a Number-average molar mass as determined by SEC, ^b $D \equiv M_w/M_n$ as determined by SEC

Tensile tests with *in-situ* fluorescence measurements

Tensile tests were performed on a Linkam TST350 tensile tester equipped with a 200N load cell. Samples were strained with a strain rate of $3 \cdot 10^{-3} \text{ s}^{-1}$ until $\sim 500\%$ engineering strain. In situ fluorescence emission spectra were recorded by an Ocean-HDX-UV-VIS portable spectrometer equipped with a QR600-7-SR-125F reflectance probe and an INLINE-SFH filter holder including a 420 nm filter in front of the detector. A separate light source of 400 nm was used to excite the sample and the probe was used for detection (**Figure 3.7**). The distance between the probe and the sample was in the mm range and optimized according to the emission read-out of the software Oceanview. Emission spectra were recorded every 10 seconds with 1s per scan.

Displacements and forces were measured. Engineering stresses and strains were calculated using matlab with the following equations:

$$\sigma = \frac{F}{A} \quad \text{Eq. 3.1}$$

$$\varepsilon = \frac{L - L_0}{L_0} \quad \text{Eq. 3.2}$$

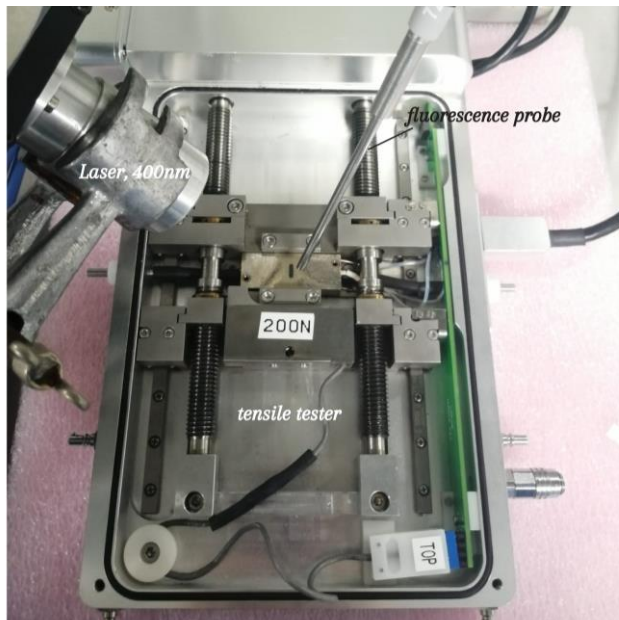


Figure 3.7. Illustration of the experimental set up for the tensile tests with *in situ* fluorescence measurements.

3.6 REFERENCES

- van de Laar, T.; Schuurman, H.; van der Scheer, P.; van Doorn, J. M.; van der Gucht, J.; Sprakel, J. Light from Within: Sensing Weak Strains and FemtoNewton Forces in Single Molecules. *Chem.* **2018**, *4*, 269–284.
- Sagara, Y.; Karman, M.; Verde-Sesto, E.; Matsuo, K.; Kim, Y.; Tamaoki, N.; Weder, C. Rotaxanes as Mechanochromic Fluorescent Force Transducers in Polymers. *J. Am. Chem. Soc.* **2018**, *140*, 1584–1587.
- Balkenende, D. W. R.; Coulibaly, S.; Balog, S.; Simon, Y. C.; Fiore, G. L.; Weder, C. Mechanochemistry with Metallosupramolecular Polymers. *J. Am. Chem. Soc.* **2014**, *136*, 10493–10498.
- Filonenko, G. A.; Khusnudinova, J. R. Dynamic Phosphorescent Probe for Facile and Reversible Stress Sensing. *Adv. Mater.* **2017**, *29*, 1–6.
- Crenshaw, B. R.; Weder, C. Deformation-Induced Color Changes in Melt-Processed Photoluminescent Polymer Blends. *Chem. Mater.* **2003**, *15*, 4717–4724.
- Filonenko, G. A.; Lugger, J. A. M.; Liu, C.; van Heeswijk, E. P. A.; Hendrix, M. M. R. M.; Weber, M.; Müller, C.; Hensen, E. J. M.; Sijbesma, R. P.; Pidko, E. A. Tracking Local Mechanical Impact in Heterogeneous Polymers with Direct Optical Imaging. *Angew. Chemie* **2018**, *130*, 16623–16628.
- Löwe, C.; Weder, C. Oligo(p-Phenylene Vinylene) Excimers as Molecular Probes: Deformation-Induced Color Changes in Photoluminescent Polymer Blends. *Adv. Mater.* **2002**, *14*, 1625–1629.
- Sagara, Y.; Karman, M.; Seki, A.; Pannipara, M.; Tamaoki, N.; Weder, C. Rotaxane-Based Mechanophores Enable Polymers with Mechanically Switchable White Photoluminescence. *ACS Cent. Sci.* **2019**, *5*, 874–881.
- Imato, K.; Yamanaka, R.; Nakajima, H.; Takeda, N. Fluorescent Supramolecular Mechanophores Based on Charge-Transfer Interactions. *Chem. Commun. (Camb.)* **2020**, *56*, 7937–7940.
- Zych, A.; Verdelli, A.; Soliman, M.; Pinalli, R.; Pedrini, A.; Vachon, J.; Dalcanale, E. Strain-Reporting Pyrene-Grafted Polyethylene. *Eur. Polym. J.* **2019**, *III*, 69–73.
- Tran-Thi, T. H.; Prayer, C.; Millié, P.; Uznanski, P.; Hynes, J. T. Substituent and Solvent Effects on the Nature of the Transitions of Pyrenol and Pyranine. Identification of an Intermediate in the Excited-State Proton-Transfer Reaction. *J. Phys. Chem. A* **2002**, *106*, 2244–2255.
- Wong, F. H. C.; Fradin, C. Simultaneous PH and Temperature Measurements Using Pyranine as a Molecular Probe. *J. Fluoresc.* **2011**, *21*, 299–312.
- Rosenbluth, H.; Weiss-Lopez, B.; Olea, A. F. Thermodynamic and Kinetic Study of the Interaction between Alkylpyridinium Ions and Pyrene Derivatives in Aqueous Solution. *Photochem. Photobiol.* **1997**, *66*, 802–809.

14. Corsaro, G. Ion Strength, Ion Association, and Solubility. *J. Chem. Educ.* **1962**, *39*, 622–626.
15. Rogulska, M.; Kultys, A.; Podkościelny, W. Studies on Thermoplastic Polyurethanes Based on New Diphenylethane-Derivative Diols. II. Synthesis and Characterization of Segmented Polyurethanes from HDI and MDI. *Eur. Polym. J.* **2007**, *43*, 1402–1414.

Chapter 4

Fluorescent visualization of bond breaking in polymer glasses

| ABSTRACT |

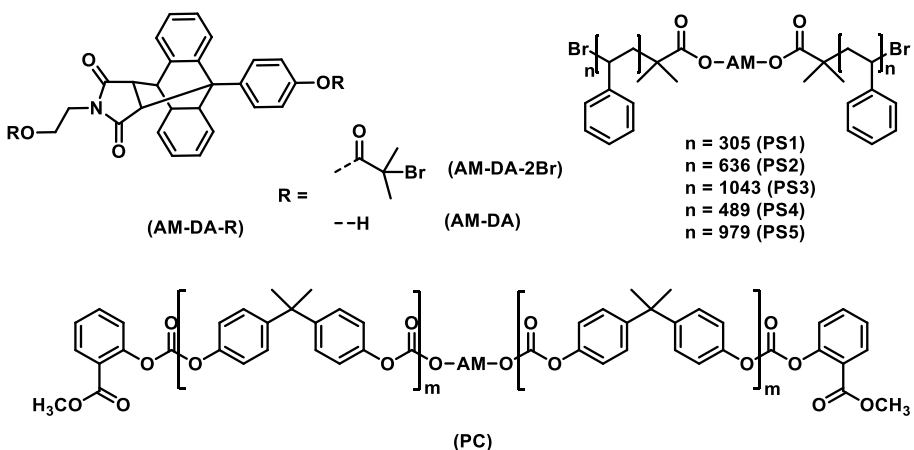
Mechanofluorescent polymer probes were used to visualize stresses and bond scission in polystyrene and polycarbonate. Sonicating polystyrene probes with a molar mass of $109 \cdot 10^3 \text{ g} \cdot \text{mol}^{-1}$ resulted in 30% activation after 1 hour, while shorter probes showed lower activation percentages. Single-asperity sliding friction tests were performed on mechanophore containing polystyrene and polycarbonate films. In polystyrene clearly visible cracks were formed with a correlated pattern in the friction force and penetration depth as well as in the fluorescent activation of the mechanophore. The mechanophore was activated significantly with an applied normal load of 100 mN for polystyrene, while for polycarbonate a normal load of 750 mN was required to activate the mechanophore.

Part of the work in this chapter will be published in:

Aerts, A.; Looijmans, S. F. S. P.; Breemen, van L. C. A.; Heuts, J. P. A.; Sijbesma, R. P.; *Fluorescent visualization of bond breaking in polymer glasses, in preparation.*

4.1 INTRODUCTION

Glassy polymers are extensively used in a wide range of demanding applications, in which they can be exposed to severe mechanical, thermal or chemical conditions. This can result in premature failure of the polymer glasses.¹⁻³ Failure often starts with a small imperfection which initiates the formation of a small crack that grows to ultimately make the material fail, limiting the useful lifetime and performance of glassy polymers.³⁻⁵ It is therefore of great importance to get a better understanding of the structure-property relationship of the polymers and their failure mechanisms in order to be able to predict the long term mechanical behavior of a material and to ensure its reliability for safety reasons.^{6,7} Numerous studies have shown that stimuli-responsive molecular units, in particular mechanophores, are good candidates to study the behavior of a polymer when stress is applied.⁸⁻¹¹ Mechanophores change their optical properties when a stress is applied and most common detection methods are mechanochromism,¹² mechanoluminescence,¹³ and mechanofluorescence.¹⁴ Mechanochromism has been studied extensively, with spirobifluorans as the most defined and well-studied example. Mechanoluminescence was introduced by our group in 2012 with the chemiluminescent response of 1,2-dioxetane upon exposure to stress.^{10,13} To study of bond scission in glassy polymers under stress, both absorption and chemiluminescence based techniques have limitations, such as low sensitivity in absorption and a limited lifetime in luminescence.¹⁵ In the current study we therefore used the well-known mechanofluorescent anthracene-maleimide Diels-Alder adduct for more sensitive and time-independent stress visualization.^{14,16} An additional challenge in the study of damage in glassy polymers with mechanophores is that usually covalent bond scission does not occur before failure. This in contrast to mechanophore studies on non-crosslinked elastomers, where the transmittance of the stress in the polymer can be visualized prior to failure since the forces are mostly transduced along the backbone. In mechanophore studies in glassy polymers, activation has mostly been achieved under specialized force conditions or by tensile forces on an adapted polymer system at elevated temperatures, or with added plasticizer.¹⁷⁻¹⁹ Recently Vidavsky²⁰ and coworkers were the first to report mechanochemical activation under tensile stresses in polycarbonate without the need of elevated temperatures^{18,19} or additives.¹⁷



Scheme 4.1. Chemical structures of the mechanophore (AM) and both mechanophore containing polymers PS1-PS5 and PC.

Here we discuss the fluorescent visualization of bond scission in polystyrene and polycarbonate glasses. A π -extended anthracene-maleimide Diel-Alder adduct (**Scheme 4.1**) was synthesized and characterized as a mechanophore and was incorporated into polystyrene and polycarbonate via a single-electron transfer-living radical polymerization (SET-LRP) and a solution transcarbonation respectively. Mechanochemical activation of these polymers was tested in solution and in the solid state.

4.2 MECHANOPHORE SYNTHESIS AND CHARACTERIZATION IN SOLUTION

Anthracene-maleimide Diels Alder cycloadduct AM-DA (**Scheme 4.1**) was synthesized and used as a mechanophore in glassy polymers. AM-DA was obtained in a multistep synthesis discussed in chapter 2 and incorporated into polystyrene (PS1-PS5, **Scheme 4.1**) or polycarbonate (PC, **Scheme 4.1**). For the polystyrene polymeric probe, a bifunctional ATRP-initiator AM-DA-2Br was synthesized, and polystyrene was grown simultaneously on both sides of the AM mechanophore via a single-electron transfer-living radical polymerization (SET-LRP), resulting in center functionalized polystyrene chains. The adjacent polymer chains play an important role in the propagation of the generated forces on the polymer towards the mechanophore. Polystyrene polymers (PS1-PS5) of five different molecular masses were synthesized. Additionally, Bisphenol-A polycarbonate was synthesized via solution polymerization described in *Chapter 2*.²¹ A prepolymer of

polycarbonate (PC-prepol), was synthesized and coupled with AM-DA to obtain a mechanophore functionalized polycarbonate (**Scheme 4.1**). In this polymer, the mechanophore is not necessarily situated in the center of the chain and in some cases more than one mechanophore is built into the polymer. Diffusion ordered spectroscopy (DOSY)-NMR was used to confirm incorporation of the mechanophore. For both polystyrene and polycarbonate the total length of the polymers significantly exceeds the molar masses between entanglements which are $M_e, PS \approx 15 \cdot 10^3 \text{ g} \cdot \text{mol}^{-1}$ and $M_e, PC \approx 2.5 \cdot 10^3 \text{ g} \cdot \text{mol}^{-1}$.²² Entanglements between the polymeric probe and the polymer matrix will enhance the transmission of the applied force towards the mechanophore. Two matrix polymers were synthesized via free radical polymerization of styrene to obtain PSS and PSL as matrix polymers.

Table 4.1. Molar masses and polydispersity of the polymers used in this study.

Polymer	M_n ^a (g·mol ⁻¹)	\mathcal{D} ^b
PS1	$32 \cdot 10^3$	1.2
PS2	$66 \cdot 10^3$	1.5
PS3	$109 \cdot 10^3$	1.2
PS4	$51 \cdot 10^3$	1.4
PS5	$102 \cdot 10^3$	1.3
PC-prepol	$10 \cdot 10^3$	2.1
PC	$31 \cdot 10^3$	1.8
PSS	$107 \cdot 10^3$	1.8
PSL	$560 \cdot 10^3$	1.9

^a Number-average molar mass as determined by SEC, ^b $\mathcal{D} \equiv M_w/M_n$ as determined by SEC.

Thermal stability

The mechanophores were tested for their thermal stability in both solid state and solution. The solid-state tests were performed on a hotplate equipped with a thermocouple. A few AM-DA-2Br crystals were put on a piece of aluminum foil on a hotplate and heated to 250 °C. Instantaneous and bright fluorescence was observed around 230 °C, which is close to the melting point of the crystals as measured by Differential Scanning Calorimetry (DSC). This suggest that fluorescent anthracene is not released from crystalline AM-2Br until the crystals melts. When AM-2Br was dissolved in *o*-DCB, the anthracene was released at lower temperatures. Percentages of activation were calculated using a

calibration curve for concentrations between $5 \cdot 10^{-8}$ M and $5 \cdot 10^{-6}$ M shown in **Figure 4.1a**. As shown in **Figure 4.1b** activation increased with temperature. Heating the mechanophore for at least 1 hour at 100 °C resulted in only 0.3% of activation. When the polymers were heated when keeping the sample at 100 °C for 24h, only 3% of the mechanophore was activated. Hence, sample preparation of mechanophore containing polymer, which takes place below 100 °C does not result in significant activation of the mechanophore.

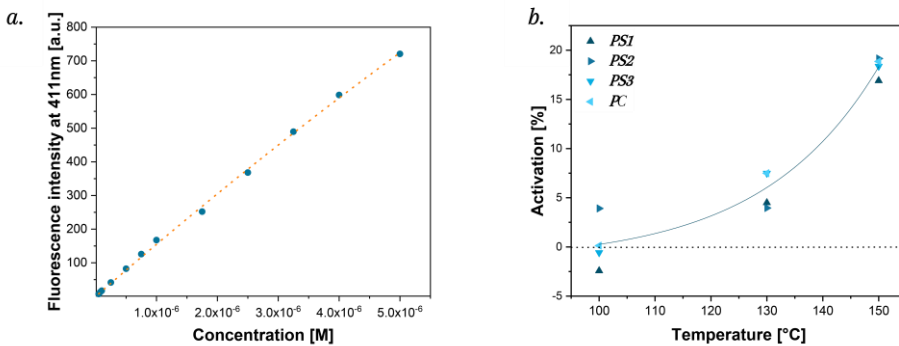


Figure 4.1. a) Calibration curve measure in THF. Mechanophore activation after heating PS1(\blacktriangle), PS2(\blacktriangleright), PS3(\blacktriangledown) and PC(\blacktriangleleft) for 1h to 100 °C, 130 °C and 150 °C. Activation was calculated from the intensity at 411 nm and was corrected for activation at $t=0$. The solid line is a guide to the eye, while the dotted line represents 0 % activation.

Mechanical activation in solution

Ultrasonication was used to investigate mechanical activation of the DA-adduct in solution. Sonication of a polymer solution with a sonication probe instead of a sonication bath results in cavitation-induced cleavage of polymers. The rate of cleavage is dependent on the molar mass and is zero below a certain critical molecular weight. Scission preferentially takes place in the middle of the polymer chain.²³ Solutions of $5 \cdot 10^{-5}$ M were sonicated for periods of 15 min and 1 hour. Fluorescence intensities of the solutions were measured to determine the fraction of activated mechanophores, and the results are shown in **Figure 4.2** and **Table 4.2**. The spectra show, as expected, that the activation of the mechanophore in solution by sonication increases with molar mass of the polymer. Percentages of activation were determined using the calibration curve shown in **Figure 4.1a**.

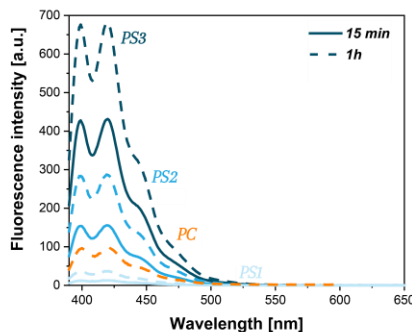


Figure 4.2. Fluorescence emission spectra after sonication of PS1-PS3 and PC for 15 minutes and 1 hour. Number average molar masses for PS1-PS3 and PC are 32, 66, 102 and 31 kg·mol⁻¹ respectively. Note: PC spectrum for 15 minutes is missing.

Table 4.2. Activation of PS1-PS3 and PC after 15 min and 1h of sonication. Percentages of activation were calculated for each polymer based on fluorescence emission at 411 nm.

Polymer	M_n (g·mol ⁻¹)	% activation	
		15 min sonication	1 hour sonication
PS1	32·10 ³	0	1.4
PS2	66·10 ³	3.1	12
PS3	109·10 ³	9.2	30
PC	31·10 ³	-	2.2

PS1 and PC have similar number-average molar mass around 30·10³ g·mol⁻¹ and show low mechanophore activation because the molar mass is close to the limiting molar mass for polymers subjected to ultrasonication.²⁴ For higher molar masses, the activation increased from 1.5 % for PS1 to 12 % and 30 % percent for PS2 and PS3, respectively. The sonication experiments show that for all polymers described in this work, the mechanophore can be activated in solution. Although the lower molar masses show little scission because they are close to the limiting molar mass for ultrasonication, the higher molar mass are significantly activated.

4.3 MECHANICAL ACTIVATION IN SOLID STATE

Multiple techniques were used to activate the mechanophore in a solid polymer film: grinding, compression, tensile tests and indentation tests. For polycarbonate (PC), only tensile and indentation tests were used, whereas the polystyrene samples were tested by grinding, compression and indentation.

Compression and grinding

Grinding and compression tests were performed on fully mechanophore functionalized polymer with a number-average molar mass of $51 \cdot 10^3 \text{ g} \cdot \text{mol}^{-1}$ (PS4) or $102 \cdot 10^3 \text{ g} \cdot \text{mol}^{-1}$ (PS5). Solvent-cast polystyrene films were manually ground for 2 minutes and subsequently dissolved in toluene. Fluorescence spectroscopy of the dissolved films showed that up to 5 % of the mechanophore was activated by grinding (**Figure 3a, c**). Activation of the higher molecular mass PS5 (3.3 %) was lower than for PS4 (4.9 %). These experiments however, clearly showed that the mechanophore was able to be activated by a mechanical force applied to the polymer film.

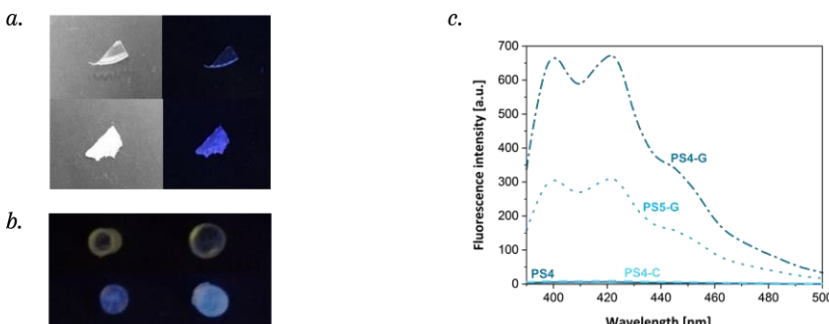


Figure 4.3. a) PS4 film before (top) and after (bottom) grinding in daylight (left) and with excitation at 366 nm (right). b) Visualisation of the fluorescence obtained before and after compression. Top left: uncompressed commercial polystyrene, top right: compressed commercial polystyrene. Bottom left: uncompressed PS4, bottom right: compressed PS4. Both commercial polystyrene samples were not fluorescent before and after compression. A fluorescent background was observed after preparing the samples of the functionalized polystyrene for compression and almost no change in fluorescence was observed after compression of the samples. c) Emission spectra of the dissolved samples. A significant increase in fluorescence intensity was observed for the ground samples (PS4-G and PS5-G), while compressing PS4 (PS4-C) did not result in a significant change in fluorescence emission.

Additionally, compression tests were performed on cylinders with a diameter of 3 mm and an aspect ratio of 1 (**Figure 4.3b**). These cylinders were prepared by solvent casting polystyrene films and stacking round cut-outs from the film in a metal cylindrical mould (**Figure 4.4**). After heating the stack of films to 140 °C, which is above the T_g of the polymer ($T_g \sim 105$ °C), for 10 minutes in a Tribotak and applying a pressure of 14 MPa with a weight of 10 kg on top of the stack of films, the stacked films were permanently attached to each other, and cylindrical polystyrene samples were obtained.

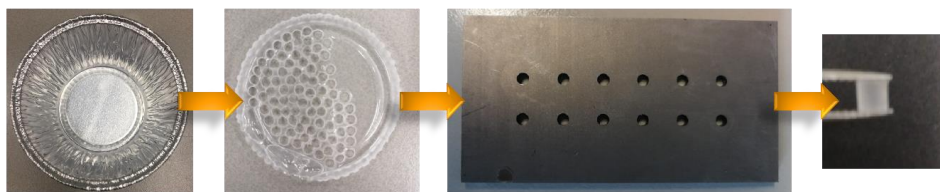


Figure 4.4. Illustration of the steps involved in the sample preparation for compression tests. A Tribotak used to stack the polystyrene films into the RVS mold to prepare cylinders with an aspect ratio of 1.

These samples were covered with Teflon tape and compressed with a uniaxial force in a tensile tester. The activation of the mechanophore was determined by dissolving the compressed sample and measuring fluorescence in solution; no change in fluorescence was observed. For polycarbonate it was impossible to prepare similar samples due to the high T_g (~140 °C) as the mechanophore is not stable at temperatures above this temperature. Hence, the mechanophore was activated via tensile tests. These tests were performed at a strain rate of 0.001 s⁻¹ and activation was determined by measuring fluorescence of the region of break dissolved in THF. No activation was measured.

Indentation tests

Indentation and scratch tests were performed on films with a thickness of ~200 µm for polycarbonate and between 300 and 400 µm for polystyrene (PSS and PSL). Thicker PC films were opaque due to solvent-induced crystallization of polycarbonate.^{25,26} Transparent films were glued onto a glass plate on top of an aluminium stud to make sure the samples were flat and immobile during indentation and scratch tests as shown in **Figure 4.5a**. At the contact edge between sample and indenter, stress location may lead to micro-crack formation in radial direction, however, no fluorescence was observed. In the indentation tests the stress is extremely localized and hence the failure of the material is also too local to be observed with a fluorescence microscope. Furthermore, the load-

displacements were plotted for the applied loads (**Figure 4.5c**). The penetration depth was slightly lower for PSL than for PSS, but this effect is negligible.

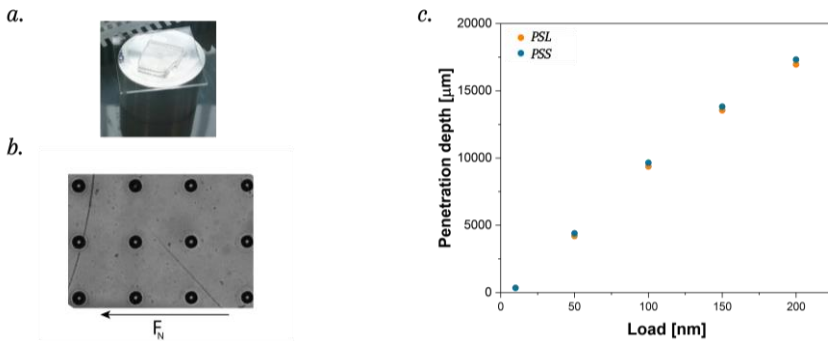


Figure 4.5. a) Illustration of the samples prepared for indentation and scratch tests. b) Bright field images of indentation tests of the five highest forces on PSL-PS1 with different normal loads of 200, 190, 180 and 160 mN from left to right. All indentations were performed in triplicate; each column of indents represent one normal load. c) Plot of penetration depth versus load, showing the penetration depth at a similar force is slightly lower for PSL compared to PSS.

Single-asperity sliding friction tests

In order to increase the amount of local deformation in a controlled way, single-asperity sliding friction tests, better known as scratch tests, were performed. The friction force generated by the sliding motion increases the local stress state and yields a larger area over which the mechanophore may be activated. These experiments were performed with an indentation machine with a conical tip with a cone angle of 90° and a top radius of 10 μm. Solvent cast polymer samples containing 0.2 wt% of AM mechanophore were glued onto a glass plate and an aluminium stud and scratched with a sliding speed of 10 μm/s with applied normal loads ranging between 50 and 400 mN for PS1-PS3 and up to 3000 mN for PC. Damage of both materials was visible in bright field microscope images (**Figure 4.6 - top**) and fluorescence microscopy images were analysed. The intensity patterns from the fluorescence microscope images are shown in **Figure 4.6 - bottom**.

Brittleness of polystyrene results in crack formation at lower forces ($F_N \leq 100$ mN) than in polycarbonate ($F_N \geq 400$ mN). Polystyrene already shows activation of the mechanophore at $F_N = 100$ mN. Crazes were observed in the bright field microscopy image (**Figure 4.6a**) and a correlating intensity pattern is present in the intensity plot. The width of the scratch and the area of mechanophore activation increase with the normal force.

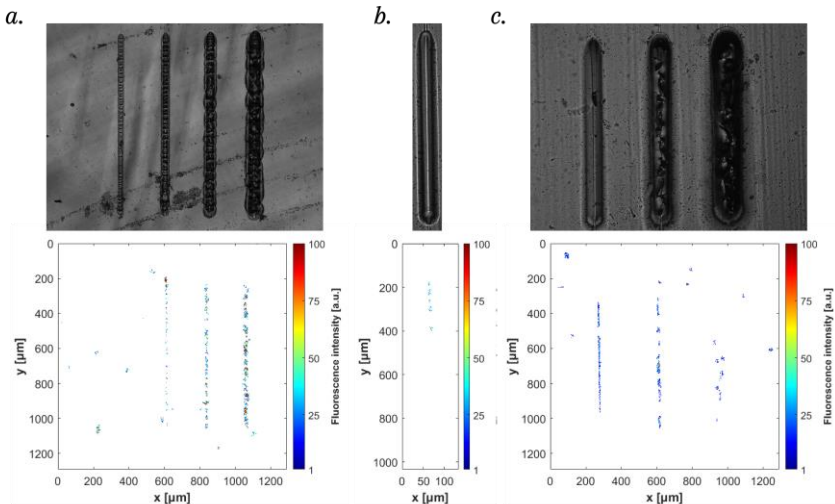


Figure 4.6. Bright field images and fluorescence intensity plots of sliding friction tests (scratch length 0.8 mm) on PSL-PS1 and PC with different normal loads of a) 50, 100, 200 and 400 mN for polystyrene, b) 400 mN on PC and c) 750, 1500 and 3000 mN for polycarbonate. The mechanophore in PSL-PS1 was visibly activated when the sample was scratched with a force up to 750 mN. No fluorescence was observed for polycarbonate while for polystyrene activation was observed above a normal force of 100 mN.

Polycarbonate, however, has more strain hardening and hence its resistance to deformation becomes higher at higher loads. When a normal force of 400 mN (**Figure 4.6b**) was applied to PC, no crazes or cracks were observed and only a minimal amount of activation was observed. An applied normal force of $F_N = 750$ mN resulted in activation of the mechanophore in the area of the tip without introducing visual cracks in the material. When the normal force was raised to 1500 mN, the polycarbonate started to detach from the glass plate and thus the stresses were not concentrated on the sample, resulting in an interrupted fluorescence intensity pattern. An even more strongly interrupted pattern was observed for a scratch test with $F_N = 3000$ mN as here most of the sample detached from the glass substrate. **Figure 4.7a** shows a comparison between scratches in polystyrene and polycarbonate applied with a normal load of 500 mN and 1000 mN of which the intensity pattern is shown in **Figure 4.7b**. PSS, PSS-PS1 and PC were used for sliding friction tests with a normal load of 500 mN. PSS and PC show a fluorescence intensity around 0, while for PSS-PS1 a strongly fluctuating fluorescence signal was observed. For PC, however, sliding friction tests with a normal load of 1000 mN show steady fluorescence over the total length of the scratch. The difference between

polystyrene and polycarbonate can be explained by a different stress distribution in these polymers. Uniaxial compression tests on both polystyrene and polycarbonate show a clear difference in mechanical behaviour after the yield point.²⁷ Polystyrene shows a large strain softening effect whereas polycarbonate undergoes some strain softening followed by strong strain hardening, resulting in a delay of local failure.²⁷ Hence, higher forces are required to reach similar damage in polycarbonate as in polystyrene.

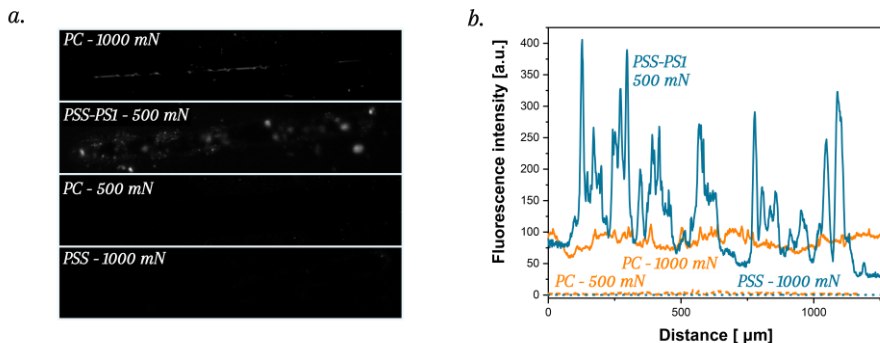


Figure 4.7. a) Fluorescence microscope images and b) intensity plots of PSS, PSS-PSI and PC scratched with $F_N = 500 \text{ mN}$ or 1000 mN . Intensity patterns were taken from the area shown in the microscope image on the left. Polycarbonate scratched at 500 mN nearly showed fluorescence intensity, while for polystyrene a relatively high alternating intensity pattern was measured. Doubling the force resulted in the activation of the mechanophore in PC with a steady intensity pattern over the total length of the scratch.

Sliding friction experiments were performed on a micro indenter and the lateral friction force and penetration depth were plotted against the distance of the scratch (**Figure 4.8a**). The penetration depth shows a significant increase in the beginning of the scratch. This effect is due to the decrease in surface contact when the tip starts moving. After the maximum was reached, the penetration depth decreased to a steady value as a consequence of the growing bow wave in front of the tip and hence an increase in surface contact. The friction force in polycarbonate was much lower than the normal force applied to the samples due to its higher strain hardening. In polystyrene, fluctuation around the horizontal asymptote at the applied normal load was observed. The mean value of this friction force and penetration depth was plotted versus the load. The standard deviation of these values increases strongly at higher loads (**Figure 4.8b** and **c**). In **Figure 4.8**, polycarbonate (shown in orange) shows a steady friction force and penetration depth up to a normal force of 1500 mN , whereas the friction force and penetration depth in polystyrene (shown in blue) start to fluctuate when a normal force of 100 mN or more was applied. The strong fluctuation friction force in polystyrene samples can be explained by the formation of crazes behind the tip, and correlates well

with the pattern mechanophore activation shown in **Figure 4.7b**. This clearly indicates a direct relation between bond scission and crack formation.

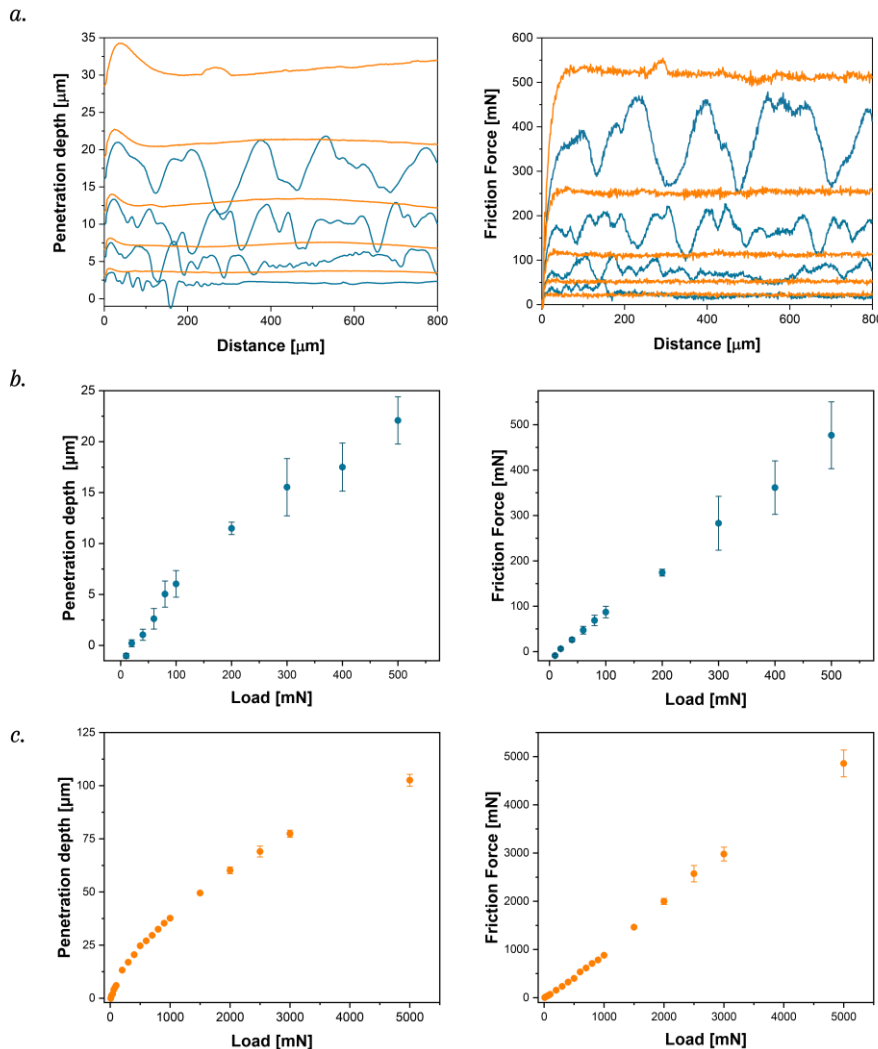


Figure 4.8. a) Penetration depth (left) and friction force (right) as a function of the distance of the scratch with loads of 50, 100, 200 and 400 mN for polystyrene (blue) and 50, 100, 200, 400 and 750 mN for polycarbonate (orange). A steadier friction force and penetration depth was observed for polycarbonate than for polystyrene. b) Penetration depth and friction force as a function of load for polystyrene. c) Penetration depth and friction force as a function of load for polycarbonate.

4.4 DISCUSSION AND CONCLUSIONS

Polystyrene is known to undergo brittle failure while polycarbonate is a more tough material.²⁷ When performing a tensile test polystyrene breaks at very low strains between 0 and 2% strain, while for polycarbonate 70-80 % strain can easily be reached.^{28,29} This difference can be explained by the post-yield intrinsic behavior of the material.²⁹ Both polymers show a decrease in stress after the yield point, which is known as strain softening of the polymer, resulting in localization of stress and strain. In polystyrene this localization is believed to initiate craze formation, while in polycarbonate the unstable behavior is counteracted by the strain hardening effect which in the increasing stress at higher strains leading to stable plastic deformation without initiation of macroscopic failure.^{27,29} In this study mechanochemistry was used to study the molecular origin of damage introduced by forces in polystyrene and polycarbonate.

Manual grinding of the polymer films showed mechanical activation of the mechanophores up to 5 %. Instrumental tests such as compression and tensile tests, did not result in measurable mechanophore activation. In both polycarbonate and polystyrene, if scission of the covalent bonds occurred during these tests, the bond breaking was extremely localized and hence undetectable by fluorescence spectroscopy. Sliding friction tests were performed at different normal forces and from these tests a clear difference in molecular origin of the mechanical behavior between polystyrene and polycarbonate was observed. Polystyrene showed mechanophore activation at a normal force of 100 mN and higher, and also formed crazes in the polymer material. Correlation of the fluorescence intensity pattern with the fluctuating friction force and penetration depth show that craze formation and bond breaking are closely related in polystyrene. The mechanophore in polycarbonate, however, was only activated at a normal force of 750 mN without the formation of visual cracks, suggesting that in the scratch tests, polycarbonate mainly undergoes plastic deformation with limited rupture of covalent bonds.

4.5 EXPERIMENTAL DETAILS

Chemicals were purchased from Sigma Aldrich, Merck, Cambridge Isotopes Laboratories or Biosolve and used as received unless stated otherwise. Bis(methyl salicyl) carbonate (BMSC, SABIC, 99+ %), bisphenol-A (BPA, SABIC, polymerization grade, > 99%) were kindly provided by SABIC. Styrene was purified on an aluminum plug prior to use. Dry solvents were obtained using the MBraun solvent purification system (MB SPS-800). *o*-DCB was

dried over mol sieves (4\AA). Reactions were monitored by either $^1\text{H-NMR}$ or thin-layer chromatography (TLC). $^1\text{H-NMR}$, $^{13}\text{C-NMR}$ spectra were recorded at room temperature using a 400 MHz Bruker UltrasShield Nuclear Magnetic Resonance spectrometer, in CDCl_3 or $\text{d}_6\text{-DMSO}$. Chemical shifts are given in ppm with tetramethyl silane (TMS, 0 ppm) as internal standard. Column chromatography was performed manually using silica (60-200 μm , 60 \AA) as stationary phase. Matrix assisted laser desorption/ionization-time of flight mass spectra (MALDI-TOF) were measured using a Bruker Autoflex Speed mass spectrometer using α -cyano-4-hydroxycinnamic acid (CHCA) or trans-2-[3-(4-tert-butylphenyl)-2-methyl-2-propenylidene]-maloneitrile (DCBT) as matrix. Size exclusion chromatography (SEC) was performed in tetrahydrofuran (THF) at 25 °C on a Shimadzu Prominence-I LC-2030C 3D equipped with a RID-20A detector and calibrated by narrow polystyrene standards. The following Mark-Houwink-Sakurada parameters were used to convert the polystyrene (PS) masses into polycarbonate (PC) masses: $K_{\text{PS}} = 1.41 \cdot 10^{-4} \text{ dL} \cdot \text{g}^{-1}$, $a_{\text{PS}} = 0.70$, $K_{\text{PC}} = 4.12 \cdot 10^{-4} \text{ dL} \cdot \text{g}^{-1}$, $a_{\text{PC}} = 0.69$.³⁰ Sonication experiments were performed at an amplitude of 25%. Polymers were dissolved in THF, transferred to a Suslick cell and cooled to 2 °C. While sonicating without pulse the solution was bubbled with methane.

Synthesis

N-[2-(2-bromoisobutyryloxy)ethyl]maleimide (M-Br): a 3-neck round bottom flask was equipped with bubbler, a septum and a cap. M-OH (2.50 g, 17.7 mmol) was dissolved in 100 mL dry DCM and triethylamine (2.84 mL, 20.41 mmol) was added under argon flow. The mixture was put on ice for 20 minutes and a solution of α -Bromoisobutryl bromide (2.52 mL, 20.41 mmol) in 30 mL dry DCM was added drop wise to the reaction mixture. The reaction was left for 3 hours and allowed to warm to room temperature. After the reaction the mixture was filtered and THF was evaporated, the obtained solid was redissolved in chloroform and washed with 5 % NaHCO_3 , demineralized water and brine subsequently. The chloroform fraction was dried *in vacuo*. The crude product was further purified by column chromatography over silica using 100% chloroform. M-Br was obtained as a white solid (64 % yield).

$^1\text{H-NMR}$ (400 MHz, CDCl_3): δ 6.73 (s, 2H), 4.33 (t, $J = 5.6$ Hz, 2H), 3.86 (t, $J = 5.3$ Hz, 2H), 1.89 (s, 6H).

$^{13}\text{C-NMR}$ (400 MHz, CDCl_3): δ 171.62, 170.33, 134.27, 62.89, 55.45, 36.60, 30.61.

Synthesis of 4-(anthracen-9-yl)phenyl 2-bromo-2-methylpropanoate (A-Br): To a 3 neck round bottom flask equipped with bubbler, a septum and a cap. A-OH (2.05 g, 7.3 mmol, 1 eq) was dissolved in 100 mL dry DCM and triethylamine (2.05 mL, 14.8 mmol, 2 eq) was added under argon flow. The mixture was put on ice for 20 minutes and a solution of α -Bromoisobutyryl bromide (1 mL, 8.8 mmol) in 30 mL dry DCM was added drop wise to the reaction mixture. The reaction was left for 3 hours and allowed to warm to room temperature. The crude product was further purified by flushing over a silica plug in 100% chloroform and recrystallization in MeOH. A-Br was filtered off and dried in vacuo resulting in 2.1 g off-white powder (67 % yield).

$^1\text{H-NMR}$ (400 MHz, DMSO-d6) : δ (ppm) = 8.49 (s, 1H), 8.05 (d, J = 8.51 2H), 7.65 (d, J = 8.51, 2H), 7.47 (m, 4H), 7.37 (m, 4H), 2.16 (s, 6H).

Synthesis of Diels-alder ATRP initiator (AM-2Br): N-[2-(2-bromoisobutyryloxy) ethyl]maleimide (1.71 g, 5.9 mmol) and 4-(anthracen-9-yl)phenyl 2-bromo-2-methylpropanoate (2.48 g, 5.9 mmol) were added to an oven dried 250 mL round bottom flask. The reactants were dissolved in 82 mL of 3:1 toluene: isopropyl alcohol (v/v). The reaction mixture was heated to 120 °C and reacted for 2 days under reflux while stirred. After the reaction the solvent was evaporated in a rotary evaporator. The obtained crude product was further purified via column chromatography (Silica, 2:1 hexane:EtOAc (v/v)). Two fractions were obtained and the second fraction containing the product was further purified via column chromatography (Silica, 2:1 hexane:EtOAc (v/v)). After evaporation of the solvent and drying in the vacuum oven AM-2Br was obtained in the form of white needles (80 % yield).

$^1\text{H-NMR}$ (400 MHz, CDCl₃): δ 8.11 (s, 1H), 7.51 – 7.29 (m, 5H), 7.25 – 7.13 (m, 4H), 7.03 (td, J = 7.6, 1.3 Hz, 1H), 6.48 (d, J = 7.7 Hz, 1H), 4.87 (d, J = 3.0 Hz, 1H), 3.90 (d, J = 8.4 Hz, 1H), 3.70 – 3.51 (m, 2H), 3.44 – 3.20 (m, 3H), 2.14 (s, 6H), 1.88 (s, 3H), 1.86 (s, 3H).

$^{13}\text{C-NMR}$ (400 MHz, CDCl₃): δ 175.79, 174.88, 170.26, 150.12, 140.12, 138.31, 127.26, 127.12, 126.89, 126.52, 125.51, 125.24, 125.10, 123.42, 61.97, 55.98, 55.62, 55.44, 49.12, 47.19, 46.13, 36.68, 30.70. Maldi-TOF MS: calculated m/z (M+Na)⁺: 732.04 found 731.99.

PSS and PSL - Free radical polymerization:

A flame dried Schlenk flask was charged with styrene, toluene and AIBN and kept on ice to avoid initiation of the polymerization. The reaction mixture was bubbled with argon for 20 minutes and afterwards heated to 75 °C. The reaction was left stirring under inert atmosphere overnight. The viscous reaction mixture was precipitated as a polymer into

MeOH and the polymer was isolated via filtration and dried at 40 °C under vacuum. Details for the polymerizations are shown in **Table 4.3**.

Table 4.3. Reaction conditions for the free radical polymerization of polystyrene

Polymer	Styrene	Toluene	AIBN	m	M _n ^a (g·mol ⁻¹)	D ^b
SS	33 mL	67 mL	32 mg	9.9 g	107·10 ³	1.8
PSL	48 mL	12 mL	1 mg	16.4 g	560·10 ³	1.9

^a Number-average molar mass as determined by SEC, ^b D ≡ M_w/M_n as determined by SEC.

PS1-PS3 - SET-LRP:

A flame dried schlenk flask was charged with AM-2Br (0.10 g, 0.14 mmol), copper(II)bromide (1.62 mg, 0.007 mmol), styrene and toluene. The reaction mixture was put on ice and bubbled with argon for 20 minutes. A 5 cm copper wire (Cu⁰) was wound around a tweezer tip and activated by immersing it in pure HCl for 30 seconds, rinsing twice demineralized water followed by acetone. 10µL N,N,N',N'',N'''-pentamethyldiethyleentriamine (0.35 eq) was added to the reaction mixture and. The reaction was followed by SEC and stopped when the desired molar mass was reached, or the dispersity started to increase. The viscous reaction mixture was filtered over basic alumina to remove the copper and afterwards the polymer was precipitated in MeOH. The resulted precipitate was filtered and dried in a vacuum oven (40 °C) overnight, obtaining a white solid.

Table 4.4. Reaction conditions for the SET-LRP PS1-PS3

Polymer	Styrene	Toluene	Reaction time	m	M _n ^a (g·mol ⁻¹)	D ^b
PS1	22.5 mL	20 mL	69 hours	2.4 g	32·10 ³	1.2
PS2	48 mL	0	76 hours	10.8 g	66·10 ³	1.5
PS3	48 mL	0	96 hours	12.9 g	109·10 ³	1.2
PS4	12.2 mL	11.5 mL	72 hours	-	51·10 ³	1.4
PS5	24 mL	0	72 hours	5.3 g	102·10 ³	1.3

^a Number-average molar mass as determined by SEC, ^b D ≡ M_w/M_n as determined by SEC.

PC – solution transcarbonation

A flame dried Schlenk flask was charged with BPA (5.1 g, 22.3 mmol), BMSC (6 g, 22.5 mmol) and NaOH (2 mg, 1.8). This solid mixture was flushed with argon and 48 mL of *ortho*-dichlorobenzene (*o*-DCB) was added. The resulting reaction mixture was heated to 60 °C while stirring under argon. After 28 hours the reaction was left to cool to room temperature overnight. A viscous white gelly mixture was obtained. Chloroform was added to dilute to a transparent viscous mixture and afterwards the polymer was precipitated into a 15-fold excess of *n*-hexane. The resulting white polymer was collected by filtration and dried in a vacuum oven at 40 °C overnight. Afterwards the polymer (3 g) was redissolved in *o*-DCB at 120 °C and AM-2OH (33 mg, 0.08 mmol) was added. The reaction mixture was stirred overnight at 120 °C under inert atmosphere. Then the mixture was left to cool to room temperature overnight and precipitated in 15-fold excess of *n*-hexane to obtain PC as a white solid.

Solvent casting polystyrene

1.25 g of PS was dissolved in 5 mL of toluene and cast into an aluminum mold with a diameter of 4 cm. The films were slowly dried under a nitrogen flow in an oven to avoid bubble formation. The film was left at room temperature overnight and another night at 35 °C. Then the temperature was increased by 5 °C per hour and the sample was left overnight at 65 °C. Afterwards the temperature was again increased stepwise to 105 °C and after 1 hour the samples were put under vacuum oven for the last drying for 12 hours.

Solvent casting polycarbonate

1.35 g of PC was dissolved in 9 mL DCM and cast into an aluminum mold with a diameter of 7.5 mm. The film was dried in the nitrogen oven overnight at room temperature. Afterwards the temperature was increased to 45 °C and the film was left overnight. Afterwards the film was put into a vacuum oven at 105 °C for 12 hours.

Sliding friction experiments tests

Single-asperity sliding friction experiments were performed on a CSM Micro Indentation Tester. A defined normal load and sliding velocity are applied to the sample and the surface penetration and lateral force are measured. A conical, diamond indenter tip geometry, with a cone angle of 90° and a top radius of 10 µm was used to apply normal loads ranging from 50 to 4000 mN. Two rotational motors control the linear, in-plane motion and are able to apply sliding velocities over three decades of magnitude. Scratch tests with a length of 0.8 mm and 1 mm were performed at scratch velocities 10 and µm/s,

all at room temperature. Each combination of sliding velocity and normal force is applied at least three times to check reproducibility of the steady-state penetration depth and friction force.

Indentation tests

Indentation tests were performed on a Nano Indentor machine equipped with a cylindrical 10 µm flat punch. Load controlled experiments were performed at a loading rate of 1 mN/s. Maximum loads were varied between 10 mN and 200 mN and all indents were performed in threefold.

Heating experiments

The thermal stability for the polymeric mechanophores was determined in of $6 \cdot 10^{-4}$ M in *o*-DCB. Samples were heated to 100 °C, 130 °C and 150 °C, the solvent was evaporated and redissolved in THF ($1.5 \cdot 10^{-4}$ M). Samples were diluted 100 times before recording the spectra.

4.6 REFERENCES

1. Dry, C. Procedures Developed for Self-Repair of Polymer Matrix Composite Materials. *Compos. Struct.* **1996**, *35*, 263–269.
2. Dry, C.; McMillan, W. A Novel Method to Detect Crack Location and Volume in Opaque and Semi-Opaque Brittle Materials. *Smart Mater. Struct.* **1997**, *6*, 35–39.
3. Awaja, F.; Zhang, S.; Tripathi, M.; Nikiforov, A.; Pugno, N. Cracks, Microcracks and Fracture in Polymer Structures: Formation, Detection, Autonomic Repair. *Prog. Mater. Sci.* **2016**, *83*, 536–573.
4. Azadi, M.; Saeedi, M.; Mokhtarishirazabad, M.; Lopez-Crespo, P. Effects of Loading Rate on Crack Growth Behavior in Carbon Fiber Reinforced Polymer Composites Using Digital Image Correlation Technique. *Compos. Part B Eng.* **2019**, *175*, 107161.
5. Pang, J. W. C.; Bond, I. P. A Hollow Fibre Reinforced Polymer Composite Encompassing Self-Healing and Enhanced Damage Visibility. *Compos. Sci. Technol.* **2005**, *65*, 1791–1799.
6. Clarijs, C. C. W. J.; Kanters, M. J. W.; van Erp, M. J.; Engels, T. A. P.; Govaert, L. E. Predicting Plasticity-Controlled Failure of Glassy Polymers: Influence of Stress-Accelerated Progressive Physical Aging. *J. Polym. Sci. Part B Polym. Phys.* **2019**, *57*, 1300–1314.
7. Meijer, H. E. H.; Govaert, L. E. Mechanical Performance of Polymer Systems: The Relation between Structure and Properties. *Prog. Polym. Sci.* **2005**, *30*, 915–938.
8. Yuan, Y.; Chen, Y. Ian. Visualized Bond Scission in Mechanically Activated Polymers. *Chinese J. Polym. Sci.* **2017**, *35*, 1315–1327.
9. Caruso, M. M.; Davis, D. A.; Shen, Q.; Odom, S. A.; Sottos, N. R.; White, S. R.; Moore, J. S. Mechanically-Induced Chemical Changes in Polymeric Materials. *Chem. Rev.* **2009**, *109*, 5755–5798.
10. Li, M.; Zhang, Q.; Zhou, Y. N.; Zhu, S. Let Spiropyran Help Polymers Feel Force! *Prog. Polym. Sci.* **2018**, *79*, 26–39.
11. Boulatov, R. *Polymer Mechanochemistry*; Springer: Switzerland, 2015; Vol. 53.
12. Davis, D. A.; Hamilton, A.; Yang, J.; Cremar, L. D.; Van Gough, D.; Potisek, S. L.; Ong, M. T.; Braun, P. V.; Martínez, T. J.; White, S. R.; Moore, J. S.; Sottos, N. R. Force-Induced Activation of Covalent Bonds in Mechanoresponsive Polymeric Materials. *Nature* **2009**, *459*, 68–72.
13. Chen, Y.; Spiering, A. J. H.; Karthikeyan, S.; Peters, G. W. M.; Meijer, E. W.; Sijbesma, R. P. Mechanically Induced Chemiluminescence from Polymers Incorporating a 1,2-Dioxetane Unit in the Main Chain. *Nat. Chem.* **2012**, *4*, 559–562.
14. Yoshie, N.; Saito, S.; Oya, N. A Thermally-Stable Self-Mending Polymer Networked by Diels-Alder Cycloaddition. *Polymer* **2011**, *52*, 6074–6079.
15. Lakowicz, J. R. *Principles of Fluorescence Spectroscopy*, 3rd ed.; Springer: Baltimore, **2006**.
16. Göstl, R.; Sijbesma, R. P. Π -Extended Anthracenes As Sensitive Probes for Mechanical Stress. *Chem. Sci.* **2016**, *7*, 370–375.

- 4
17. Beiermann, B. A.; Kramer, S. L. B.; Moore, J. S.; White, S. R.; Sottos, N. R. Role of Mechanophore Orientation in Mechanochemical Reactions. *ACS Macro Lett.* **2012**, *1*, 163–166.
 18. Beiermann, B. A.; Davis, D. A.; Kramer, S. L. B.; Moore, J. S.; Sottos, N. R.; White, S. R. Environmental Effects on Mechanochemical Activation of Spiropyran in Linear PMMA. *J. Mater. Chem.* **2011**, *21*, 8443–8447.
 19. Kim, J. W.; Jung, Y.; Coates, G. W.; Silberstein, M. N. Mechanoactivation of Spiropyran Covalently Linked Pmma: Effect of Temperature, Strain Rate, and Deformation Mode. *Macromolecules* **2015**, *48*, 1335–1342.
 20. Vidavsky, Y.; Yang, S. J.; Abel, B. A.; Agami, I.; Diesendruck, C. E.; Coates, G. W.; Silberstein, M. N. Enabling Room-Temperature Mechanochromic Activation in a Glassy Polymer: Synthesis and Characterization of Spiropyran Polycarbonate. *J. Am. Chem. Soc.* **2019**, *141*, 10060–10067.
 21. Kamps, J. H.; Groote, R.; Baus, M.; Vermeulen, H.; Hoeks, T.; van der Heijden, R.; Sijbesma, R. P.; Heuts, J. P. A. Activated Carbonates: Enabling the Synthesis of Differentiated Polymers via Solution Carbonation. *Eur. Polym. J.* **2020**, *135*, 109901.
 22. Wool, R. P. Polymer Entanglements. *Macromolecules* **1993**, *26*, 1564–1569.
 23. Odell, J. A.; Muller, A. J.; Narh, K. A.; Keller, A. Degradation of Polymer Solutions in Extensional Flows. *Macromolecules* **1990**, *23*, 3092–3103.
 24. May, P. A.; Moore, J. S. Polymer Mechanochemistry: Techniques to Generate Molecular Force via Elongational Flows. *Chem. Soc. Rev.* **2013**, *42*, 7497–7506.
 25. Ruvolo-filho, A.; Murakami, M. M. Transport Properties of Water in Glassy Polycarbonate Films. Effects of the Processing and Thickness. *J. Macromol. Sci. - Phys.* **1998**, *37*, 627–643.
 26. Su, Y.; Ran, S.; Fang, Z.; Guo, Z. Fullerene-Induced Crystallization toward Improved Mechanical Properties of Solvent Casting Polycarbonate Films. *Appl. Phys. A Mater. Sci. Process.* **2020**, *126*, 293.
 27. Looijmans, S. F. S. P.; de Bie, V. G.; Anderson, P. D.; van Breemen, L. C. A. Hydrostatic Stress as Indicator for Wear Initiation in Polymer Tribology. *Wear* **2019**, *426–427*, 1026–1032.
 28. Milisavljević, J.; Petrović, E.; Ćirić, I.; Mančić, M.; Marković, D.; Dordević, M. Tensile Testing for Different Types of Polymers. *29th DANUBIA-ADRIA Symp. Adv. Exp. Mech. DAS 2012* **2012**, No. September, 266–269.
 29. Smit, R. J. M.; Brekelmans, W. A. M.; Meijer, H. E. H. Predictive Modelling of the Properties and Toughness of Polymeric Materials: Part I Why Is Polystyrene Brittle and Polycarbonate Tough? *J. Mater. Sci.* **2000**, *35*, 2855–2867.
 30. Mori, S.; Barth, H. G. *Size Exclusion Chromatography*; Springer-Verlag, **1999**.

Chapter 5

Investigation of interfacial stresses in composites using mechanofluorescent silica fillers

| ABSTRACT |

Silica particles of 200 nm were synthesized via a Stöber method in which the amount of solvent was changed to tune the diameter of the particles. The π -extended anthracene - maleimide Diels-Alder mechanophore was linked to the silica particles via a three-step synthesis. Successful functionalization was confirmed using heating and sonication experiments in solution. Composite films were solvent cast and tensile test were performed. Activation of the mechanophore was studied using fluorescence microscopy and a clear increase in fluorescence as a consequence of mechanical activation was observed at a strain of 0.025, which is much lower than the strain of 0.2 at which debonding was observed in SEM. Hence stresses and rupture of covalent bonds at the surface of the particles was shown to be the molecular origin of debonding of the particles with the interface.

The work in this chapter was performed in collaboration with Martijn Scholten.

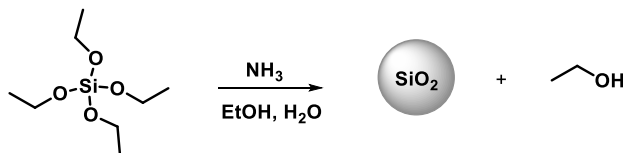
5.1 INTRODUCTION

Due to their unique mechanical properties, composites are increasingly being used in demanding applications and it is of great importance to understand the effect of relatively high and recurring forces on their performance. Silica particles are particulate fillers that are often added to thermosets and thermoplastics to improve their mechanical properties.¹⁻³ Polycarbonate is a widely industrially applied polymer due to its excellent mechanical and thermal stability and its transparency, and its properties have been further enhanced by filling with silica particles.⁴ The addition of hard phase particulate fillers to polymers results in toughening or strengthening. Toughening requires a good interaction between the polymer matrix and the filler because mechanical energy is dissipated at the interface between matrix and filler.^{2,5,6} When small particles with a large surface to volume ratio are added to a polymer, the mechanical properties of the composite are improved. The relation between particle loading and enhancement of mechanical properties is complex, but a general trend is that after initial increase, mechanical properties decrease beyond a certain particle loading. Many studies on the failure of polymer composites have led to competing theories to explain this behavior.⁷⁻⁹ Particle agglomeration in highly filled polymers leads to stress concentration in the composite which causes debonding of the particles and failure of the composite material.^{5,10,11} Additionally one of the options is that yielding of the matrix results in final failure. In order to study the localization of stresses and the ultimate origin of failure, the interaction between fillers and matrix need to be investigated at the molecular level. Mechanophores can play an important role in such studies; they can covalently connect matrix to filler and visualize the early stages of void formation around the particles. If matrix yielding is a relevant mechanism of failure of composites, the mechanism can be studied by incorporating mechanophores in the polymer matrix. Both pathways of mechanophore activation can be compared and give additional information of the failure modes in polycarbonate composites. In this chapter we focus on studying matrix-filler interactions using silica fillers functionalized with mechanofluorescent groups in a polycarbonate matrix.

5.2 SYNTHESIS OF MECHANOFLUORESCENT SILICA FILLERS

Synthesis of silica particles

Silica particles with a size of 200 nm were synthesized via an adapted Stöber method (**Scheme 5.1**).¹² Since the Stöber method is sensitive to small changes in temperature and concentration, the particle size can be tuned very precisely.^{13,14} In the current work, the amount of solvent was used to tune the particle diameter using the size-solvent relationship shown in **Figure 5.1a**.¹⁵ Silica particles with different sizes were synthesized by varying the volume of ethanol, but fixing all other reaction conditions. The volume ratio of TEOS : H₂O : NH₃ (25%) was kept to 6 ml : 3 ml : 8 ml and all reactions were performed at 60 °C for 2h. Particle sizes between 100 and 350 nm were obtained by varying the amount of ethanol from 78 to 130 mL. The results are shown in **Figure 5.1b**.



Scheme 5.1: Synthetic scheme of the silica particle synthesis.

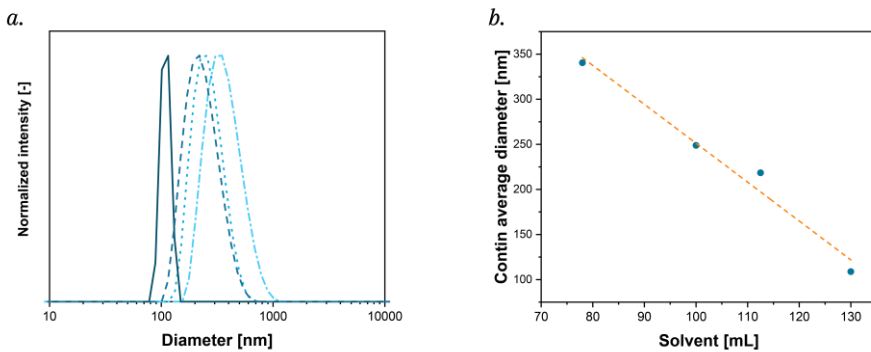


Figure 5.1. a) Size distribution for silica particles synthesized by varying the amount of ethanol. b) Average diameter of silica particles obtained at different concentrations of ethanol.

Silica particles with a diameter of 200 nm were synthesized using this modified Stöber method at 60 °C.¹⁵ The size of the particles was determined with dynamic light scattering (DLS) and confirmed by Scanning Electron Microscopy (SEM). According to the fit shown in **Figure 5.1b**, 112 mL of solvent was required to obtain particles with a diameter of 200 nm. Under SEM the particles are spherical and relatively monodisperse with an average diameter of 196 ± 12 nm. DLS gave a slightly higher average diameter of 218 nm.

The difference is attributed to the fact that SEM measures the number average particle diameter while for DLS the diameter is measured as an intensity related average.

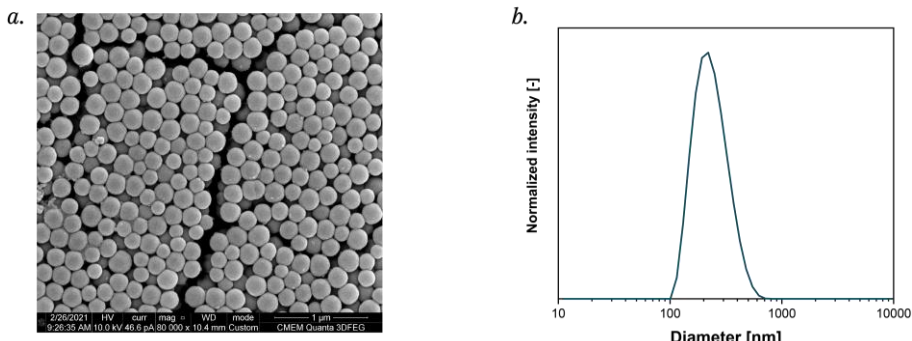
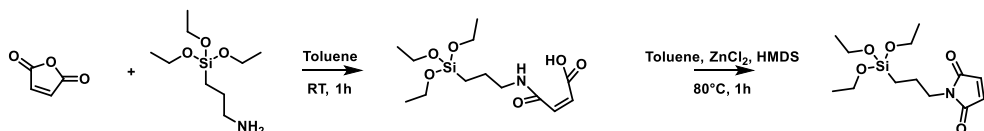


Figure 5.2. a) SEM image of silica particles synthesized with the modified Stöber method. Average size is 196 ± 12 nm determined of a population with 188 particles b) DLS of the particles measured in ethanol with an average diameter is 218 nm.

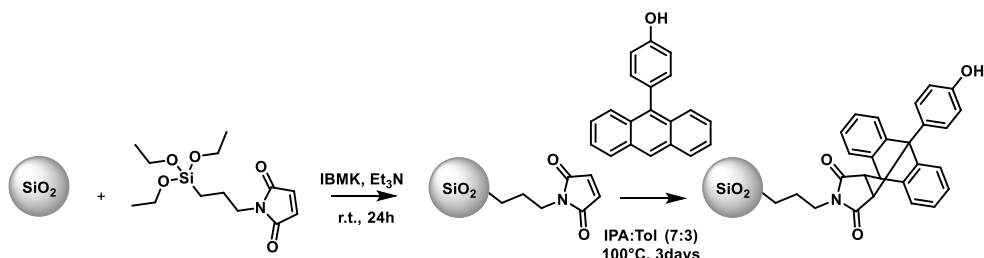
Surface functionalization

In order to use the silica particles as stress reporters, they were surface-functionalized with a mechanophore. The most straightforward method to functionalize silica nanoparticles is with a triethoxy silane derivative.¹⁶ To this end, maleic anhydride was silane-functionalized in a one-pot, two step reaction (**Scheme 5.2**). Ring opening of maleic anhydride with 3-(aminopropyl)triethoxysilane at room temperature was followed by ring closure of the maleimide with the aid of hexamethyldisilazane (HMDS) at 80°C.



Scheme 5.2. Synthetic pathway towards the silane functionalized maleimide.

Silane functionalized maleimide was used to functionalize the 200 nm silica particles in isobutyl methyl ketone (IBMK) (**Scheme 5.3**) using triethyl amine as a base.



Scheme 5.3. Synthetic overview of the functionalization of silica particles.

The mechanophore was formed in a Diels-Alder reaction between 9-(4-hydroxyphenyl) anthracene (synthetic details see *Chapter 2*) and maleimide on the surface of the particles. Covalent attachment of the mechanophore to the surface was estimated with thermogravimetric analysis (TGA) and heating experiments in solution. TGA measurements were performed to determine the difference in weight loss for both the unfunctionalized and functionalized silica particles (**Figure 5.3a**). An increase in weight loss was observed for SiP-Mal, indicating that the first functionalization step was successful. In contrast, for the SiP-DA particles no clear increase was observed and thus TGA did not prove successful functionalization of the nanoparticles. Therefore an additional heating experiment in solution was performed.

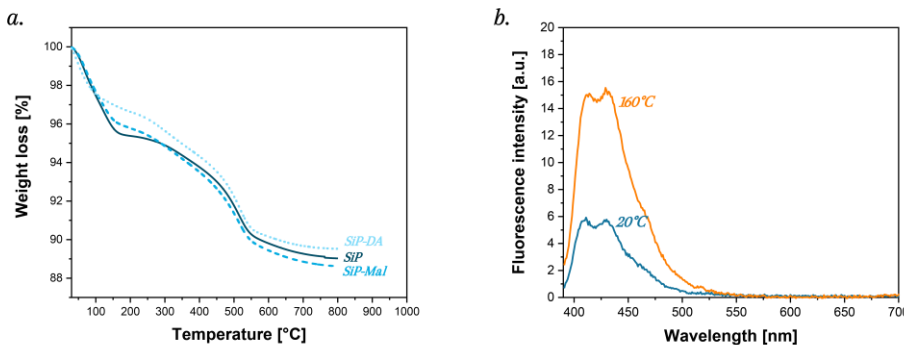


Figure 5.3. a) TGA traces for both unfunctionalized (SiP) and functionalized (SiP-Mal and SiP-DA) silica particles. b) Fluorescence intensity spectra for the heating experiment. The fluorescence intensity increased upon heating.

Heating of a particle dispersion in *ortho*-dichlorobenzene to 160°C for 1 hour resulted in a significant increase in fluorescence intensity due to the release of the fluorescent anthracene by the retro-Diels-Alder reaction (**Figure 5.3b**). The sample kept at room temperature showed a fluorescence background due to residual free 9-(4-hydroxyphenyl) anthracene in the sample.

Elongation of the mechanophore with polycarbonate

In order to optimize the interaction between the particles and the polymer matrix, the mechanophores were extended with polycarbonate chains. A polycarbonate prepolymer with a number-average molar mass of $M_n = 26.8 \cdot 10^3 \text{ g} \cdot \text{mol}^{-1}$ (synthetic details see *Chapter 2*) was reacted in dry THF with the Diels-Alder adduct on the surface of the

silica particles in the presence of NaOH at 65 °C for 5 days. The particles were isolated by centrifugation and thoroughly washed with THF. TGA was measured and a small increase in the weight loss was observed compared to the SiP-DA particles (**Figure 5.4a**), indicating that the polycarbonate coupling was successful to a small extent. Additional confirmation for successful functionalization was obtained by ultra sonication of a SiP-DAPC particle dispersion in THF and it was used to measure increased fluorescence by the mechanochemical effects of cavitation on the polymer chains that result in rupture of the mechanophore (**Figure 5.4b**). Ultrasonication of the polycarbonate functionalized particles resulted in a clear increase of the fluorescence emission, whereas no activation of the SiP-DA precursor was observed (**Figure 5.4b**). This observation confirms successful functionalization of the particles with polycarbonate.

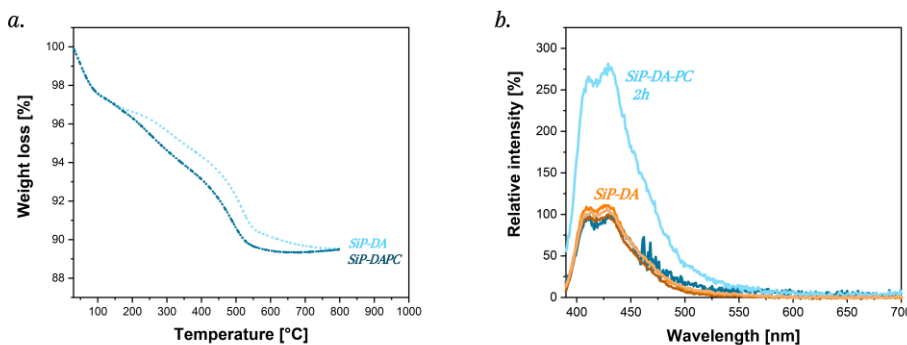


Figure 5.4. a) TGA traces normalized for the mass at 200°C. Polycarbonate functionalized particles (SiP-DA-PC) show a relatively small increased weight loss compared to SiP-DA. b) Fluorescence intensity spectra for sonication experiments. An increase in fluorescence was observed for the PC functionalized particles (SiP-DA-PC).

A calibration curve was measured in both toluene and THF to estimate the average amount of activated anthracenes being released from the surface (**Figure 5.5**) for both heating and sonication experiments. For the estimation of released anthracenes by heating, a calibration curve in toluene was used, while for the sonication experiments a calibration curve in THF was used to determine the released anthracene molecules. Heating experiments (**Figure 5.3b**) were estimated to release 83 anthracene molecules per particle while after functionalization with polycarbonate, this number was reduced to 9 anthracene moieties per particle released after sonication (**Figure 5.4b**). This clearly shows that functionalization of the particles was successful but only to a low extent.

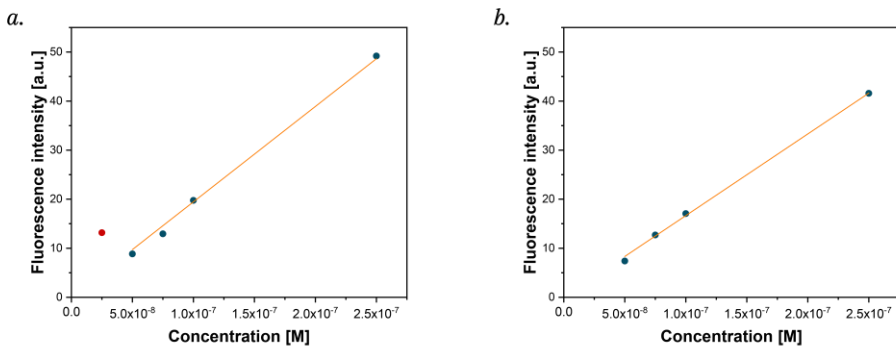


Figure 5.5. Calibration curves measured in a) toluene and b) THF to estimate the number of released anthracene molecules per particle. Toluene was used for the estimation from heating, while THF was used for the estimation after sonication. These curves were used to estimate the concentration of released anthracene molecules.

5.3 COMPOSITE FILMS

Solvent casting of polycarbonate films was a challenge because solvent-induced crystallization occurred under many casting conditions.^{17,18} Opaque and non-planar films were obtained when films thicker than 210 µm were dried.

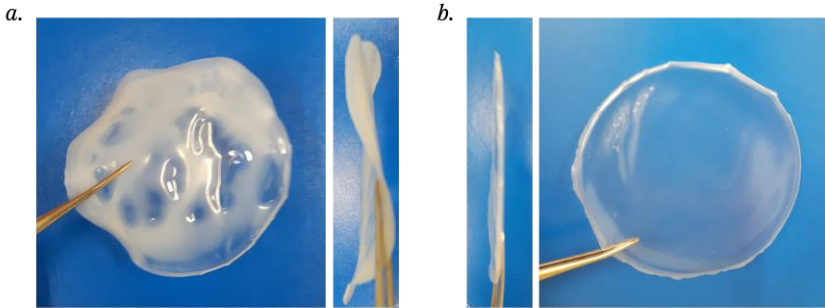


Figure 5.6. Illustrations of the solvent cast polycarbonate films. a) 1.25 g in 7 ml (179 g/L) DCM, cast at 25 °C. b) 0.85 g in 6.7 ml (127 g/L) DCM cast at 25 °C, a transparent film with a thickness of 150-195 µm was obtained.

Figure 5.6 shows a sample cast from a 179 g/L solution of polycarbonate in dichloromethane with large inhomogeneities in thickness. When casting a thinner film from a 127 g/L solution, a thin, flat and transparent film was obtained. Although literature

reports claim that transparent films of polycarbonate were obtained at elevated temperatures, in this work all films were cast at 25 °C under nitrogen flow.

The maximum thickness that could be obtained without crystallization spots was around 200 µm. In general, the addition of silica particles to the polymer resulted in more turbid films caused by facilitation of crystallization by the particles and by the formation of large aggregates of particles. In order to maintain sufficient transparency, the thickness of the films needed to be reduced to around 50 µm, and the content of silica fillers had to be limited to 5 to 15 weight percent. The total amount of composite per film was reduced, and thinner films with large aggregates were obtained. Aggregate free films were obtained by sonicating the solutions in an ultrasonic bath for one hour before casting. **Figure 5.7a** is a SEM image of the composite cast from the untreated solution, which contains large particle aggregates, whereas a film cast from a sonicated solution did not contain large aggregates (**Figure 5.7b**)

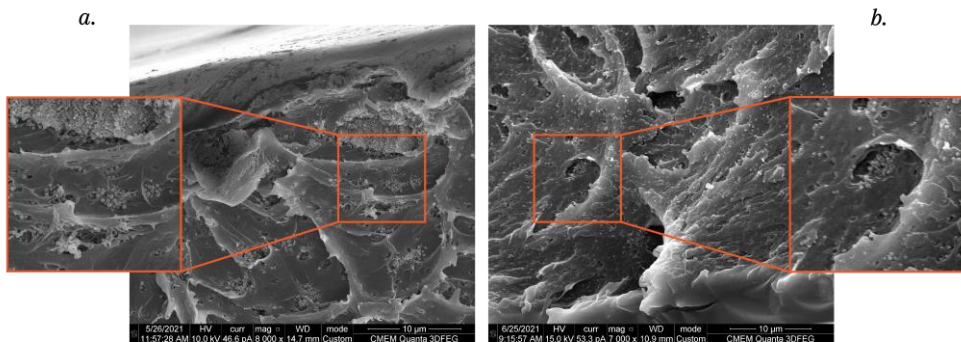


Figure 5.7. SEM images of a solvent cast polycarbonate film with 5 weight percent of the silica fillers a) before sonication b) after sonication of the solution prior to casting. Both images have a square insert of 10 µm.

5

5.4 STRESSES IN A POLYCARBONATE COMPOSITE

Solvent cast films with a thickness of 40-60 µm containing 5-15 wt% of mechanofluorescent silica particles were subjected to tensile testing on dogbone shaped samples. Tensile tests were performed at a strain rate of 0.001 s⁻¹ and stopped at strains of 0.025, 0.05, 0.1, 0.2, 0.4, 0.8 and at break to determine activation of the mechanophores (**Figure 5.8a-c**).

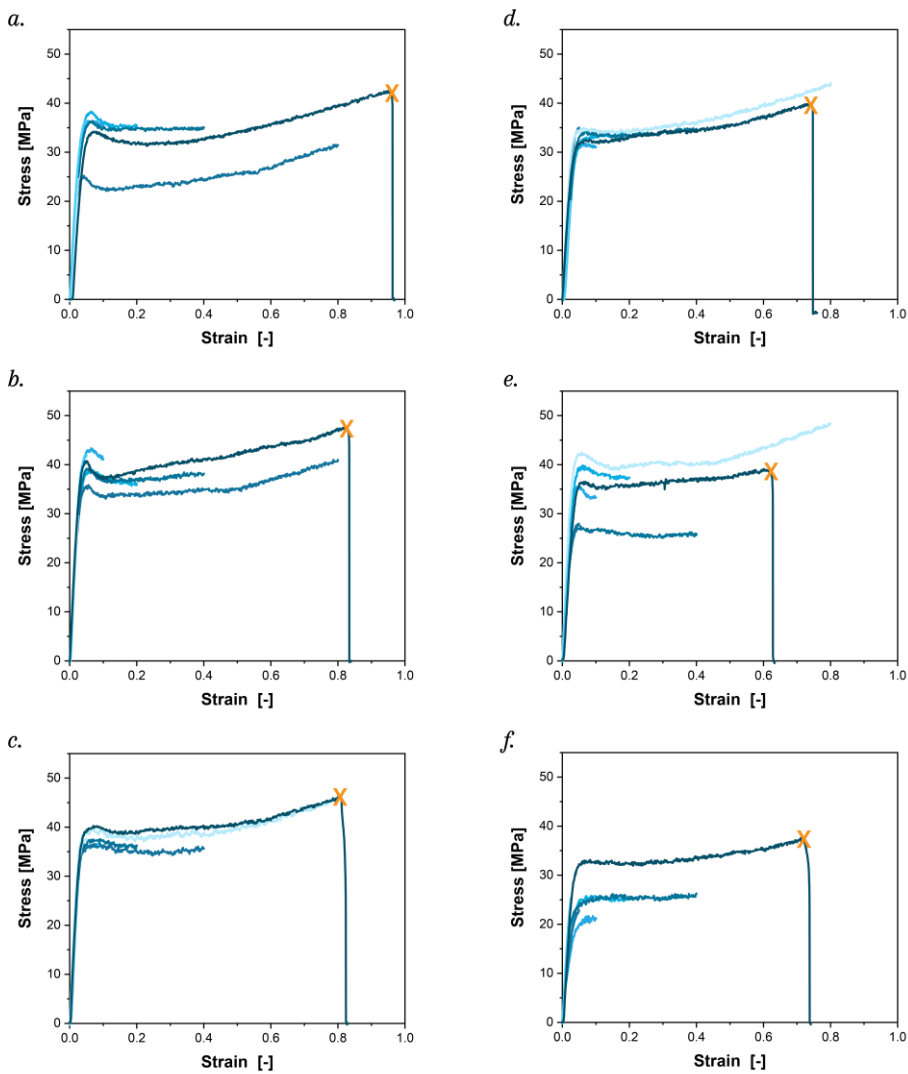


Figure 5.8. Stress-strain curves for different composites strained at 0.001 s^{-1} : a) 5 wt% SiP-DAPC, b) 10 wt% SiP-DAPC, c) 15 wt% SiP-DAPC and d) 5 wt% SiP, e) 10 wt% SiP, f) 15 wt% SiP. Different colors illustrate the measurements for one type of composite stopped at different strains or break (from light to dark blue with increasing strain). The cross (X) represents the strain at which the sample breaks.

As control experiments, films containing silica particles without mechanophore were tested (**Figure 5.7 d-f**). An overlay of all tensile tests per film is shown in **Figure 5.8 a-f**. Different colors show the experiments stopped at different strains (from light to dark blue with increasing strain) and measurement with orange cross (X) represents the sample

strained until break. Since all samples were stamped from the same composite film, the tensile curves were expected to overlap, but this was not the case. The overall shape of the curves was observed to be similar for most of the samples, which is dominated by the polycarbonate matrix of the composite. The yield stress and Young's modulus, however, fluctuates significantly for most of the composite films except for SiP-5 wt% (**Figure 5.8d**). These variations might be caused by small particle clusters in the composite film or a slightly variable thickness in the film. Unfilled polycarbonate was measured to have a yield stress of 50 MPa, which is higher compared to the filled systems. This shows that there is no improvement of the mechanical properties of the composites which is in contrast with literature that reports an increase in both the yield stress and Young's modulus.¹⁹ The fact that the moduli and yield point were lower than in the parent polycarbonate can be attributed to artefacts in the polymer composites due to solvent casting or due to the low functionalization degree of the particles resulting in a weak interaction between the particle and the polymer matrix. When the interaction is poor, voids can form at the interface resulting in a decrease in mechanical properties.

A consistent trend that was observed in all silica filled samples was that they became opaque at strains larger than of 0.1 or 0.2. **Figure 5.9** illustrates the gradual whitening of the samples, whereas unfilled polycarbonate remained fully transparent upon straining.

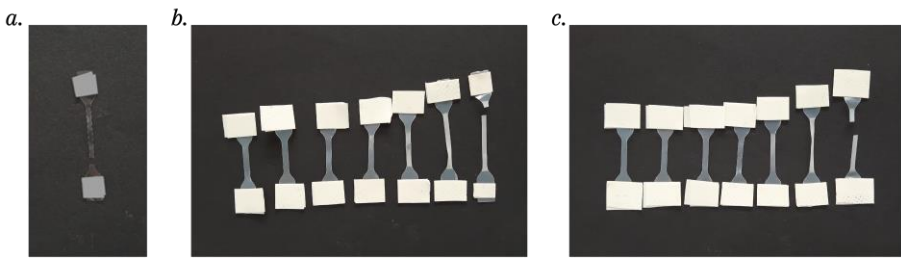


Figure 5.9. Illustration of the whitening of the samples upon straining. a) Unfilled polycarbonate remains transparent. An increase in opaqueness was observed for both b) filled polycarbonate with b) 5% SiP and c) 5% SiP-DAPC. For the other polycarbonate composites a similar trend was observed.

More insight in the whitening mechanism was obtained by imaging the tensile bars with SEM. A part from the middle of the tensile bar was cut for imaging of the surface at different strains and the samples at break were imaged at both the cross section and the surface. All samples at break showed voids around the particles and a significant increase of void size with strain was observed (**Figure 5.10**). Debonding starts to be visible in SEM

at a strain of 0.2. The nanometer displacement of the polymer at the particle interface at these strains is larger than needed for activation of the mechanophores which is therefore expected to happen at strains well below 0.2.

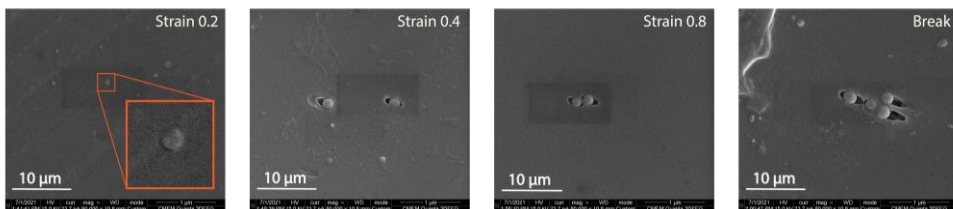


Figure 5.10. Illustration of the increasing debonding of the silica particles from the matrix with increasing strain at 0.2, 0.4, 0.8 and break in 15 wt% SiP-DAPC filled polycarbonate films.

Mechanophore activation was studied with fluorescence microscopy. If debonding of the particles occurs, release of fluorescent anthracene is expected. After applying strains 0.025, 0.05, 0.1, 0.2 or 0.4, the center part of the functionalized composite samples was cut and placed between two glass plates for imaging. At higher strains, light could not penetrate into the films due to the whitening of the samples (**Figure 5.11**), and useful fluorescence images could not be obtained.

Experiments were performed for both the unfunctionalized SiP composites and the functionalized SiP-DAPC composites at various particle loadings. Background intensity correction was performed and for the SiP no intensity or increase in fluorescence was observed with strain, whereas a higher intensity for strained than for unstrained SiP-DAPC samples was measured. However no clear increase in intensity with strain was observed. This suggests the start of debonding of the matrix and the nanoparticles occurred before 0.025 strain was reached, which was before the yield point of the composite materials (**Figure 5.8**). Since forces in composites are transduced across the Interface and SiO_2 particles can act as stress concentrators, even at low strains the interface can experience high stresses compared to the polymer matrix.²⁰

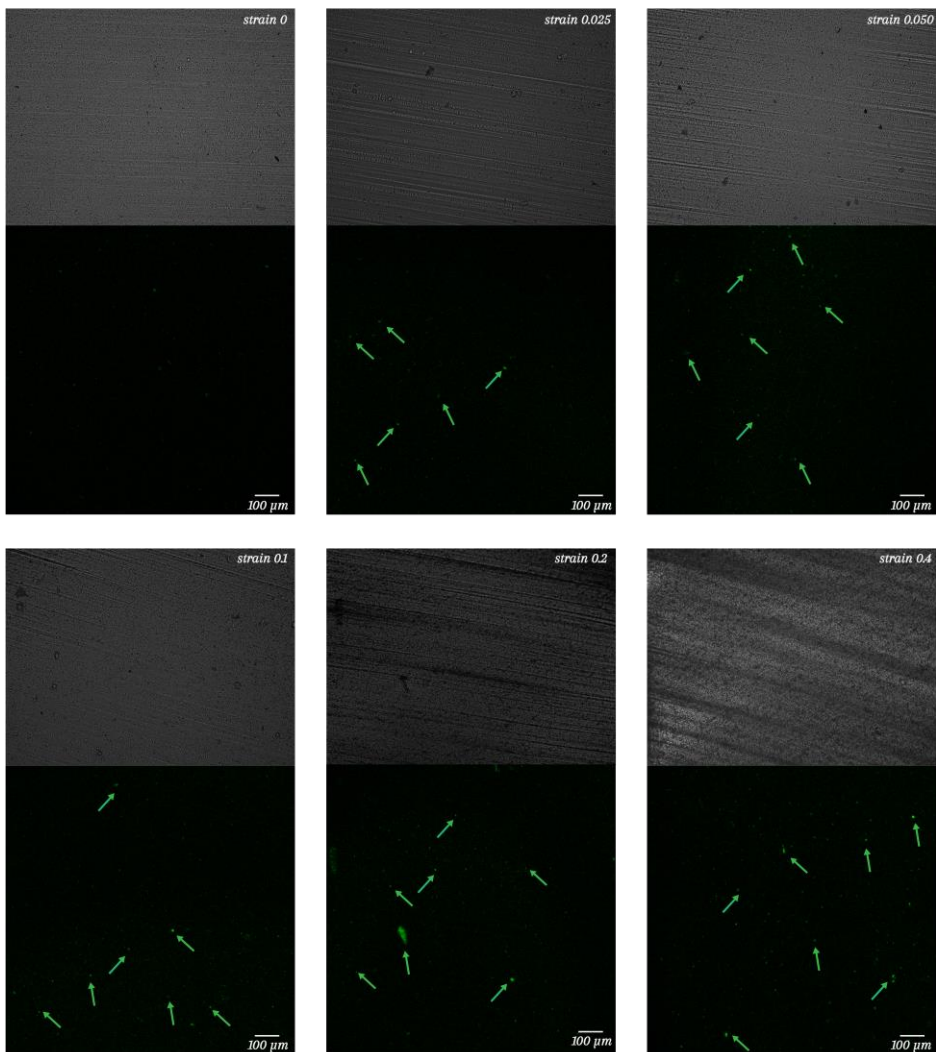


Figure 5.11. Bright field and fluorescence microscope images for 15 wt% SiP-DAPC filled polycarbonate at different strains: a) no strain, b) 0.025 strain, c) 0.05 strain, d) 0.1 strain, e) 0.2 strain and f) 0.4 strain. The green arrows point towards the fluorescent spots in the image.

5.5 CONCLUSIONS

In conclusion, a better understanding of the molecular origin of debonding at the filler interface was created using mechanoﬂuorescent silica ﬁllers. Silica particles with the desired size of 200 nm diameter were synthesized via a Stöber method in which the concentration of TEOS was changed to tune the diameter of the particles. The particles were successfully functionalized with the mechanophore on the surface and used to prepare composites. Straining of the composites in a tensile test resulted in the whitening of the material at higher strains than 0.1 and using SEM we clearly showed that this was due to the formation of voids around the particles, caused by debonding of the polymer material. Activation of the mechanophore was studied using fluorescence microscopy and a clear increase in fluorescence upon straining samples was observed as a consequence of mechanical activation starting before a strain of 0.025 was reached. This is much lower than when debonding of the polymer matrix was visible in SEM since the nanometer displacement of polymer at the particle interface at these strains is larger than needed for activation of the mechanophores. The overall intensity of the fluorescence was observed to be rather low due to the low degree of functionalization of the silica ﬁllers. With this mechanoﬂuorescent activation we showed that stresses and rupture of covalent bonds occur at the surface of the particles which is the molecular origin of debonding of the particles with the interface. With SEM the macroscopic effect of the stresses at the interface is visualized, which resulted in a void around the particle. This study can be expanded by investigating the effect of polymer matrix yielding by integrating the mechanophore in the polycarbonate interface instead of at the surface.

5.6 EXPERIMENTAL DETAILS

The chemicals used were purchased from Sigma Aldrich, VWR, Fisher Scientiﬁc, STREM Chemicals, Biosolve, Tokyo Chemical Industry and Cambridge Isotopes Laboratories. All compounds were used as received unless stated otherwise. Sodium hydroxide was dried in a vacuum oven at 80 °C before use. Toluene was dried over 4 Å mol sieves under N₂ atmosphere. Anhydrous DMF and THF were collected from a solvent puriﬁcation system (MB-SPS-800, MBRAUN). Deionised water was obtained from a Behropur B5 demineralisator connected to tap water.

All NMR spectra were recorded using a 400 MHz Bruker UltraShield Nuclear Magnetic Resonance spectrometer at room temperature. Tetramethyl silane (TMS) was used as internal standard in CDCl₃, and chemical shifts are given in ppm with TMS as reference

at 0 ppm. The shaker used was a VWR OS-500. Scanning Electron Microscope (SEM) images were obtained with a Quanta 3DFEG, equipped with an Everhart-Thornley Detector (ETD). Voltages, current and magnifications are provided with the respective pictures. Matrix-assisted laser desorption/ionization-time of flight mass spectra (MALDI-TOF) were measured using a Bruker Autoflex Speed mass spectrometer using α -cyano-4-hydroxycinnamic acid (CHCA) or trans-2-[3-(4-tert-butylphenyl)-2-methyl-2-propenylidene]-malononitrile (DCBT) as the matrix.

Dynamic Light Scattering (DLS) experiments were performed on an ALV/CGS-3 MD-4 Goniometer System equipped with a 50 mW Nd:YAG laser operating at 532 nm. The temperature was regulated at 20.0 ± 0.2 °C using a Lauda RM6-S Refrigerated Circulating Bath. The light scattering intensity was recorded under an angle of 90°. Characteristic decay rates (Γ) obtained from the normalized intensity autocorrelation function were used to calculate the translational diffusion coefficient (D_T). The size distribution of the particle hydrodynamic radii (R_H) was obtained using the Stokes-Einstein relation and the CONTIN method in AfterALV (v1.0).

Thermal stability studies were performed on a TA Instruments TGA Q500 instrument under an N₂ atmosphere. Samples were heated at 10 °C/min from 25 to 800 °C. Temperature calibration was performed using the Curie points of high purity aluminum, nickel and perkalloy standards. Size Exclusion Chromatography was performed on a Shimadzu Prominence-I LC-2030C 3D equipped with a RID-20A detector. The SEC was used with THF as solvent and polystyrene as the calibration standard.

Fluorescence emission spectra in solution were acquired using JASCO FP6500 spectrofluorometer. All experiments were performed at room temperature in a 10x10 mm quartz cuvette (3500 µL chamber volume, Hellma). The fluorescence spectra were recorded with an excitation wavelength of 365 nm between 390-700 nm. Excitation and emission monochromator slits were positioned at 3 nm and measured with 100 nm·min⁻¹ scanning speed.

Particle synthesis and functionalization

Silica particles: Ethanol (1125 ml) was added to a 3-neck round bottom flask and heated to 60 °C. After equilibrating at this temperature, deionized water (30 ml) and 25% ammonia in water (80 ml) were added dropwise using a syringe. The mixture was left to homogenize for 15 minutes under vigorous stirring, while heating to 60 °C. Tetraethyl orthosilicate (TEOS, 60 ml) was added in a time span of 1.5 minutes. The reaction was left

overnight, after which the particles were spun down in a centrifuge at 3500 rpm for 10 minutes, the supernatant was poured off and the particles were redispersed in fresh ethanol to wash out impurities. The centrifuging-washing cycle was repeated 3 times. After the last washing cycle, the particles were dried in a vacuum oven at 80 °C. The product was obtained as a white solid, with a weight of 17.66 g.

1-(3-(triethoxysilyl)propyl)-1*H*-pyrrole-2,5-dione: A 2-step-1-pot synthesis was applied.^{21,22} Maleic anhydride (1.24 g, 12.4 mmol) was dissolved in dry toluene (20 ml) in a dried 3-neck flask equipped with a dropping funnel and under N₂ atmosphere at room temperature. (3-aminopropyl)triethoxysilane (APTES, 2.9 ml 12.4 mmol) was added dropwise as a solution in 10 ml dry toluene. Conversion was followed with ¹H-NMR, when conversion was complete after 45 min, zinc chloride (1.70 g, 12.4 mmol) was added as a solid. Then hexamethyldisilazane (HMDS, 2.6 ml, 12.4 mmol) was added dropwise as a solution in 10 ml toluene while heating the reaction mixture to 80 °C under reflux. Reaction was followed with ¹H-NMR every 60 minutes, when complete conversion had been reached, the zinc chloride was filtered off. The solvent and leftover HMDS were evaporated off using a rotary evaporator in a fume hood, after which the product was dried in a vacuum oven at 40 °C. The product was obtained as a sticky oily liquid in good yield (3.08 g, 82%) with less than 5 mol% HMDS as impurity.

Step 1: ¹H-NMR (400 MHz, CDCl₃): δ 8.17 (s, 1H), 6.44 (d, J = 13.0 Hz, 1H), 6.30 (d, J = 12.0 Hz, 1H), 3.83 (q, J = 7.3 Hz, 6H), 3.38 (q, J = 6.5 Hz, 2H), 1.74 (p, J = 7.1 Hz, 2H), 1.23 (t, J = 7.3 Hz, 9H), 0.68 (t, J = 8.0 Hz, 2H).

Step 2: ¹H-NMR (400 MHz, CDCl₃): δ 6.68 (s, 2H), 3.80 (q, J = 7.1 Hz, 6H), 3.51 (t, J = 7.5 Hz, 2H), 1.70 (p, J = 7.7 Hz, 2H), 1.21 (t, J = 7.0 Hz, 9H), 0.58 (t, J = 9.0 Hz, 2H)

¹³C-NMR (400 MHz, CDCl₃): δ 170.85, 134.00, 58.46, 40.42, 22.11, 18.32, 7.74.

SiP-mal: The silica particles (4.0 g, 0.4 mmol OH) were first dispersed in isobutyl methyl ketone (IBMK, 300 ml) overnight. The triethylamine (Et₃N, 0.5 ml, 3.7 mmol) was added and after one hour 1-(3-(triethoxysilyl)propyl)-1*H*-pyrrole-2,5-dione (1.12 g, 3.7 mmol) was added in 30 ml of IBMK. After reacting for 24 hours, the particles were collected by centrifugation and redispersed in acetone. This cycle was repeated 3 more times. After the last washing step, the maleimide functionalized particles (SiP-mal) were dried in a vacuum oven at 60 °C. The product was obtained as a white powder (3.30g).

SiP-DA: The maleimide functionalized particles (SiP-mal, 1.50 g, 0.139 mmol OH) were dispersed in a isopropanol : toluene mixture (v/v - 7:3) with a total volume of 125 ml. After dispersing overnight, the phenol anthracene (0.7547 g, 1.396 mmol) was added and the reaction mixture was heated to 100 °C under reflux and left to react for 3 days. The particles with full mechanophore (SiP-DA) were obtained by centrifugation, followed by washing-centrifugation cycles with acetone until the fluorescent signal was maximum 3 times the solvent signal (background). The particles were dried in a vacuum oven at 60 °C. The product was obtained as a white powder (1.27 g).

SiP-DAPC: Previously synthesized polymer and SiP-DA (0.900 g, 0.08375 mmol OH) and polycarbonate ($M_n=26\cdot10^3 \text{ g}\cdot\text{mol}^{-1}$, 1.794 g, 0.084 mmol) were weighed and added to a dry round bottom flask under N₂ atmosphere. 3 vacuum-N₂ cycles were applied. Dry THF (54 ml) was added, and the polycarbonate was dissolved at room temperature while the particles were dispersed. When fully dissolved and dispersed, the solution was heated to 65 °C and NaOH (1.1 mg, 0.027 mmol) was added as a catalyst. The reaction was kept refluxing for 5 days. The particles were collected by centrifugation of the reaction mixture. The particles were washed by cycles of redispersing them in THF and centrifugation until no clear signal was observed in SEC. The particles were dried in a vacuum oven at 60 °C. The product was obtained as a white powder (0.84 g).

Characterization and preparation of composites

Heating experiment for confirmation of successful functionalization

SiP-DA (20 mg) were dispersed in 1 ml of *o*-DCB for one hour in an ultrasonic bath. Two vials, one placed in an oven at 160 °C and the other one kept at room temperature, were left for 1.5 hours. The vial in the oven was quenched in an ice batch to prevent the forward Diels-Alder reaction to take place. The mixtures were filtered over 0.1 µm MDI sy13vf syringe filters to filter off the particles and fluorescence was measured, after adding 1.5 ml of *o*-DCB to fill the cuvette.

Sonication experiment for confirmation of successful functionalization

120 mg particles were dispersed in THF for 30 minutes and then transferred to a Suslick cell which was cooled with water at 3 °C. Ultrasonication was conducted using a pulsed setting, the probe being on and off for 1 second repeatedly, at 25% amplitude. Every hour of time in the Suslick cell a sample was taken, and 0.8 ml was filtered over a 0.1 µm MDI

sy13vf syringe filter to remove the particles. To this, 1.5 ml THF was added to fill the cuvette to a sufficient level and a fluorescence spectrum was measured.

DLS measurements

DLS samples were prepared by making a dispersion of 0.5 mg/ml dispersions or 0.2 mg/ml, when the higher concentration was still not fully transparent, in ethanol. 10 runs of 10 seconds were measured under an angle of 90°, after optimizing the laser intensity. Data was analyzed by loading the data in AfterALV (v1.0, build 5520) and using the spectrum from roughly 2 decades before and after the curve becomes horizontal.

SEM sample preparation

SEM samples from particles were prepared by drop-casting from the DLS sample on a silicon wafer attached with carbon tape. Samples of films/composites were attached to the stud with copper tape. Cross-sections to check particle dispersion were created by breaking a piece of the film in liquid nitrogen after immersing in isopropyl alcohol.

Tensile tests

Dog bone shapes were obtained by die cutting with a punch press. Dimensions of the linear part: length 12 mm, width 2 mm. The thickness was measured with a digital caliper with 3 decimals in millimeter size. Tensile tests were performed on a Lloyd instruments EZ20 tensile tester in combination with a 500 N load cell and Nxygen plus software. The samples were clamped in the machine with double-sided tape to prevent slippage. In order to generate reproducible results, all samples were elongated with a constant rate of 0.72 mm/min, which compares to 0.001 s⁻¹, until pre-defined strain or failure.

Fluorescence microscopy

The fluorescence images were taken on a Leica confocal microscope after clamping the samples between 2 glass slits. The wavelength of excitation was 405 nm at a laser intensity of 12.5%. Signal was detected with a hybrid detector at a gain of 100%. Images were taken with a zoom of 1 in a 1024x1024 pixel format. The bright-field images were taken with a light intensity of 125 and a resolution of 1920x1440 pixels. After the images were taken, the images were analyzed by subtracting the average intensity from the unstretched sample from the pictures.

General procedure for solvent casting of polycarbonate composites

Polymer and particles were weighed and the solvent was added. The polymer was dissolved in the solvent by putting it on the shaker for approximately 1 hour. To disperse the

particles, the solution was put in an ultrasonic bath for approximately 1 hour. Aluminium mold was cleaned with CHCl₃ and blown dry with strong N₂ flow. Aluminium mold was placed in preheated oven with slight N₂ flow and the polymer-particle mixture was poured in from the vial. After 3 hours, the solvent was evaporated sufficiently to remove the film from the mold. Before further analysis or use, the films were dried in a vacuum oven at 60°C. Thickness was measured with an Elcometer 415 coating tool on a metal surface as a background.

5.7 REFERENCES

- Tzetzis, D.; Mansour, G.; Tsiafis, I.; Pavlidou, E. Nanoindentation Measurements of Fumed Silica Epoxy Reinforced Nanocomposites. *J. Reinf. Plast. Compos.* **2013**, *32*, 163–173.
- Yang, F.; Nelson, G. L. Polymer/Silica Nanocomposites Prepared via Extrusion. *Polym. Adv. Technol.* **2006**, *17*, 320–326.
- Pfaller, S.; Possart, G.; Steinmann, P.; Rahimi, M.; Müller-Plathe, F.; Böhm, M. C. Investigation of Interphase Effects in Silica-Polystyrene Nanocomposites Based on a Hybrid Molecular-Dynamics-Finite-Element Simulation Framework. *Phys. Rev. E* **2016**, *93*, 1–12.
- León, S.; Van Der Vegt, N.; Delle Site, L.; Kremer, K. Bisphenol a Polycarbonate: Entanglement Analysis from Coarse-Grained MD Simulations. *Macromolecules* **2005**, *38*, 8078–8092.
- Zhou, R. J.; Burkhardt, T. Mechanical and Optical Properties of Nanosilica-Filled Polycarbonate Composites. *J. Thermoplast. Compos. Mater.* **2010**, *23*, 487–500.
- Evans, A. G.; Williams, S.; Beaumont, P. W. R. On the Toughness of Particulate Filled Polymers. *J. Mater. Sci.* **1985**, *20*, 3668–3674.
- Chen, Q.; Chasiotis, I.; Chen, C.; Roy, A. Nanoscale and Effective Mechanical Behavior and Fracture of Silica Nanocomposites. *Compos. Sci. Technol.* **2008**, *68*, 3137–3144.
- Chen, J.; Liu, J.; Yao, Y.; Chen, S. Effect of Microstructural Damage on the Mechanical Properties of Silica Nanoparticle-Reinforced Silicone Rubber Composites. *Eng. Fract. Mech.* **2020**, *235*, 107195.
- Devaprakasam, D.; Hatton, P. V.; Möbus, G.; Inkson, B. J. Nanoscale Tribology, Energy Dissipation and Failure Mechanisms of Nano- and Micro-Silica Particle-Filled Polymer Composites. *Tribol. Lett.* **2009**, *34*, 11–19.
- Kim, T. A.; Lamuta, C.; Kim, H.; Leal, C.; Sottos, N. R. Interfacial Force-Focusing Effect in Mechanophore-Linked Nanocomposites. *Adv. Sci.* **2020**, *7*, 1903464.
- Zare, Y. The Roles of Nanoparticles Accumulation and Interphase Properties in Properties of Polymer Particulate Nanocomposites by a Multi-Step Methodology. *Compos. Part A Appl. Sci. Manuf.* **2016**, *91*, 127–132.
- Stöber, W.; Fink, A.; Bohn, E. Controlled Growth of Monodisperse Silica Spheres in the Micron Size Range. *J. Phys. Ther. Sci.* **1968**, *26*, 62–69.
- Meier, M.; Ungerer, J.; Klinge, M.; Nirschl, H. Synthesis of Nanometric Silica Particles via a Modified Stöber Synthesis Route. *Colloids Surfaces A Physicochem. Eng. Asp.* **2018**, *538*, 559–564.

14. Fernandes, R. S.; Raimundo, I. M.; Pimentel, M. F. Revising the Synthesis of Stöber Silica Nanoparticles: A Multivariate Assessment Study on the Effects of Reaction Parameters on the Particle Size. *Colloids Surfaces A Physicochem. Eng. Asp.* **2019**, *577*, 1–7.
15. Gao, W.; Rigout, M.; Owens, H. Facile Control of Silica Nanoparticles Using a Novel Solvent Varying Method for the Fabrication of Artificial Opal Photonic Crystals. *J. Nanoparticle Res.* **2016**, *18*, 387.
16. Liberman, A.; Mendez, N.; Trogler, W. C.; Kummel, A. C. Synthesis and Surface Functionalization of Silica Nanoparticles for Nanomedicine. *Surf. Sci. Rep.* **2014**, *69*, 132–158.
17. Su, Y.; Ran, S.; Fang, Z.; Guo, Z. Fullerene-Induced Crystallization toward Improved Mechanical Properties of Solvent Casting Polycarbonate Films. *Appl. Phys. A Mater. Sci. Process.* **2020**, *126*, 293.
18. Ruvolo-filho, A.; Murakami, M. M. Transport Properties of Water in Glassy Polycarbonate Films. Effects of the Processing and Thickness. *J. Macromol. Sci. - Phys.* **1998**, *37*, 627–643.
19. Krop, S.; Meijer, H. E. H.; Van Breemen, L. C. A. Global and Local Large-Deformation Response of Sub-Micron, Soft- and Hard-Particle Filled Polycarbonate. *J. Mech. Phys. Solids* **2016**, *87*, 51–64.
20. Kim, T. A.; Lamuta, C.; Kim, H.; Leal, C.; Sottos, N. R. Interfacial Force-Focusing Effect in Mechanophore-Linked Nanocomposites. *Adv. Sci.* **2020**, *7*, 1903464.
21. Engel, T.; Kickelbick, G. Thermoreversible Reactions on Inorganic Nanoparticle Surfaces: Diels-Alder Reactions on Sterically Crowded Surfaces. *Chem. Mater.* **2013**, *25*, 149–157.
22. Reddy, P. Y.; Kondo, S.; Toru, T.; Ueno, Y. Lewis Acid and Hexamethyldisilazane-Promoted Efficient Synthesis of N-Alkyl- and N-Arylimide Derivatives. *J. Org. Chem.* **1997**, *62*, 2652–2654.

Chapter 6

Epilogue

The work in this chapter was partially performed in collaboration with Steffijn de Koning

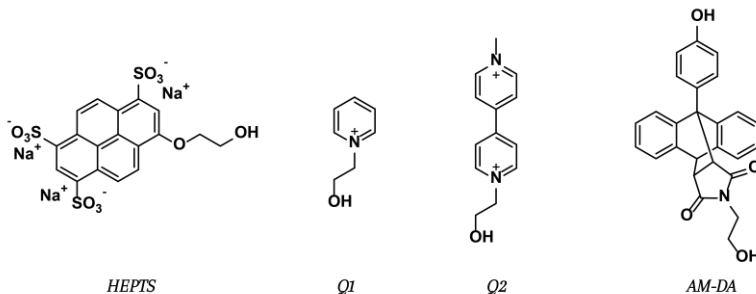
6.1 SUMMARY AND CONCLUSIONS

Due to the increasing interest in replacing currently used materials in, for example, construction and aerospace applications with polymers, it is of great importance to investigate the molecular origin of macroscopic deformation or damage in polymer materials and composites.¹ Mechanochemistry provides a unique toolbox to study the effect of mechanical force on the molecular level.²

In this thesis the development of two new mechanophores, a supramolecular and a covalent mechanophore, was described. A supramolecular mechanophore based on ion-paired complexes was developed and a covalent mechanophore based on a π-extended anthracene-maleimide Diels-Alder adduct was synthesized. The mechanophores were applied to develop a method to study stresses in both elastic and glassy polymers as well as in composites.

First, supramolecular mechanophores based on HEPTS aggregates and ion-paired complexes with pyridinium derivates were developed. The systems were integrated in MDI-based polyurethanes and a clear difference in strength of the complexes was observed (*Chapter 3*). Tensile tests were performed on solvent cast polymer films and mechanical activation of the mechanophore was monitored *in situ*. HEPTS aggregates were found to be the weakest mechanophores; activation of the mechanophore occurred at the transition from elastic to plastic deformation. HEPTS fluorescence was quenched with pyridinium derivatives via the formation of ground-state complexes. These complexes were stronger due to their ionic interactions and needed larger deformations compared to HEPTS aggregates. An increase in mechanical activation was observed at the onset of strain hardening, when the hard blocks start to dissociate. Thus, HEPTS aggregates detect plastic deformation in hard segment containing polyurethanes. Additionally, they are activated at lower forces than complexes of HEPTS with quenchers. Additionally, a covalent mechanophore was developed based in a π-extended anthracene-maleimide Diels-Alder adduct which was developed to study the molecular origin of damage in polystyrene and polycarbonate (*Chapter 4*) and in polycarbonate composites (*Chapter 5*). The thermal stability of the mechanophore was determined in solution and the Diels-Alder moiety cannot be used above 100 °C for longer than 1 hour. Polystyrene and polycarbonate thin films were solvent cast from toluene and DCM, respectively. Compression and tensile tests were performed on the solvent cast materials but no increase in fluorescence was observed, indicating that a very limited number of bonds was ruptured during these tests and if bond breakage occurred it is extremely localized.

Single asperity sliding friction experiments were performed and showed significant activation of the mechanophores starting at a normal load of 100 mN for polystyrene. At this load, polystyrene showed clear craze formation combined with mechanical activation, indicating that crazing is closely related to rupture of covalent bonds. Polycarbonate, however, only showed plastic deformation and minimal activation of the mechanophore at lower forces. At higher loads of 750 mN, a significant amount of mechanophores were activated without the formation of visual cracks, suggesting that in the scratch tests, polycarbonate mainly undergoes plastic deformation with limited rupture of covalent bonds.



Scheme 6.1. Chemical structures of the mechanophores used in this thesis. HEPTS, can form an aggregate with itself or an ion-paired complex with one of the quenchers Q1 or Q2. AM-DA is a Diels-Alder adduct as a mechanophore.

To extend this study towards composites, mechanofluorescent silica fillers were added to polycarbonate matrices to investigate stresses at the interface between the polymer matrix and the silica filler. Silica fillers with a 200 nm diameter were synthesized via the Stöber method and covalently functionalized with mechanophore and a polymer chain. Polycarbonate composite films were prepared via solvent casting from DCM. Tensile tests were performed and investigated at different stages during the tensile test. Activation of the mechanophore at the surface was observed at low strains starting from 0.025, while visual debonding in SEM was observed at 0.2 strain. It was shown that the molecular origin of debonding is breaking of multiple bonds at the interface between the polymer and the particulate filler, which starts well before macroscopic debonding is visible in SEM.

6.2 FURTHER DEVELOPMENTS IN COMPOSITES

Much of the molecular origins of macroscopic deformation in polymer composites remains unknown. Mechanochemistry can help elucidate mechanisms as mechanophores can be introduced on the surface of the particles and in the polymer matrix. The research reported in this thesis has focused on the origin of debonding in polycarbonate composites, however, there is insufficient evidence to decide whether bonds rupture only at the interface or fracture takes place at the interface and in the polymer matrix simultaneously.^{3,4} Hence it is important to investigate bond rupture in the matrix, complementing the study of bond breaking at the interface.

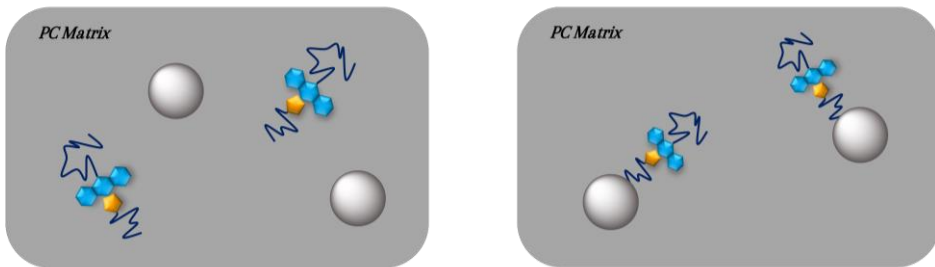


Figure 6.1. Illustration of two systems designed to investigate the failure mechanisms in polymer composites in more detail. a) a system with the mechanophore built into the polymer material will give more insight in the shear yielding of the polymer matrix, while b) mechanofluorescent fillers will give a warning when debonding of the polymer at the interface starts.

Two systems can be designed for this study: one system with the mechanophore on the particulate filler and one with the mechanophore build into the polymer chain of the matrix (**Figure 6.1**). Performing these experiments in parallel at different strains will give more insight in which bonds rupture first and which mechanism will dominate fracture in composites.

Additionally, similar experiments can be performed with soft fillers to investigate the differences in behavior of soft and hard particulate filled composites. Krop *et. al.* reported modelling results on the differences in local stresses in soft and hard particulate filled polycarbonate systems in which they used TiO₂ particles as hard fillers and methacrylate-butadiene styrene (MBS) rubber particles as soft fillers.⁵ They showed that in soft filled systems the highest stresses were present at the poles of the particles while for hard particles, the highest stresses were found in the polycarbonate matrix. With mechanofluorescent labeling of either particles or matrix (**Figure 6.1**), the site of highest

stress can be visualized. The hardness of silica particles is comparable to those of TiO₂ fillers, but since their synthesis and functionalization is easier, silica particles were used for the research in this thesis. MBS particles can be functionalized with mechanophores on the surface via a seeded emulsion polymerization in water. Some preliminary results on this functionalization are shown in **Figure 6.2**. Particles were dispersed in water and functionalized with a protected maleimide containing methacrylate groups (**I**). After functionalization, the particles were isolated and dried at 120 °C to induce a retro Diels-Alder reaction of the protected maleimides on the surface of the particles. Preparation of mechanophore functionalized MBS particles was completed by reaction of the maleimide groups with phenol anthracene. A polycarbonate prepolymer was synthesized and attached to the mechanophore on the surface of the particles.

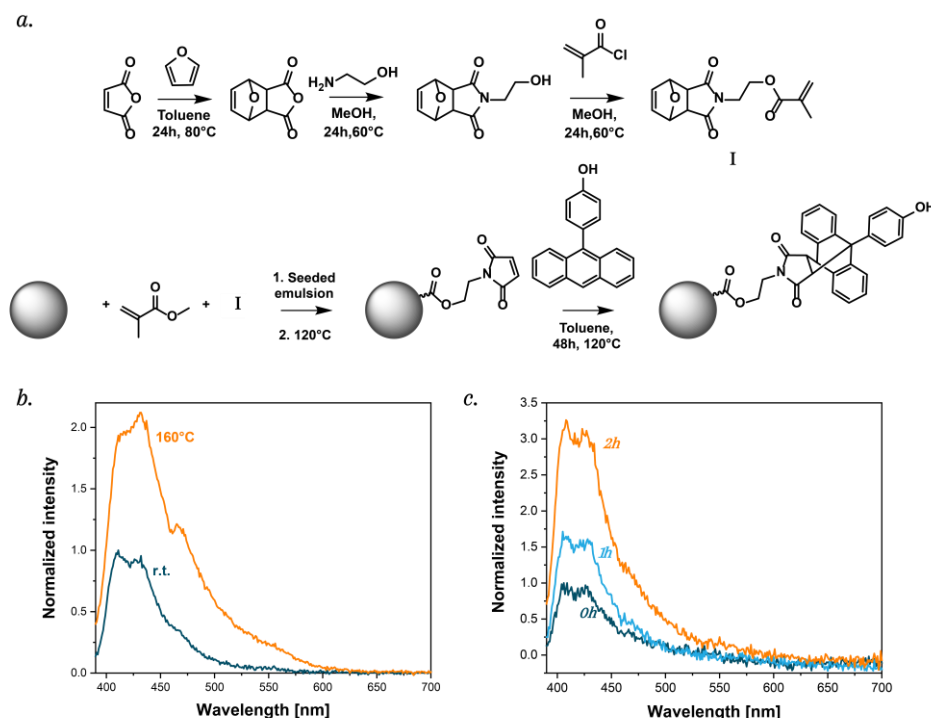


Figure 6.2. a) schematic overview of the functionalization of the MBS particles via a seeded emulsion polymerization using a mixture of methyl methacrylate and the synthesized maleimide methacrylate I. b) After heating the functionalized particles to 160 °C an increase in fluorescence was observed. c) When the mechanophore on the surface was further functionalized with PC, sonication of the particles resulted in an increase in fluorescence intensity.

Similarly as for the silica particles in *Chapter 5*, functionalization of the particles was confirmed in heating and sonication experiments although with low loading. Further investigation on the formation of stresses in composites will be done by comparing the matrix functionalized materials with the particle functionalized materials.

An additional study which can be performed to create a better understanding of the relationship between the macroscopic behavior and events at the molecular level is incorporating the mechanophore inside MBS particles. This can be done by synthesizing a crosslinker of the mechanophore and incorporate this into spherical particles synthesized via an emulsion polymerization. Also here the functionalized matrix and surface functionalized composites can be compared to the particle functionalized composites.

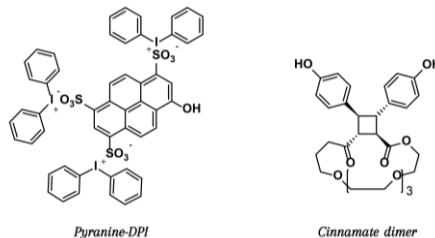
6.3 APPLICATION OF MECHANO CHEMISTRY IN BULK POLYMERS

The conventional route for bisphenol-A polycarbonate via a melt trans carbonation requires high temperatures. By exchanging the diphenyl carbonate donor by an activated carbonate like bis(methyl salicyl) carbonate (BMSC) the polymerization temperature is lowered but still does not allow incorporation of thermolabile monomers or mechanophores.^{6,7} The solution transcarbonation reported by Kamps allows incorporation of thermolabile compounds as described in *Chapter 4*.⁸ High molar mass polycarbonates can be synthesized, but due to the low thermal stability of the mechanophore only solvent casting can be used to prepare polymer materials. Therefore, mechanophores with a low thermal stability, such as the Diels-Alder mechanophore proposed in this thesis, cannot be integrated into industrially relevant materials.

HEPTS derivatives are thermally more stable than the Diels-Alder mechanophore, for example pyranine with diphenyliodonium counterions (**Scheme 6.2**) is reported to be stable up to ~200 °C.⁹ and their applicability is broader. An interesting feature of ionic HEPTS is that it can be converted into a bifunctional monomer, allowing the production of ionomers. Ionomers are known to exhibit significantly improved mechanical properties compared to their non-ionic analogues.¹⁰ When the ionic groups also act as mechanophore, these moieties are the perfect tool for detection of plastic deformation and chain slippage in polymer materials with a processing temperature below 200 °C.

Another mechanophore which has been reported to have high thermal stability is based on cinnamate dimers that contain a cyclobutane ring (**Scheme 6.2**). Boulatov and coworkers reported this mechanophore to have a half-life of longer than one hour

at 300 °C.¹¹ This mechanophore can also be incorporated in polymer chains if the synthetic procedure requires high temperatures. This would facilitate incorporation of the mechanophore in bulk polycarbonate samples.



Scheme 6.2. Chemical structures of the tris(diphenyliodonium) pyranine and the cinnamate dimers. Both mechanophores contain OH-functionalities, allowing for relatively easy functionalization.

6.4 CONCLUSIONS

In this thesis it has been shown that mechanofluorescent molecules are good candidates to develop a method to create a better understanding of the structure-to-property relationship of polymers and composites. These mechanophores were applied in three different types of materials: brittle polystyrene, tougher polycarbonate and elastic polyurethanes. In all three systems the mechanophores could be activated mechanically by performing tensile tests or sliding friction tests. Additionally, visualization of stress was expanded towards silica filled polycarbonate composites in which debonding of the polymer matrix was shown to start at the very early stages of deformation. Further investigation on the failure mechanisms is required and can be performed with mechanochemical experiments with the mechanofluorescent labeling either in the particle, at the surface of the particle or in the polymer matrix. Performing these tests on both hard and soft filled polymer composites is expected to give a more complete insight in the failure mechanisms of polymer composites.

6.5 REFERENCES

1. Jancar, J.; Douglas, J. F.; Starr, F. W.; Kumar, S. K.; Cassagnau, P.; Lesser, A. J.; Sternstein, S. S.; Buehler, M. J. Current Issues in Research on Structure–Property Relationships in Polymer Nanocomposites. *Polymer* **2010**, *51*, 3321–3343.
2. Chen, Y.; Mellot, G.; Van Luijk, D.; Creton, C.; Sijbesma, R. P. Mechanochemical Tools for Polymer Materials. *Chem. Soc. Rev.* **2021**, *50*, 4100–4140.
3. Onitiri, M.; Ubi, P. A. Failure Modes in Particle Filled Plastic Matrix. *J. Eng. Sci. Technol.* **2021**, *5*, 78–96.
4. German, R. M. *Particulate Composites: Fundamentals and Applications*; 2016.
5. Krop, S.; Meijer, H. E. H.; Van Breemen, L. C. A. Global and Local Large-Deformation Response of Sub-Micron, Soft- and Hard-Particle Filled Polycarbonate. *J. Mech. Phys. Solids* **2016**, *87*, 51–64.
6. Kamps, J. H.; Hoeks, T.; Kung, E.; Lens, J. P.; McCloskey, P. J.; Noordover, B. A. J.; Heuts, J. P. A. Activated Carbonates: Enabling the Synthesis of Differentiated Polycarbonate Resins via Melt Transcarbonation. *Polym. Chem.* **2016**, *7*, 5294–5303.
7. Freitag, D.; Fengler, G.; Morbitzer, L. Routes to New Aromatic Polycarbonates with Special Material Properties. *Angew. Chemie Int. Ed. English* **1991**, *30*, 1598–1610.
8. Kamps, J. H.; Groote, R.; Baus, M.; Vermeulen, H.; Hoeks, T.; van der Heijden, R.; Sijbesma, R. P.; Heuts, J. P. A. Activated Carbonates: Enabling the Synthesis of Differentiated Polymers via Solution Carbonation. *Eur. Polym. J.* **2020**, *135*, 109901.
9. Tarumoto, N.; Miyagawa, N.; Takahara, S.; Yamaoka, T. Diphenyliodonium Salts with Pyranine Conk as an Environment-Friendly Photo-Acid Generator and Their Applications to Chemically Amplified Resists. *Polym. J.* **2005**, *37*, 545–549.
10. Eisenberg, A.; King, M. *Ion-Containing Polymers*, 1st editio.; Academic press, **1977**.
11. Zhang, H.; Li, X.; Lin, Y.; Gao, F.; Tang, Z.; Su, P.; Zhang, W.; Xu, Y.; Weng, W.; Boulatov, R. Multi-Modal Mechanophores Based on Cinnamate Dimers. *Nat. Commun.* **2017**, *8*, 1147.

Curriculum Vitae



Annelore Aerts was born on the 14th of March 1994 in Mol, Belgium. After finishing her secondary education at Campus Het Spoor in Mol, she began her studies in chemistry and life sciences at Hasselt University in 2012. In her bachelor graduation project she investigated a CuAAC reaction of biomolecules on hydrophilic poly(*p*-phenylene ethynylene) films. In 2015 she started her masters in Chemical Engineering and Chemistry at Eindhoven University of Technology her graduation project under supervision of R.A.J. Janssen focused on the application of thiophene-fused 1,10-phenanthroline conjugated polymers in polymer solar cells. After completion of her internship at CSIRO in Melbourne, Australia, she obtained her masters degree. In 2017 she started her PhD in the Supramolecular Polymer Chemistry Group at Eindhoven University of Technology under supervision of R.P. Sijbesma and Hans Heuts. Her research focused on the probing damage in polymers and composites using mechanochemistry. The most important results are presented in this thesis.

Publications

This thesis is based on the following publications:

Aerts, A., Lugger, S.J.D., Heuts, J.P.A., Sijbesma, R.P.; Pyranine Based Ion-Paired Complex as a Mechanophore in Polyurethanes; *Macromolecular Rapid Communications* **2021**, *42*, 2000476.

Aerts, A., Kroonen, C.C.E., Kamps, J.H., Sijbesma, R.P., Heuts, J.P.A.; High Molar Mass Polycarbonate via Dynamic Solution Transcarbonation Using Bis(methyl salicyl) Carbonate, an Activated Carbonate; *Macromolecular Chemistry and Physics* **2021**, *222*, 2100186.

Aerts, A., Looijmans, S.F.S.P., van Breemen, L.C.A., Heuts, J.P.A., Sijbesma, R.P.; Fluorescent visualization of bond breaking in polymer glasses; to be submitted.

The author has also contributed to the following publication:

Aerts, A., Lewis, R.W., Zhou Y., Malic,N., Moad, G., Postma, Almar; Light-Induced RAFT Single Unit Monomer Insertion in Aqueous Solution—Toward Sequence-Controlled Polymers; *Macromolecular Rapid communications* **2018**, *39*, 1800240.

Acknowledgements

De afgelopen vier jaren zijn voorbij gevlogen en net zoals iedere belangrijke mijlpaal in mijn leven, was ook mijn promotieonderzoek en het schrijven van dit proefschrift onmogelijk zonder de hulp en steun van heel veel lieve vrienden, familie en collega's. Graag zou ik iedereen daar enorm hard voor willen bedanken en een aantal mensen in het bijzonder.

The last four years have flown by and like every important milestone in my life, this PhD-research and the writing of this dissertation was impossible without the help of many dear friends, family and colleagues. I would like to thank everyone for that and a number of people in particular.

Allereerst wil ik graag mijn promotoren Rint en Hans heel erg bedanken voor het vertrouwen, de begeleiding en de steun gedurende de afgelopen vier jaar. Rint, mijn allereerste sollicitatiegesprek in het hostel in Brisbane waarin u zei: 'Hans en ik hebben besloten om jou aan te nemen.' herinner ik me nog als de dag van gisteren. En dat zelfs nog nadat ik meteen volop de cocktails ben in gevlogen. Ik heb gedurende de afgelopen vier jaren ontzettend veel van u geleerd en ik ben enorm gegroeid op zowel professioneel als persoonlijk vlak en ik weet zeker dat ik nog veel meer van u kan leren. Ik heb gigantisch bewondering voor uw toewijding aan de wetenschap en uw fantastische (en af en toe gekke) wetenschappelijke ideeën. Super bedankt voor alle opportuniteiten die ik gedurende mijn PhD heb gekregen.

Hans, al sinds het vak 'inleiding tot polymeerchemie' tijdens de master had ik suuuuuuper veel bewondering voor u. Altijd blij, enthousiast en bereid om zaken toe te lichten en te verduidelijken. Nooit was ook maar iets een tikkeltje teveel gevraagd; ook dat was heel duidelijk tijdens mijn PhD en dat apprecieer ik enorm! Uw deur stond altijd open voor het bespreken van de resultaten, het fine-tunen van presentaties, maar ook gewoon voor een babbeltje. De uurtjes bij u op kantoor waren voor mij enorm waardevol; je had altijd goede ideeën en super tips en je enthousiasme is erg aanstekelijk en daardoor kon ik ook iedere keer weer happy de peppy en vol goede moed verder met mijn onderzoek. Hartelijk bedankt voor al je tijd, moeite en geduld!

I would also like to thank my committee members prof. dr. Katja Loos, prof dr. Costantino Creton, dr. Stefan Meskers and dr. Lambèrt van Beemen for their time to assess this thesis and for taking part in the defense. Costantino, I'd also like to thank you for the nice and fruitful discussions during the annual DPI progress meetings. Stefan, hartelijk bedankt voor de hulp bij de opbouw van mijn optische set-up gedurende de laatste weken van mijn PhD, ook uw deur stond altijd open en dat apprecieer ik ten zeerste. Lambèrt, ook wil ik u in het bijzonder bedanken voor alle hulp, suggesties en feedback met betrekking tot het mechanisch testen van onze materialen. Ik vond het een zeer leuke samenwerking! Finally, special thanks go to prof. dr. Fausto Gallucci for chairing the defense.

The research described in this thesis formed part of the research programme of DPI, project #805t15. I would like to thank Denka for chairing all annual DPI meetings and our progress meetings together with Costantino. I would also like to express my gratitude to all ICP's involved in my project for their useful feedback and suggestions.

Deze thesis was nooit in deze vorm tot stand gekomen zonder samenwerkingen met collega's en studenten. Stan, graag wil ik jou heeeeel erg bedanken voor al je steun, hulp, suggesties, peptalks en gezellige koffietjes! Ik hoop echt dat we hoofdstuk 3 en 4 nog samen kunnen publiceren. Diederik, je bent zoooo ongelooflijk slim en ik ben zo dankbaar dat ik ook tijdens mijn domme momentjes even bij jou kon aankloppen. Dankjewel voor alle leuke mechanochemie discussies en gezellige koffietjes. Souma, thanks for always being super helpfull. Tobi, my favorite fellow lab supervisor! Thanks for your help with and suggestions for my first paper, for taking care of everything and all happy times on the lab. Camiel, Sean, Naomi, Martijn en Steffijn, jullie hebben fantastisch werk geleverd en me enorm vooruit geholpen met mijn onderzoek. Ieder hoofdstuk bevat wel een bijdrage van een van jullie. Superveel thaanksiess voor jullie inzet en gezelligheid, ik heb jullie orecht met heel veel plezier begeleid. Sean, jou wil ik in het bijzonder nog even bedanken voor je steun, vele geduld en en alle hulp gedurende de laatste weekjes van 2021!

Ook de vaste staf die SMO draaiende houdt verdient het om in de bloemetjes gezet te worden. Hans, bedankt voor het doorvoeren van alle bestellingen en voor je handige harry tips wanneer ik een rotavap of een oven moest repareren. Martina, Margot en Carla jullie zijn absoluut onmisbaar voor SMO, dank om er steeds voor te zorgen dat alles op rolletjes loopt en voor het organiseren van de zeer leuke en gezellige activiteiten en borrels. Martina en Margot, ik kon altijd bij jullie terecht voor ook maar iedere kleine pietluttigheid of gewoon een gezellige babbeltje en dat vond ik geweldig! Dankjulliewel!

Gedurende de jaren van mijn PhD zijn er heel veel mensen gekomen en ook weer gegaan. Ik ben de tel ondertussen alweer kwijt, maar dus bij deze zou ik heel graag ieder (ex)-SMO-lid willen bedanken voor hun steentje dat ze hebben bijgedragen. *During the years of my PhD, many people have come and gone. I already lost the count, but here I would like to express my gratitude for all (ex)-SMO members that contributed one's bit.* Ook wil ik heel graag SFD bedanken voor de mogelijkheden om experimenten te kunnen uitvoeren op jullie labs. Simon, Stijn, Fabian, Jeroen & Jeroen, Davey, Gilles, Marc, en alle andere ameazing vriendjes, bedankt om mij te adopteren voor gezellige lunchtijden en onvergetelijke ameazing avonturen!

Lieve Henk, wat heb ik toch genoten van onze dagelijkse koffiekransjes. Ik ben heel blij dat we deze koffiemomentjes hebben doorgezet samen met Michel, Joris, Maarten, Jolanda en Sandra. Ik vond het altijd megagezellig en ik ga deze momentjes ook enorm hard missen! Michel, naast de leuke koffietjes wil ik je ook nog bedanken voor het meedenken en 3D-printen van labeltjes e.d. voor Mammelien! Heel leuk, dankjewel! Sandra, jij bent echt een geweldig leuke en lieve persoon. Je staat altijd klaar voor alles en iedereen en daar heb ik veel bewondering voor. Daarnaast ben je ook de beste bakartiest allertijden, heel erg bedankt voor al je overheerlijke bakcreaties die ik gedurende mijn PhD heb mogen proeven. Jolandaaaaaa, wat ben je toch een topmadam en mijn god wat moest ik toch zonder jou! Koffietjes, babbeltjes, lunchjes en zelfs samen sporten; we hadden altijd goude momentjes. Je ben echt de meest praktisch denkende persoon op aarde. Ik heb echt superduper veel bewondering voor jou en snap eigenlijk ook na vier jaar nog steeds niet hoe je het toch altijd zo goed voor mekaar krijgt. Ik heb enorm veel van jou geleerd en werkelijk zonder jou had mijn onderzoek helemaal niks geworden.

As the baby of our little PhD squat I'm suuuper grateful for all the tips, tricks and suggestions and of course all the support and love I received from you guys! Elisabeth, Huiyi, Shidong, Patri and Jie I'm grateful that I could share these happy times with you and I'm sooooo proud of you all! I love you, guys! Jie, my friend, my officemate, I really appreciate you for who you are. You're a very sweet and kind person and you're always happy to help! Angelooo, my friend and (temporary) office mate, you are amazing! I really admire you for both your scientific dedication and kindness and happiness! We had so much fun, I really enjoyed your little 'fights' with Jie as well. Additionally, I would like to thank our Wednesday writing retreat club! I really enjoyed our dinners together and thanks for making my Wednesday evenings fun and productive.

Of course, I would like to express my extremely special thanks to my lovely paranymphs. Eveline, oh my god ik ben zooooo blij dat je ook mijn paranymph wilde zijn! Al heel snel werden we echt goede maatjes. Ik ben je enorm dankbaar voor alles wat je voor me gedaan

hebt! Alle leuke koffietjes, circuit traininkjes, dinertjes en ga zo maar door. Zelfs het controleren van elkaars berekeningen en uitwerkingen was gezellig. Ik zou bijna zeggen dat corona helemaal poep was en alles verpest heeft, maar ik ben dat vieze virusje toch ook heel dankbaar dat we nog een heeeeel korte periode wel kantoorgenootjes konden zijn. Dit waren misschien niet de meest productieve weken van mijn PhD, maar zeker wel enkele van de leukste! Dikke Kus! Lieve Patri, brownie, eigenlijk zou ik dit nu in het Nederlands moeten doen, maar goed ik zal even lief zijn en switchen naar Engels. From the first day when I started my PhD we had a lot of fun and even within a few weeks we had the first person entering our office to ask us to shut up, ooooopss... But in the end it never changed. Lovely paranympths, thanks for all the happiness, love, support and my favorite delicious TimTams!

Aan alle lieve vrienden, familie en schoonfamilie, daaaankk julllieee weeeeell! Ik ben jullie allemaal heel erg dankbaar voor alle steun en liefde die ik gedurende de jaren heb gekregen. Thijs, bedankt voor de gezellige koffietjes, borrels en dinertjes! Lioba, lieve puppy, de vriendschap die ik met jou heb opgebouwd is onbetaalbaar; ik kan altijd bij jou terecht om te lachen, te gieren en te brullen of gestoord en gek te doen, maar ook om even te zeuren of uit te huilen. Dankjewel! #Puppylove

In het bijzonder wil ik nog even mijn allerliefste ouders, plusouders en mijn broer bedanken voor alle liefde, steun en toeverlaat. Ik kan altijd met alles bij jullie terecht (ook in het verre Spanje) en zonder jullie had ik hier nu niet gestaan! Mammie, dankjewel voor alle paren schoenen die je ooit voor mij hebt meegebracht, zonder jou had ik ook die shoe-challenge niet gehaald. Lovies, knuffel en een dikke kus!

Als laatste natuurlijk Stefan, muppet, moppie, dankjewel voor al je hulp, liefde, steun en ook vooral je geduld gedurende de afgelopen jaren. Sorry de snorry voor alle momenten dat ik om 5 uur thuis zou zijn en het dan toch half 7 werd. Ik ben blij dat ik dit heb kunnen doen met jou aan mijn zijde. We hebben ongelooflijk leuke tijden beleefd hier in Eindhoven en ik kijk heel erg uit naar onze vervolgavonturen tussen de schaapjes in het Belgische Reppel! Ik hou ontzettend veel van jou!

Lots of Lovies,

Annelore

